HALL EFFECT OF HOLES IN ANTHRACENE

by

ABRAHAM I. KORN

A dissertation submitted to the Graduate Faculty in Physics in partial fulfillment of the requirements for the degree of Doctor of Philosophy, The City University of New York.

1969

This manuscript has been read and accepted for the Graduate Faculty in Physics in satisfaction of the dissertation requirement for the degree of Doctor of Philosophy.

May 23, 1969
date

Arthur C. Danauk
Chairman of Examining Committee

May 23, 1969
date

Executive Officer

Dr. Richard A. Arndt

Prof. Milton Furst

Prof. Robert D. Hatcher

Prof. George Skorinko
Supervisory Committee

The City University of New York

To my wife, Tina, and my parents, without whose constant encouragement and help this work could not have been completed.

Acknowledgments

The author wishes to express his sincere gratitude to his advisor, Professor Arthur C. Damask. The skills and values which he imparted were as significant as his explicit help in providing the facilities, equipment, and encouragement that made this work possible.

The author also wishes to express his appreciation to Doctor Richard A. Arndt for discussions, frequent suggestions, and his valuable advice.

Appreciation is here expressed for the support of this research by The Army Research Office, Durham. The author has also benefited by the use of the facilities provided by Brookhaven National Laboratory and by a Summer appointment as a Visiting Research Assistant at Brookhaven National Laboratory.

Gratitude is also expressed to New York City Community College of the City University of New York for a leave of absence granted to complete this research.

TABLE OF CONTENTS

TABLES

FIGURES

1. Introduction

This work is on the bulk measurement of the Hall effect of holes in single crystals of high purity anthracene. In this chapter, the theories regarding charge transport in organic semiconductors, band theory, hopping motion, and tunneling models are contrasted. It will be shown that this work indicates that band theory gives the best description of charge transport in anthracene. Previous Hall effect measurements in anthracene are reviewed, and the objectives of this investigation are stated.

A. General Characteristics of Organic Semiconductors

Most organic semiconductors should really be designated as insulators because of their low electrical conductivity. They are called semiconductors because their dark electrical conductivity increases exponentially with temperature as $\sigma = \sigma_o \exp(-E/kT)$. The conductivity arises from the injection of charge carriers into the organic semiconductor by some extrinsic means such as by **contacts, adsorbed gases, or impurities.**
For anthracene, a typical organic semiconductor, $E \approx 0.85$ eV, $\sigma_o \approx 2.5 \times 10^{-31}$ (ohm cm)$^{-1}$, and $\sigma_{20^oC} \approx 10^{-15}$ (ohm cm)$^{-1}$.[1] Since $2E$ is smaller than the band gap, given below, for anthracene, the conduction must be extrinsic and not intrinsic. However, since this investigation is concerned with the transport of charge carriers once they reach the conduction band, the actual method of charge carrier

generation is only important for the following reasons: a determination of the type of charge carrier present and the provision of a sufficient number of charge carriers in the conduction band so that an observation of the Hall effect can be made.

Organic semiconductors belong to the class of solids known as molecular crystals. The binding forces of these crystals are Van der Waals forces, and the molecules are relatively far from one another. Anthracene, a planar polycylcic aromatic hydrocarbon (see Figs. 1.1 and 1.2), has been used in scintillation counters for many years. Thus, being readily available commercially, in what was believed to be an adequately pure crystalline form, anthracene has long been considered by many to be a prototype material for the investigation of the properties of organic semiconductors.

Due to the weak crystal forces, the molecular energy levels are relatively undisturbed in a molecular crystal. In order to obtain charge transport, it is necessary, at the very least, to excite an electron into one of these molecular states. The electronic states of aromatic molecules are assumed to factor into noninteracting sets of σ-orbitals and π-orbitals. The σ-orbitals are symmetrical around the bond axis, giving localized C-C and C-H bonds. The π-orbitals are perpendicular to the molecular plane. Fig. 1.3 is a composite sketch of three benzene molecular orbitals for anthracene. The composite was made from a sketch of the molecular orbitals of a

Fig. 1.1. The molecular structure of anthracene, $C_{14}H_{10}$. The C-C bond lengths are approximately 1.4 Å, and the C-H bond lengths are approximately 1.1 Å at 290 K.[2]

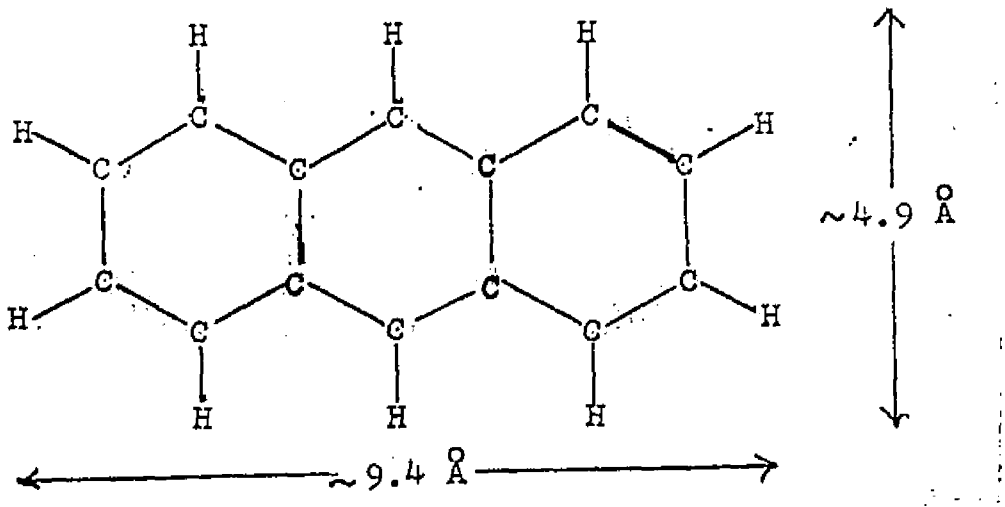

Fig. 1.2. The crystal structure of anthracene. The crystal is monoclinic and the space group is C_{2h}^5-$P2_1/a$ (twofold screw axis normal to the glide plane). The molecules are stacked in herring-bone array in sheets, which are parallel to the ab cleavage plane of the crystal. The lattice parameters, given below, were obtained by Mason.[2]

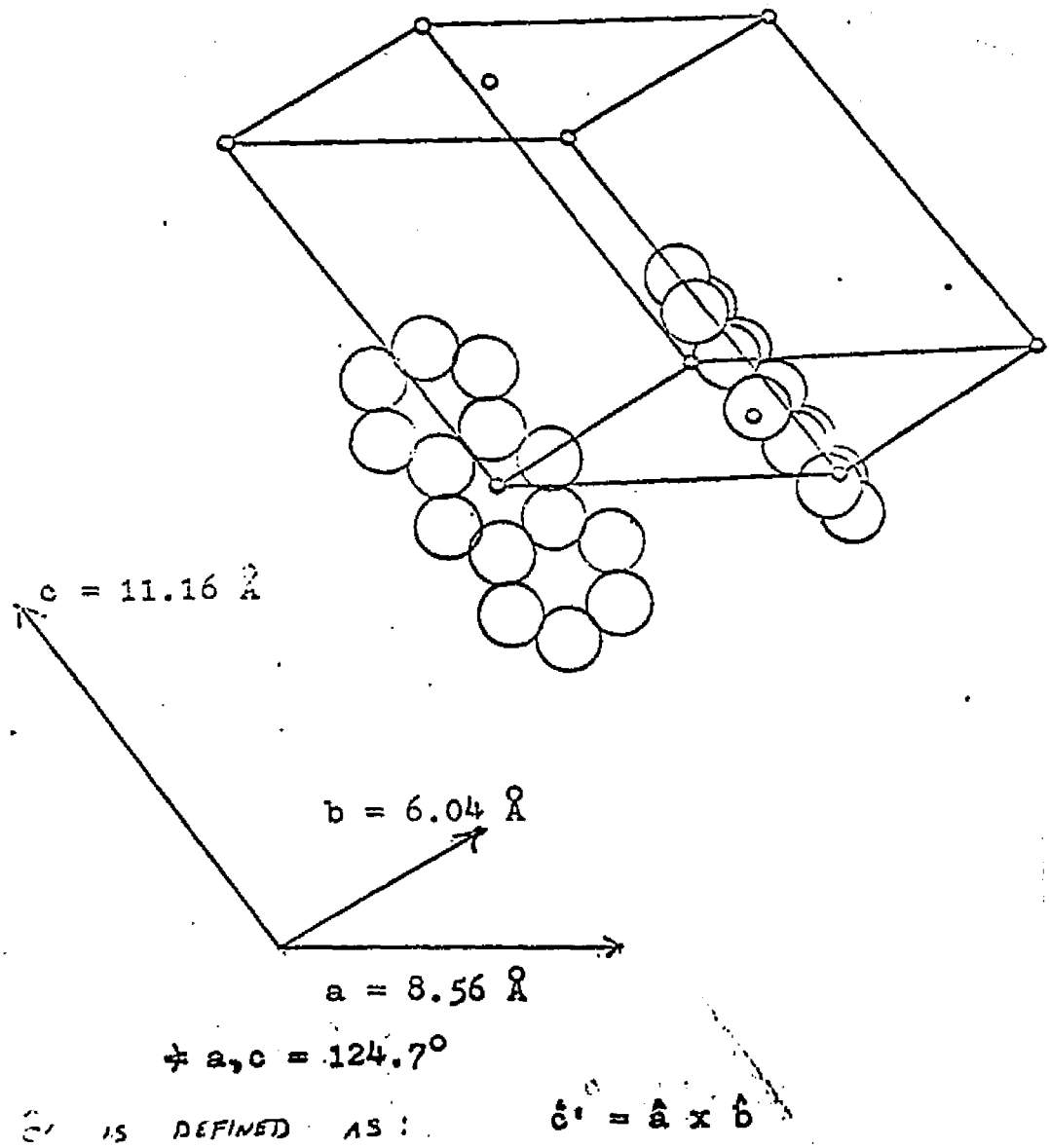

FIG. I.3. ANTHRACENE MOLECULAR ORBITALS.
(a) LOCALIZED σ-ORBITALS; (b) UNLOCALIZED π-ORBITALS.

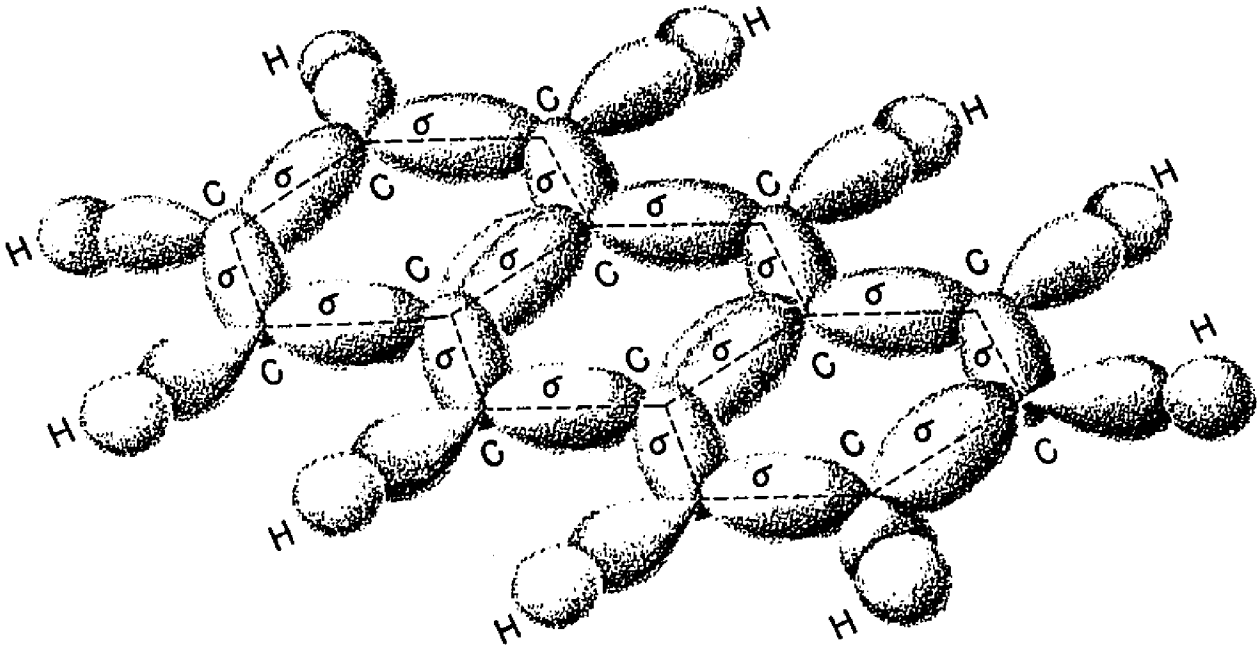

(a)

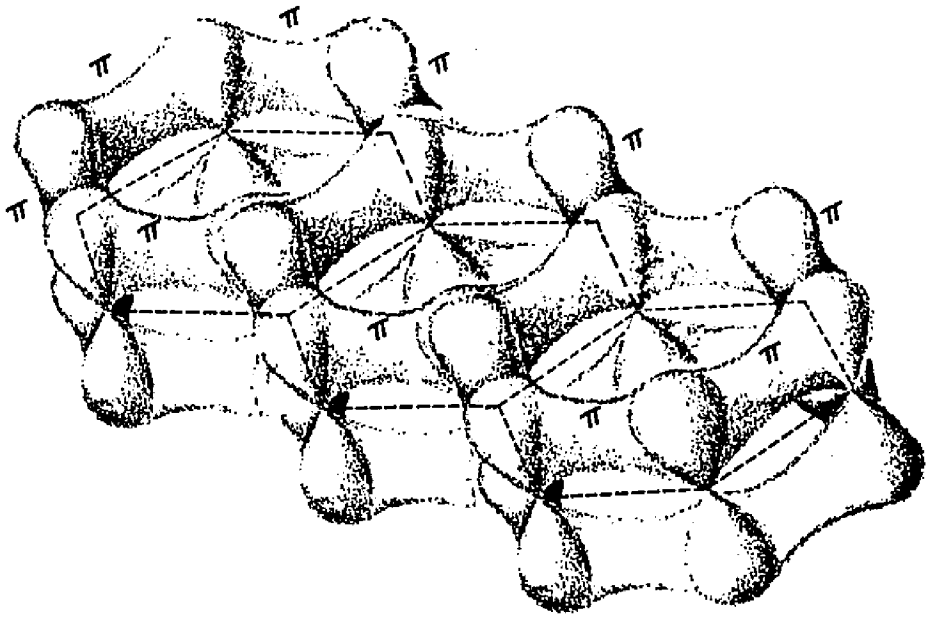

(b)

benzene molecule[3] and is used to give a schematic representation of the σ and π-orbitals. Any π-orbital overlaps both of its neighbors equally so that the π electrons are completely delocalized.

Considering only the π-orbitals, the ground state of the molecule is obtained by placing pairs of electrons, with opposite spin, into the lowest orbitals. The resultant ground state is therefore a singlet state since there are an even number of electrons. An excited state may be obtained by removing an electron from the uppermost filled orbital of the ground state to a vacant orbital of higher energy. If the spin of the excited electron is conserved in this process, the total spin of the excited state is zero, giving rise to an excited singlet state. If there is a spin reversal, the total spin is one, resulting in a triplet state. The first excited singlet and triplet states of an anthracene crystal are shown schematically relative to the singlet ground state in Fig. 1.4. Thus, the band gap must be greater than 3.42 eV.

The theories which can be used to describe charge transport in molecular crystals are band theory, the hopping model, and the tunneling model.

Band theory considers charge carriers to be completely shared by the entire crystal lattice. Bloch momentum eigenfunctions of the perfect lattice are used as basis functions, and crystal imperfections, phonon or other, are treated as perturbations that scatter carriers among the perfect lattice states. In this model, the π-orbitals,

Fig. 1.4. The first excited singlet and triplet states of anthracene single crystals.[4]

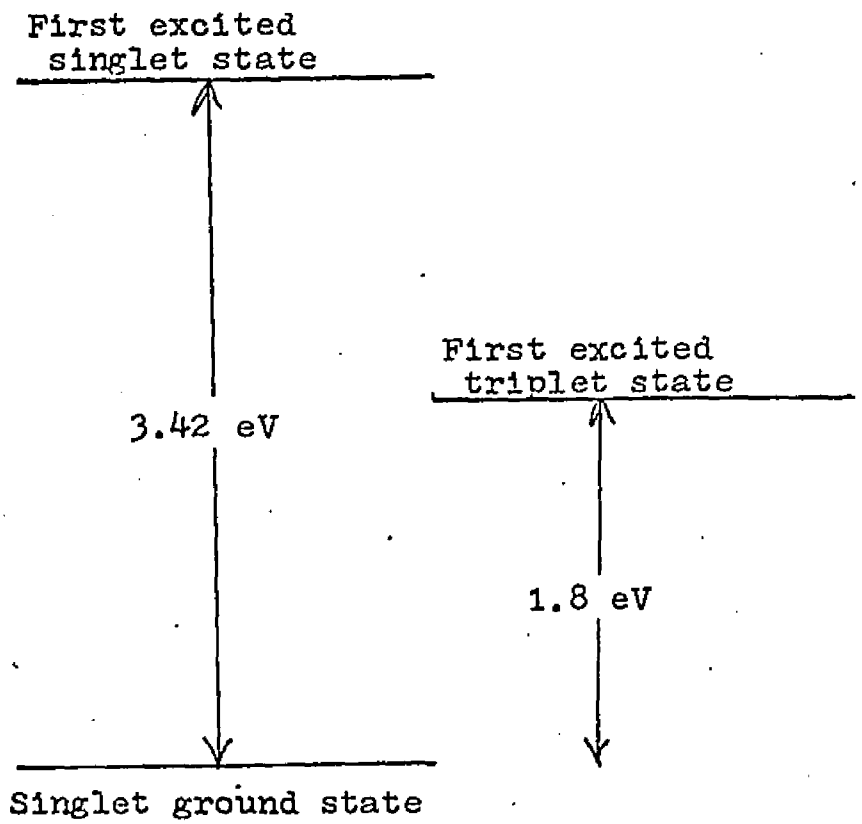

extending from the molecular planes, overlap with one another so that their energy levels split into bands belonging to the entire crystal. In order to be physically meaningful, the band model must satisfy restrictions imposed by the uncertainty principle.[5] From the uncertainty principle, $W > \hbar/\tau$, where W is the bandwidth and τ is the relaxation time. $\tau = \ell/v$, where ℓ is the mean free path of carriers with respect to scattering, and v is the carrier velocity, given by $v = (1/\hbar)\partial\mathcal{E}(k)/\partial k$. The maximum value of v is $v_{max} \sim Wa/\hbar$, where a is a lattice spacing. For $W < kT$, narrow bands, the statistical average of v^2 is of the order of v_{max}^2 so that the inequality from the uncertainty principle may be written as $\ell > a$. Since the drift mobility may be written as $\mu_D = (e/kT)\langle \tau v^2 \rangle$ (equation 2.28 of chapter 2), one has: $\mu_D > (ea^2/\hbar)(W/kT)$. Using anthracene lattice spacings, one obtains: $\mu_D > 0.1(W/kT)$. Calculations for anthracene lead to values of the mean free path that are between 1 and 5 lattice spacings.[6,7,8,9,10]

Calculations of the energy band structure for anthracene have been performed by LeBlanc,[6] Thaxton et. al.,[7] Katz et. al.,[8] Silbey et. al.,[9] Glaeser and Berry,[10] and Chojnacki.[11] These calculations are discussed in more detail in Chapter 3. The tight binding approximation was used in all the calculations because of the relatively small binding energy of the molecules in a molecular crystal compared to excitation energies of the various excited electronic states of the molecule (and crystal). The anisotropy of the drift mobility was then calculated by assuming either a constant

relaxation time or a constant mean free path. Although these calculations have been criticized for failure to take into account molecular vibrations, lattice expansion, self trapping, and the hydrogen atoms, they predict, quite well, the anisotropy of the drift mobility, and predict a decreasing mobility with increasing temperature. It should be noted that the temperature dependence of the drift mobility does not conflict with the temperature dependence of the dark conductivity, given above. This is because $\sigma = en\mu_D$ for one type of charge carrier, where n is the charge carrier concentration and μ_D is the drift mobility. It is the temperature dependence of n that is responsible for the temperature dependence of σ.

An important feature of band theory for this investigation is the prediction of Hall mobilities.[12,13,14] In particular, if an anthracene crystal is oriented with either its a or c' axis (see Fig. 1.2 for a definition of the c' direction) along the direction of an applied magnetic field, band theory predicts the Hall mobility should have an anomalous sign. That is, charge carriers should be deflected in the "wrong" direction (opposite to the direction determined by the Lorentz force) for these orientations. This effect occurs because the bands are sufficiently narrow for an electron (or hole) to be thermally excited into the top of the conduction band (bottom of the valence band) where it would be in a negative effective mass state. In the presence of a

magnetic field, an electron (or hole) in a negative effective mass state would be deflected in the opposite direction from one in a positive effective mass state. Then, depending on how the contributions from each state are statistically weighted, it is possible, according to band theory, for the Hall effect to be anomalous for electrons and holes.

The hopping model considers electrons to be localized on a particular molecule. In this process, an electron sits on a particular lattice site for a time, corresponding to the relaxation time, before acquiring enough thermal energy from phonons to jump over the molecular potential barrier from one excited state to the other excited state of an adjacent molecule. Hopping models usually predict an increasing drift mobility with increasing temperature.[15] If the electron relaxation time is long compared with the periods of lattice vibrations, the lattice around the electron has time to distort. That is, if the electron-lattice interaction is sufficiently strong, the surrounding lattice particles are displaced to new equilibrium positions providing a deep potential well for the electron. The electron occupies a bound state and is unable to move unless accompanied by the induced lattice deformation. The motion of an electron together with its induced lattice deformation is called polaron motion.[16] Polaron motion results in drift mobilities that increase exponentially with temperature when $T > \frac{1}{2}\theta_{Debye}$.[17] Below this temperature, the motion is described in terms of a polaron

band theory, where the drift mobility is a decreasing function of temperature. Hopping models do not predict an anomalous Hall effect.

The tunneling model considers a π electron excited into an empty level, and tunneling through a potential barrier between one molecule and its neighbor.[18] In this model, the temperature dependence of the drift mobility is obtained from a variation of the potential barrier width as the moleclues undergo lattice vibrations. This model results in drift mobilities that increase exponentially with temperature, and depend on such parameters as barrier height and lattice spacing.[19] A difficulty with this model is that before tunneling occurs, one has an excited molecule next to an unexcited molecule. After tunneling, one has a positive molecular ion next to a negative molecular ion. The Coulomb attraction between the two ions will prevent the electron from traveling on in the crystal, unless it is provided with extra energy.[20] Resolving this difficulty leads one to the band theory described above.

Measurement of the drift mobility and its temperature dependence should distinguish between hopping and band models. Ordinarily, the hopping model is used when $\mu_D \leq 1$ cm^2/V sec and band theory is used when $\mu_D \gtrsim 1$ cm^2/V sec. Measurements performed on anthracene by Kepler[21] and verified for holes in this investigation, are given in Table 1.1. They indicate that the drift mobility is of the order of 1 cm^2/ V sec, and depends on the direction of drift and the type of charge carrier. This value is in the

Table 1.1. The anisotropy of the drift mobility in anthracene, at room temperature.

Drift Direction	μ_D in $cm^2/Vsec$	
	HOLES	ELECTRONS
a	1.0	1.7
b	2.0	1.0
c'	0.8	0.4

The hole drift mobilities are those obtained in this investigation and are the same as the values obtained by Kepler.[21] The electron drift mobilities are those obtained by Kepler.

transition region between a localized, hopping model and a delocalized, band theory, and is thus, equally well described by both.[22] Measurement of the temperature dependence indicates that the drift mobility decreases with increasing temperature.[23] This particular feature is most directly described by band theory. It should be noted that mobilities of the order of 1 cm^2/Vsec. are in accord with the restriction imposed by the uncertainty principle (see above).

As discussed above, the measurement of the Hall effect can distinguish between the use of band theory and the hopping model for the description of charge transport in anthracene. The results of this investigation indicate that band theory must be used to account for the observation of the anomalous Hall effect of holes that was observed.

B. Previous Hall Effect Experiments in Anthracene .

There have been a number of Hall effect measurements in anthracene. They differ from one another and were not taken in all possible orientations of electric and magnetic fields. They are discussed below in chronological order.

Dresner[24] measured the Hall effect of surface carriers in the ab plane and found Hall mobilities of 50 cm^2/Vsec for electrons and 30 cm^2/Vsec for holes. Except for a measurement on a crystal where $\mu_H < 5$ cm^2/Vsec, the sign

of the Hall voltage was not anomalous. The directions in which the measurements were made was not specified. Surface properties are not necessarily the same as bulk properties. Since two carrier effects were found to predominate, the measured Hall voltage could not be directly related to the Hall mobility of either holes or electrons.

Delacote and Schott[25] measured a Hall effect for holes using a pulsed light technique similar to Kepler's pulsed photoconductivity technique for measuring the drift mobility. They generated carriers near the front electrode by a 2 μsec light pulse. They used a rear electrode, that was split in half, to collect the charge carriers that drifted across the crystal. When a magnetic field is applied, the deflection of the charge carriers causes an inbalance in the two collecting currents which is the Hall current. One of the disadvantages of this method is that the Hall current is approximately .1% of the primary current so that the measurement involves the difference of two large quantities. Since Delacote and Schott used plates that were about 2.8mm thick, one may assume that these were cleavage plates so that the current was largely holes in the c' direction. They found for holes, a Hall mobility to drift mobility ratio of -25 ± 10, although the direction of the magnetic field was not specified.

Pethig and Morgan[26] measured the Hall mobility with dark conductivity and report 5.5 cm^2/V sec perpendicular

to the ab plane. The electric field direction was not specified nor was the carrier sign determined. They used the analysis of Dobrovol'skii and Gritsenko,[27] treating anthracene as a semiconductor. Since any current obtained in the dark was due to injection from the electrodes, which were evaporated gold, they did not know which charge carrier (or both) was responsible for their observations. Thus, they could not verify the anomalous Hall effect.

Toombs[14] measured the Hall effect using a split rear electrode technique. The charge carriers were photo-injected holes drifting along the c' direction. The magnetic field was oriented either along the a or b directions. Hall mobilities ranged between 0.2 and 2 cm^2/V sec and were not anomalous in sign. His method, called a low frequency a.c. phase sensitive method, used an a.c. magnetic field and a d.c. electric field. The magnetic field had a low frequency of f cps, and the sample current a frequency of f' cps obtained by chopping the light that generated the charge carriers. The Hall current was detected at the difference frequency of f-f' cps. Two sets of frequencies were used. The first set was f = 9 cps and f' = 12 cps. The second set used f = 60 cps and f' = 48 cps.

Smith[28] used a modification of the Redfield method[29] and has measured Hall mobilities of 0.8 ± 0.3 and 2.5 ± 1.0 cm^2/V sec with the primary current along the a and b directions, respectively, and with the magnetic field perpendicular to the ab plane. He did not observe an

anomalous Hall effect. Since he illuminated the crystal uniformly by using weakly absorbed light, he apparently observed both types of charge carriers simultaneously.

C. Thesis Objectives.

One of the two goals of this investigation was to measure the Hall effect in high purity anthracene crystals in each of six possible combinations of magnetic field and electric field orientations in order to make a complete comparison with the theoretical predictions.

The other goal was to develop an experimental technique for measuring the Hall voltage that may provide the necessary sensitivity for the study of the Hall effect in other organic semiconductors. In the method, used in this work, one type of charge carrier (holes) was photo-injected via a directly illuminated, transparent electrode in contact with one end of an anthracene crystal. The photo-injecting electrode was maintained at a positive bias with respect to ground. The charge carriers drifted across the crystal and were collected at an opaque, collecting electrode, maintained at a negative bias with respect to ground. The crystal was fitted with a guard ring near the directly illuminated electrode, which was masked around the edges so that surface currents were maintained four orders of magnitude below the bulk current. A magnetic field up to 40 kilogauss intensity, generated by a superconducting magnet, and a photocurrent density of 5×10^{-11} A/cm^2

permitted Hall voltages to be measured with vibrating reed electrometers connected to the Hall probes, which were spring-loaded point contacts. This method was limited to the measurement of the Hall effect for holes, however, because the electron current, being smaller, placed their measurement just beyond the limits of sensitivity of the apparatus.

References - Chapter 1

1. K. Hasegawa, Japan J. Appl. Phys. 3, 633 (1964).

2. R. Mason, Acta Cryst. 17, 547 (1964).

3. M. Alonso and E.J. Finn, Fundamental University Physics (Addison-Wesley Publishing Co., Inc., Reading, Mass., 1968), Vol. III, p.211.

4. R.G. Kepler, J.C. Caris, P. Avakian, and E. Abramson, Phys. Rev. Letters 10, 400 (1963).

5. H. Fröhlich and G.L. Sewell, Proc. Phys. Soc. 74, 643 (1959).

6. O.H. LeBlanc Jr., J. Chem. Phys. 35, 1275 (1961).

7. G.D. Thaxton, R.C. Jarnagin, and M. Silver, J. Phys. Chem. 66, 2461 (1962).

8. J.I. Katz, S.A. Rice, S. Choi, and J. Jortner, J. Chem. Phys. 39, 1683 (1963).

9. (a) R. Silbey, J. Jortner, S.A. Rice, and M.T. Vala Jr., J. Chem. Phys. 42, 733 (1965); (b) R. Silbey, J. Jortner, S.A. Rice, and M.T. Vala Jr., J. Chem. Phys. 43, 2925 (1965).

10. R.M. Glaeser and R.S. Berry, J. Chem. Phys. 44, 3797 (1966).

11. H. Chojnacki, Molecular Crystals 3, 375 (1967).

12. O.H. LeBlanc Jr., J. Chem. Phys. 39, 2395 (1963).

13. L. Friedman, Phys. Rev. 133, A1668 (1964).

14. T. Toombs, Ph.D. Thesis, Princeton University (unpublished, 1968).

15. F. Seitz, Modern Theory of Solids (McGraw Hill, New York, 1940), p.547.

16. T. Holstein, Annals of Phys. 8, 325 (1959).

17. L. Friedman and T. Holstein, Annals of Phys. 21, 494 (1963).

18. D.D. Eley and G.D. Parfitt, Trans. Faraday Soc., 51, 1529 (1955).

19. R.H. Tredgold, Proc. Phys. Soc. 80, 807 (1962).

20. J. Kommandeur, Conductivity in D. Fox, M.M. Labes, and A. Weisberger eds., Physics and Chemistry of the Organic Solid State (Interscience Publishers, New York, 1963), Vol. II, 1, p.1.

21. R.G. Kepler, Charge Carrier Mobility and Production in Anthracene in J.J. Brophy and J.W. Buttrey eds., Organic Semiconductors (Macmillan, New York, 1962), p.1.

22. S.H. Glarum, J. Chem. Solids 24, 1577 (1963).

23. D.C. Hoesterey and G.M. Letson, J. Phys. Chem. Solids 24, 1609 (1963).

24. J. Dresner, Phys. Rev. 143, 558 (1966).

25. G. Delacote and M. Schott, Solid State Comm. 4, 177 (1966).

26. R. Pethig and K. Morgan, Nature 214, 266 (1967).

27. V.N. Dobrovol'skii and Yu. I. Gritsenko, Soviet Physics - Solid State 4, 2025 (1963).

28. G.C. Smith, Bull. Amer. Phys. Soc. 14, 370 (1969).

29. A.G. Redfield, Phys. Rev. 94, 526 (1954).

2. The Hall Effect

A. Elementary Theory for One Type of Charge Carrier

It is assumed that only one type of charge carrier is present. Referring to Fig. 2.1, positive charge carriers are deflected towards the negative y direction as a result of the Lorentz force, $\vec{v} \times \vec{B}$. An excess concentration of positive carriers builds up at the V_2 face of the material until an electrostatic field, E_H, is generated which exactly balances the Lorentz force so that:

$$E_H = v_x B_z \qquad 2.1$$

(MKS units are being used). This is an oversimplified analysis where it is assumed that all charge carriers have the same drift velocity, v_x. In the next section, it will be shown how one averages over a distribution of drift velocities, using the Boltzmann **transport equation.** Since the current density is given by:

$$J_x = nev_x, \qquad 2.2$$

where n is the number of positive charge carriers per unit volume, the Hall field, E_H, may be written as:

$$E_H = (1/ne) J_x B_z \qquad 2.3$$

The Hall coefficient, R_H, is usually defined by:

$$E_H \equiv R_H J_x B_z. \qquad 2.4$$

Fig. 2.1. The normal Hall effect for positive charge carriers.

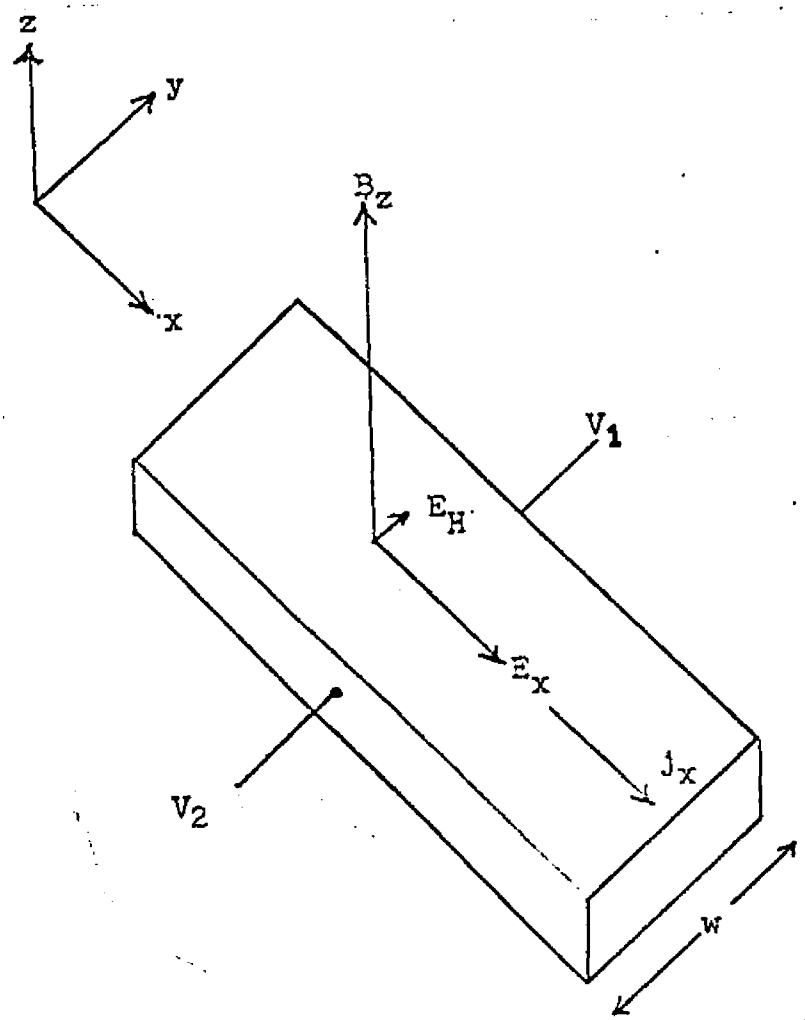

Thus, it is seen that in the simple analysis, the Hall coefficient is inversely proportional to the concentration of charge carriers.

One defines the Hall mobility as:

$$\mu_H \equiv R_H \sigma , \qquad 2.5$$

where σ is the electrical conductivity of the sample given by:

$$\sigma \equiv ne\mu_D, \qquad 2.6$$

where μ_D is the drift mobility. Combining equations 2.5 and 2.6, it is seen that, for this simple analysis, μ_H is equivalent to μ_D. For the general analysis, described in section B, one finds that μ_H and μ_D are not necessarily equivalent.

The Hall field can be obtained from the measurement of the Hall voltage, V_H, given by:

$$V_H \equiv E_H w = V_2 - V_1, \qquad 2.7$$

where w is the sample width, and V_1 and V_2 are potentials of the Hall probes relative to ground potential, as shown in Fig. 2.1. Since $j_x = \sigma E_x$, one obtains by combining equations 2.4, 2.5,2.6 and 2.7:

$$\mu_H = V_H/wE_xB_z. \qquad 2.8$$

Since equations 2.4, 2.5, 2.6, and 2.7 are definitions, they may be used, together with equation 2.8, in the general case described in the following sections.

B. General Theory for One Type of Charge Carrier.

For electrons, the Boltzmann transport equation may be written as:[1]

$$-(f-f_o)/\tau = -e(\vec{E} + \vec{v} \times \vec{B}) \cdot \vec{\nabla}_p f + \vec{v} \cdot \vec{\nabla}_r f. \qquad 2.9$$

$f(\vec{p},\vec{r},t)d\vec{p}d\vec{r}$ represents the number of electrons in the volume element $d\vec{r}$, which, at the instant t, have momenta in the range $d\vec{p}$. f_o represents this distribution in the absence of external fields at thermal equilibrium, i.e. when $\vec{E} = \vec{B} = 0$. f_o is the Fermi-Dirac distribution function given by:

$$f_o = \left[\exp\left[(\mathcal{E}-\mathcal{E}_F)/kT\right] + 1\right]^{-1}. \qquad 2.10$$

The energy scale that is used to measure $\mathcal{E}$ and $\mathcal{E}_F$ is shown in Fig. 2.2. The relaxation time, τ, has the following meaning: when the external fields are removed, $f-f_o$ decays to zero as:

$$(f-f_o)_t = (f-f_o)_{t=0} \exp(-t/\tau). \qquad 2.11$$

For a uniform material at a constant temperature, the distribution function must be the same in every part of the sample so that $\vec{\nabla}_r f$ is zero.

The Boltzmann transport equation is now solved, using a method developed by Jones and Zener.[2] f is written as:

$$f = f_o - \phi(\partial f_o/\partial \mathcal{E}), \qquad 2.12$$

Fig. 2.2. Energy scale for the measurement of $\mathcal{E}$ and $\mathcal{E}_F$ for electrons. The direction of $\mathcal{E}$ is reversed for the case of positive charge carriers, holes.

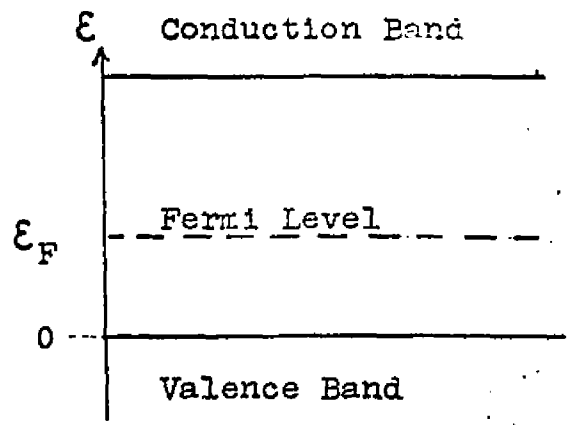

where ϕ is a function to be determined below. Since $\vec{p} = \hbar\vec{k}$ and $\vec{v} = \vec{\nabla}_p \mathcal{E} = (1/\hbar)\vec{\nabla}_k \mathcal{E}$, where $\vec{p}$ is the electron momentum and $\vec{k}$ is the propagation vector associated with the delocalized wave representing the electron, when the gradient of f is taken with respect to $\vec{p}$, using equation 2.12, one obtains:

$$\vec{\nabla}_p f = (1/\hbar)\vec{\nabla}_k f_o - (1/\hbar)(\vec{\nabla}_k \phi)(\partial f_o/\partial \mathcal{E}) - (1/\hbar)\phi.\vec{\nabla}_k(\partial f_o/\partial \mathcal{E})$$

$$\vec{\nabla}_p f = -\vec{v}\left[(\partial f_o/\partial \mathcal{E}) - \phi(\partial^2 f_o/\partial \mathcal{E}^2)\right] - (1/\hbar)(\vec{\nabla}_k \phi)(\partial f_o/\partial \mathcal{E}). \qquad 2.13$$

Thus, since $\mathbf{v} \times \mathbf{v} = 0$, it is seen that:

$$(1/\hbar)(\vec{v} \times \vec{B})\cdot \vec{\nabla}_k f = (1/\hbar)\vec{B}\cdot(\vec{\nabla}_k f \times \vec{v})$$

$$= (1/\hbar)(\partial f_o/\partial \mathcal{E})\vec{B}\cdot(\vec{v} \times \vec{\nabla}_k \phi). \qquad 2.14$$

Choosing the magnetic field, $\vec{B}$, along the $\underline{z}$ direction, equation 2.14 becomes:

$$(1/\hbar)(\vec{v} \times \vec{B})\cdot \vec{\nabla}_k f = (B_z/\hbar^2)(\partial f_o/\partial \mathcal{E})\left[(\partial \mathcal{E}/\partial k_x)(\partial \phi/\partial k_y) - (\partial \mathcal{E}/\partial k_y)(\partial \phi/\partial k_x)\right]$$

$$= (B_z/\hbar^2)(\partial f_o/\partial \mathcal{E})\,\Omega_z \phi, \qquad 2.15$$

where $\vec{\Omega}$ is an operator defined by:

$$\vec{\Omega} = \vec{\nabla}_k \mathcal{E} \times \vec{\nabla}_k . \qquad 2.16$$

Equations 2.12 and 2.15 are substituted into the Boltzmann transport equation, 2.9, in order to obtain an equation for the unknown function $\phi = \phi(k)$. It is assumed that $f-f_o$ is small, i.e. equation 2.12 is assumed to be a first order

expansion of f in terms of the electric field so that terms proportional to E^2 are neglected (see Appendix A). Upon substitution, one obtains a linear first order equation for ϕ:

$$\phi/\tau + (e/\hbar)\vec{E}\cdot\vec{\nabla}_k\mathcal{E} + (e/\hbar^2)B_z\Omega_z\phi = 0, \qquad 2.17$$

where a term proportional to $\vec{E}\phi$ has been neglected. It can be seen that this term is proportional to E^2 when the solution for ϕ is obtained from equation 2.17. The solution for ϕ was first obtained by Jones and Zener. They used an iteration in ascending powers of B and obtained (see Appendix B):

$$\phi = -(e/\hbar)\left[\tau\vec{E}\cdot\vec{\nabla}_k\mathcal{E} - (e/\hbar^2)\tau\vec{B}\cdot\vec{\Omega}(\tau\vec{E}\cdot\vec{\nabla}_k\mathcal{E}) + (e^2/\hbar^4)\tau\vec{B}\cdot\vec{\Omega}\left[\tau\vec{B}\cdot\vec{\Omega}(\tau\vec{E}\cdot\vec{\nabla}_k\mathcal{E})\right] + \ldots\right]. \qquad 2.18$$

The current density, $\vec{j}$, is given by:

$$\vec{j} = -(2e/8\pi^3)\int_{\substack{\text{All k}\\\text{space}}}(f-f_o)\vec{v}\,d\vec{k} = (e/4\pi^3)\int_{\substack{\text{All k}\\\text{space}}}\phi(\partial f_o/\partial\mathcal{E})\vec{v}\,d\vec{k}. \qquad 2.19$$

From equation 2.10, it follows that:

$$-(\partial f_o/\partial\mathcal{E}) = f_o(1-f_o)/kT. \qquad 2.20$$

If the density of electrons in the conduction band is small enough that $f_o \ll 1$, i.e. if the system is non-degenerate so that it may be described by classical Boltzmann statistics, equation 2.20 reduces to:(see appendix):

$$-(\partial f_o/\partial\mathcal{E}) \approx f_o/kT. \qquad 2.21$$

Thus, equation 2.19 becomes:

$$\vec{J} = -(e/4\pi^3)(1/kT)\int_{\substack{\text{All k}\\\text{space}}} \vec{v}\,\phi\, f_o\, d\vec{k}. \qquad 2.22$$

In order to calculate the drift mobility, it is assumed that an electric field, E_x, is along the x direction, and that there is no magnetic field. Then the equation for ϕ reduces to:

$$\phi = -(e/\hbar)\tau E_x(\partial\mathcal{E}/\partial k_x) = -e\tau E_x v_x. \qquad 2.23$$

Substituting equation 2.23 into equation 2.22, one obtains:

$$J_x = +(e^2/4\pi^3)(E_x/kT)\int_{\substack{\text{All k}\\\text{space}}} v_x^2\, f_o\, \tau\, dk. \qquad 2.24a$$

Equation 2.24a can be written as:

$$J_x = (ne^2/kT)E_x\langle\tau v_x^2\rangle, \qquad 2.24b$$

where n is the number of charge carriers (electrons) per unit volume given by:

$$n = (1/4\pi^3)\int_{\substack{\text{All k}\\\text{space}}} f_o\, d\vec{k}, \qquad 2.25a$$

The brackets denote the usual statistical average given by:

$$\langle G\rangle = \frac{\int G\, f_o\, d\vec{k}}{\int f_o\, d\vec{k}}. \qquad 2.25b$$

The limits of integration in equation 2.25b are over all k space. In tensor notation, one has:

$$j_i = \sum_j \sigma_{ij} E_j, \qquad 2.26$$

where the indices i and j correspond to x, y, or z directions. For electrons:

$$j_x = \sigma_{xx} E_x = -ne \mu_x E_x, \qquad 2.27$$

where μ_x is the drift mobility in the x direction. Combining equations 2.24b and 2.27, one obtains:

$$\mu_{\dot{x}} = -(e/kT) \langle \tau v_{\dot{x}}^2 \rangle, \text{(etc. for y and z)} \qquad 2.28$$

for the drift mobility in the $\dot{x}$ direction.

In order to calculate the Hall mobility from the Hall voltage, external fields are chosen such that the electric field is: $\vec{E} = E_x \hat{x} + E_H \hat{y}$; and the magnetic field, B_z, is oriented along the z direction. Then, using equation 2.18, ϕ is:

$$\phi = -(e/\hbar) \tau \left[E_x (\partial \mathcal{E}/\partial k_x) + E_H (\partial \mathcal{E}/\partial k_y) \right]$$
$$+ (e^2/\hbar^3) \tau B_z \Omega_z \tau \left[E_x (\partial \mathcal{E}/\partial k_x) + E_H \partial \mathcal{E}/\partial k_y) \right]. \qquad 2.29$$

Substituting equation 2.29 into equation 2.22, the current density in the y direction is:

$$j_y = (e^2/4\pi^3)(1/kT) \int \tau v_y (E_x v_x + E_H v_y) f_o \, \vec{dk}$$
$$-(e^3/4\pi^3\hbar^2)(B_z/kT) \int \tau v_y \Omega_z \left[\tau (E_x v_x + E_H v_y) \right] f_o \, \vec{dk}, \qquad 2.30$$

where the integration limits are over all k space.

From equation 2.26, j_y can be expressed as:

$$j_y = \sigma_{yx}E_x + \sigma_{yy}E_y = \sigma_{yx}E_x + \sigma_{yy}E_H . \qquad 2.31$$

For the steady state, j_y must be zero, so that:

$$\frac{E_H}{E_x} = \frac{-\sigma_{yx}}{\sigma_{yy}} = \frac{(e/\hbar^2)B_z \langle \tau v_y \Omega_z(\tau v_x)\rangle - \langle \tau v_x v_y\rangle}{\langle \tau v_y^2\rangle - (e/\hbar^2)B_z \langle \tau v_y \Omega_z(\tau v_y)\rangle}, \qquad 2.32$$

where equation 2.30 has been modified by equation 2.25b and then combined with equation 2.31. $\langle \tau v_x v_y\rangle$ must be small because $j_y \approx$ zero in the absence of a magnetic field. $(e/\hbar^2)B_z \langle \tau v_y \Omega_z(\tau v_y)\rangle$ is a magneto-resistance term. Frankevich and Sokolik[3] have measured a variation in the photocurrent as large as 8% when anthracene crystals were placed in a magnetic field of 3 kilogauss. However, this Frankevich effect occurs when charge carriers are photo-injected by a light intensity of 10^{18} quanta/cm^{2}sec or greater. For lower light intensities the Frankevich effect cannot be measured. Since this is the only variation of a longitudinal current with magnetic field that has been reported, it is reasonable to assume that magneto-resistance effects are negligible in anthracene. Therefore, the second term in the numerator and denomiator of equation 2.32 may be neglected. From equations 2.4, 2.5, and 2.7, the Hall mobility is:

$$\mu_H = \sigma_{xx}R_H = E_H/E_xB_z. \qquad 2.33$$

Therefore, substituting equation 2.32 into 2.33, one obtains (with the negelct of the two small terms):

$$\mu_H = \frac{(e/\hbar^2)\langle \tau v_y \Omega_z (\tau v_x)\rangle}{\langle \tau v_y^2 \rangle} \qquad 2.34$$

Combining equations 2.30 and 2.31, and using equations 2.25a and 2.25b, one finds that σ_{yx} is:

$$\sigma_{yx}(B_z) = -(ne^3 B_z/\hbar^2 kT)\langle \tau v_y \Omega_z (\tau v_x)\rangle , \qquad 2.35$$

where $\langle \tau v_x v_y \rangle$ has been neglected. Expanding the operator, Ω_z, as defined by equation 2.16, one finds that:

$$\langle \tau v_y \Omega_z (\tau v_x)\rangle = \hbar^2 \langle \tau^2 (v_y v_x M_{yx}^{-1} - v_y^2 M_{xx}^{-1})\rangle + \langle \tau v_y v_x \Omega_z \tau \rangle , \qquad 2.36$$

where M_{ij}^{-1} is the symmetric, effective mass tensor, defined as:

$$M_{ij}^{-1} = (1/\hbar^2)(\partial^2 \mathcal{E}/\partial k_i \partial k_j). \qquad 2.37$$

The two simplified models one usually considers are: (1) constant relaxation time (τ is a constant); and (2) constant mean free path ($\tau = \tau(\vec{k})$ which is inversly proportional to $|\vec{v}(\vec{k})|$. When one assumes model (1), a constant relaxation time, equations 2.28, 2.34, and 2.36 may be combined to obtain the following expression for the ratio of the Hall mobility, μ_H, to the drift mobility, μ_D:

$$\frac{\mu_H}{\mu_D} = \frac{kT\langle v_y^2 M_{xx}^{-1} - v_y v_x M_{yx}^{-1}\rangle}{\langle v_x^2\rangle\langle v_y^2\rangle} \cdot \qquad 2.38$$

μ_D is due to carriers drifting in the x direction. If model (2), a constant mean free path, is assumed, one must consider the second term on the right side of equation 2.36. Expanding the operator, Ω_z, in this term, one obtains:

$$\hbar\langle \tau v_y v_x [v_x(\partial\tau/\partial k_y) - v_y(\partial\tau/\partial k_x)]\rangle$$

$$= \hbar\langle [\partial(\tfrac{1}{2}\tau^2 v_y v_x^2)/\partial k_y - \tfrac{1}{2}\tau^2\partial(v_y v_x^2)/\partial k_y - \partial(\tfrac{1}{2}\tau^2 v_y^2 v_x)/\partial k_x$$

$$+ \tfrac{1}{2}\tau^2\partial(v_y^2 v_x)/\partial k_x]\rangle$$

$$= +\hbar^2\langle \tfrac{1}{2}\tau^2(2v_x v_y M_{xy}^{-1} + v_y^2 M_{xx}^{-1} - 2v_y v_x M_{yx}^{-1} - v_x^2 M_{yy}^{-1})\rangle$$

$$+ \hbar\langle [\partial(\tfrac{1}{2}\tau^2 v_y v_x^2)/\partial k_y - \partial(\tfrac{1}{2}\tau^2 v_y^2 v_x)/\partial k_x]\rangle. \qquad 2.39$$

The second term, on the right side of the last expression in equation 2.39, is expanded using equations 2.25a and 2.25b. Then, using Green's theorem, one obtains:

$$\hbar\langle \partial(\tfrac{1}{2}\tau^2 v_y v_x^2)/\partial k_y - \partial(\tfrac{1}{2}\tau^2 v_y^2 v_x)/\partial k_x\rangle$$

$$= (\hbar/4\pi^3 n)\int_{\substack{\text{closed}\\ S\to\infty}} f_o \tfrac{1}{2}\tau^2(v_y v_x^2 - v_y^2 v_x)\, dS$$

$$-(\hbar/4\pi^3 n)\int_{\substack{\text{All k}\\ \text{space}}} \tfrac{1}{2}\tau^2 [v_y v_x^2(\partial f_o/\partial k_y) - v_y^2 v_x(\partial f_o/\partial k_x)]\, d\vec{k}. \qquad 2.40$$

The surface integral in equation 2.40 is zero because the integrand is an odd function of k, i.e. it is assumed that $\tau(k) = \tau(-k)$. Since $f_o = f_o(\mathcal{E})$,

$$\partial f_o/\partial k_i = \hbar v_i(\partial f_o/\partial \mathcal{E}). \qquad 2.41$$

Therefore, the volume integral in equation 2.40 is also zero. Thus, equation 2.36 has been reduced to:

$$\langle \tau v_y \Omega_z(\tau v_x)\rangle = \tfrac{1}{2}\hbar^2\langle \tau^2(2v_y v_x M_{yx}^{-1} - 2v_y^2 M_{xx}^{-1} + 2v_x v_y M_{xy}^{-1} + v_y^2 M_{xx}^{-1} - 2v_y v_x M_{yx}^{-1} - v_x^2 M_{yy})\rangle. \qquad 2.42$$

Thus, for constant mean free path, μ_H/μ_D is obtained from equations 2.28, 2.34, and 2.42 as:

$$\frac{\mu_H}{\mu_D} = \frac{\tfrac{1}{2}kT\langle \tau^2(v_x^2 M_{yy}^{-1} - 2v_x v_y M_{xy}^{-1} + v_y^2 M_{xx}^{-1})\rangle}{\langle \tau v_x^2\rangle\langle \tau v_y^2\rangle}. \qquad 2.43$$

Onsager's relation is:

$$\sigma_{yx}(B_z) = \sigma_{xy}(-B_z). \qquad 2.44$$

Thus, with equations 2.35, 2.42, and 2.44, equation 2.43 becomes:

$$\frac{\mu_H}{\mu_D} = \frac{kT\langle \tau^2(v_y^2 M_{xx}^{-1} - v_y v_x M_{yx}^{-1})\rangle}{\langle \tau v_x^2\rangle\langle \tau v_y^2\rangle}. \qquad 2.45$$

If instead of a Hall voltage, one desires to measure a Hall current, j_H, then E_H is zero and $j_y = j_H$. The Hall mobility may then be expressed as:

$$\mu_H = j_H/j_x B_z. \qquad 2.46$$

One then obtains an equation, similar to equation 2.32, for j_H/j_x which is:

$$\frac{j_H}{j_x} = \frac{E_x\left[-(e/\hbar^2)B_z \langle \tau v_y \Omega_z \tau v_x \rangle + \langle \tau v_x v_y \rangle\right]}{E_x\left[\langle \tau v_x^2 \rangle - (e/\hbar^2)B_z \langle \tau v_x \Omega_z \tau v_x \rangle\right]} . \qquad 2.47$$

Carrying through the above analysis, one then obtains:

$$\frac{\mu_H}{\mu_D} = \frac{-kT\langle \tau^2 (v_y^2 M_{xx}^{-1} - v_y v_x M_{yx}^{-1}) \rangle}{\langle \tau v_x^2 \rangle \langle \tau v_x^2 \rangle} . \qquad 2.48$$

It is seen that, for an anisotropic material such as anthracene, μ_H/μ_D as calculated from a Hall voltage is not equal to μ_H/μ_D calculated from a Hall Current.

The above equations for μ_H/μ_D can be applied to positive charge carriers, holes, if e is changed to -e and the energy, $\mathcal{E}$, is changed to $-\mathcal{E}$.

C. Computation of the Hall Mobility from the Measured Hall Voltage.

A coordinate system, x,y,z, shown in Fig. 2.3, is chosen such that the photocurrent and the primary electric field, E_x, are along the x direction, the Hall voltage is measured along the y direction, and the magnetic field, B_z, is along the z direction. The sample is located in the region: $-\frac{1}{2}\ell \leq x \leq +\frac{1}{2}\ell$, $-\frac{1}{2}w \leq y \leq +\frac{1}{2}w$, and $-\frac{1}{2}t \leq z \leq +\frac{1}{2}t$. The directly illuminated, hole-injecting electrode, located at $x = -\frac{1}{2}$, $-\frac{1}{2}w \leq y \leq +\frac{1}{2}w$, $-\frac{1}{2}t \leq z \leq +\frac{1}{2}t$, is at a positive bias, V_L, with respect to ground. The collecting electrode, located at $x = +\frac{1}{2}$, $-\frac{1}{2}w \leq y \leq +\frac{1}{2}w$, $-\frac{1}{2}t \leq z \leq +\frac{1}{2}t$, is at a negative bias, V_D, with respect to ground. ℓ, w, and t are the sample dimensions along the x, y, and z directions respectively. V_M is the voltage measured at one of the Hall probes with respect to ground. As a result of the finite dimensions of the sample and space charge effects, V_H, given by equation 2.8 is not equal to $2V_M$. Since the observed photocurrent density varied as the square of the applied voltage, V_L+V_D, ohmic conditions were not satisfied and it was necessary to consider space charge effects. Thus, E_x was not equal to E_o, where E_o is given by:

$$E_o = (V_L+V_D)/\ell \,. \qquad 2.49$$

(1) Calculation of the Primary Electric Field Distributiion.

For convenience, an x',y,z coordinate system

Fig. 2.3. Orientation of a sample relative to the x,y,z coordinate system used to measure the Hall voltage.

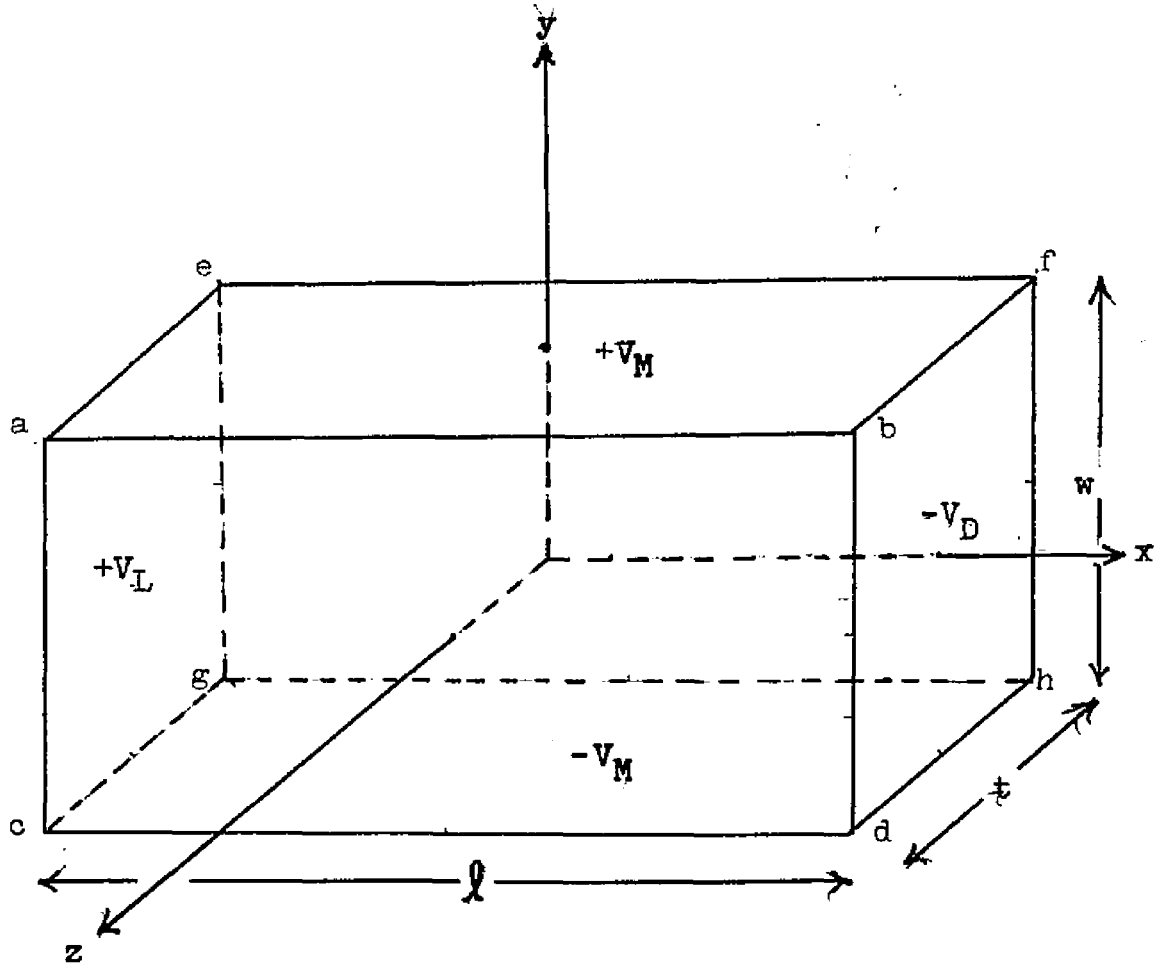

The Hall probes are located at the centers of faces abcd and efgh.

is chosen so that:

$$x' = x + \tfrac{1}{2}\ell \ . \qquad 2.50$$

Assuming that the sample is homogeneous, one may consider that $E_x = E_x(x')$, with the conditions that $V_x(x'=0) = +V_L$ and $V_x(x'=+\ell) = -V_D$. Since j_x is proportional to V_x^2, one may assume **Child's law for solids holds for the electric field** distribution[4,5] so that:

$$E_x = K\, x'^{\frac{1}{2}} \ . \qquad 2.51$$

Integrating equation 2.51 and applying the boundary conditions, mentioned above, one obtains:

$$-(V_L+V_D) = -\int_0^{\ell} K\, x'^{\frac{1}{2}}\, dx' = -(2/3)K\, \ell^{3/2},$$

or
$$K = (3/2)(V_L+V_D)\ell^{-3/2}. \qquad 2.52$$

Substituting equation 2.52 into equation 2.51 leads to the following expression for the electric field distribution:

$$E_x(x') = (3/2)(x'/\ell)^{\frac{1}{2}}(V_L+V_D)/\ell = E_x(x). \qquad 2.53$$

The potential distribution is obtained by integrating equation 2.53 from zero to x'. One obtains:

$$V_x(x') = V_L - \int_0^{x'} Kx'^{\frac{1}{2}}\, dx' = V_L - (2/3)K\, x'^{3/2}$$

or
$$V_x(x') + V_D = (V_L+V_D)\left[1 - (x'/\ell)^{3/2}\right] = V_x(x). \qquad 2.54$$

If one arbitrarily adjusts V_L and V_D so that the Hall probe potential, $V_x(x_o')$, is zero, x_o'/ℓ may be obtained

FIG. 2.4. THE ELECTRIC FIELD DISTRIBUTION, $E_x(x)$, AS GIVEN BY EQUATIONS 2.50 AND 2.53. E_x IS MEASURED IN UNITS OF $(3/2)(V_L + V_D)/\ell$, AND x IS MEASURED IN UNITS OF ℓ.

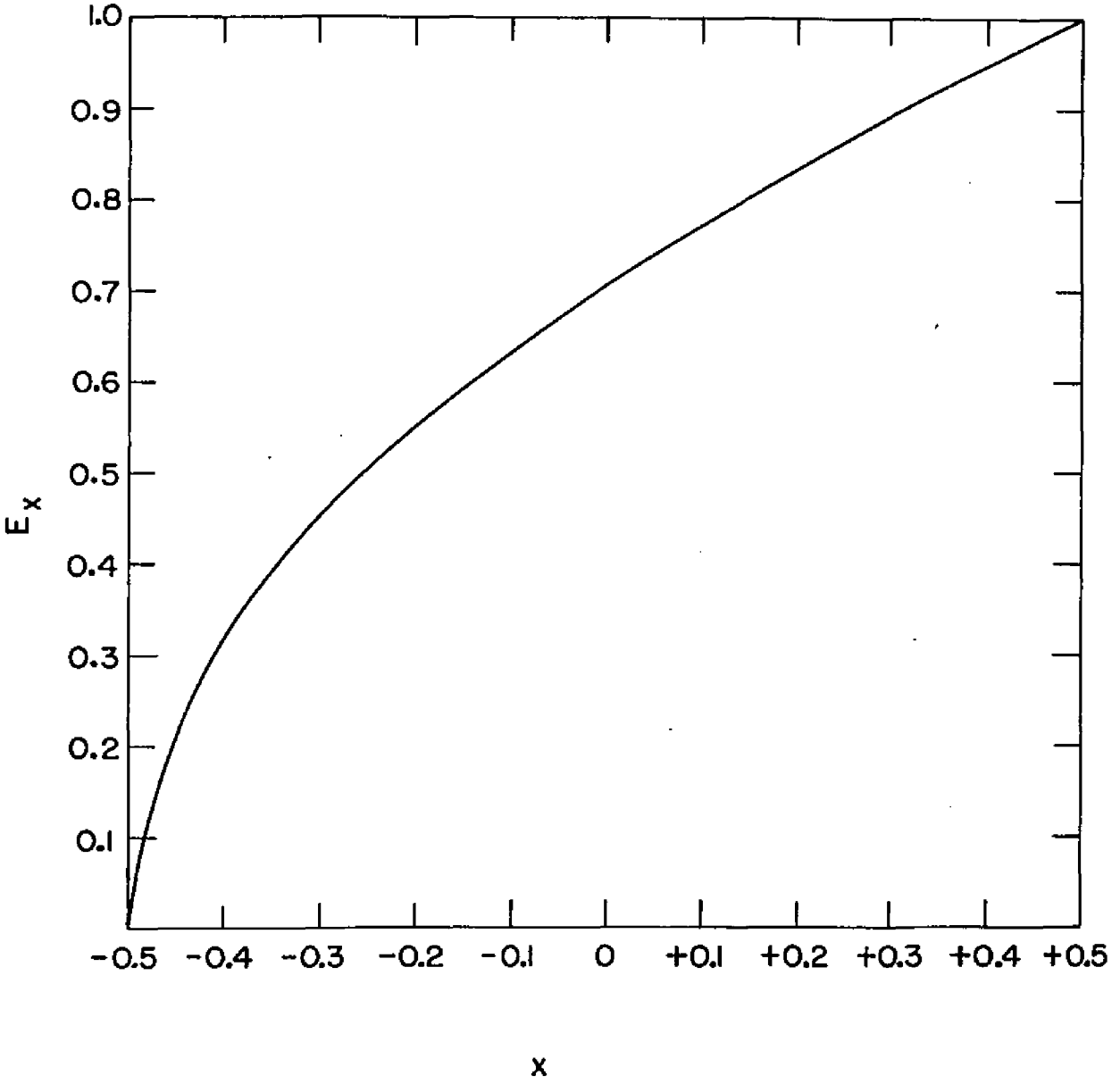

FIG. 2.5. THE POTENTIAL DISTRIBUTION, $V_x(x)$, AS GIVEN BY EQUATIONS 2.50 AND 2.54. $V_x + V_D$, MEASURED IN UNITS OF $V_L + V_D$, IS PLOTTED AGAINST x, MEASURED IN UNITS OF ℓ.

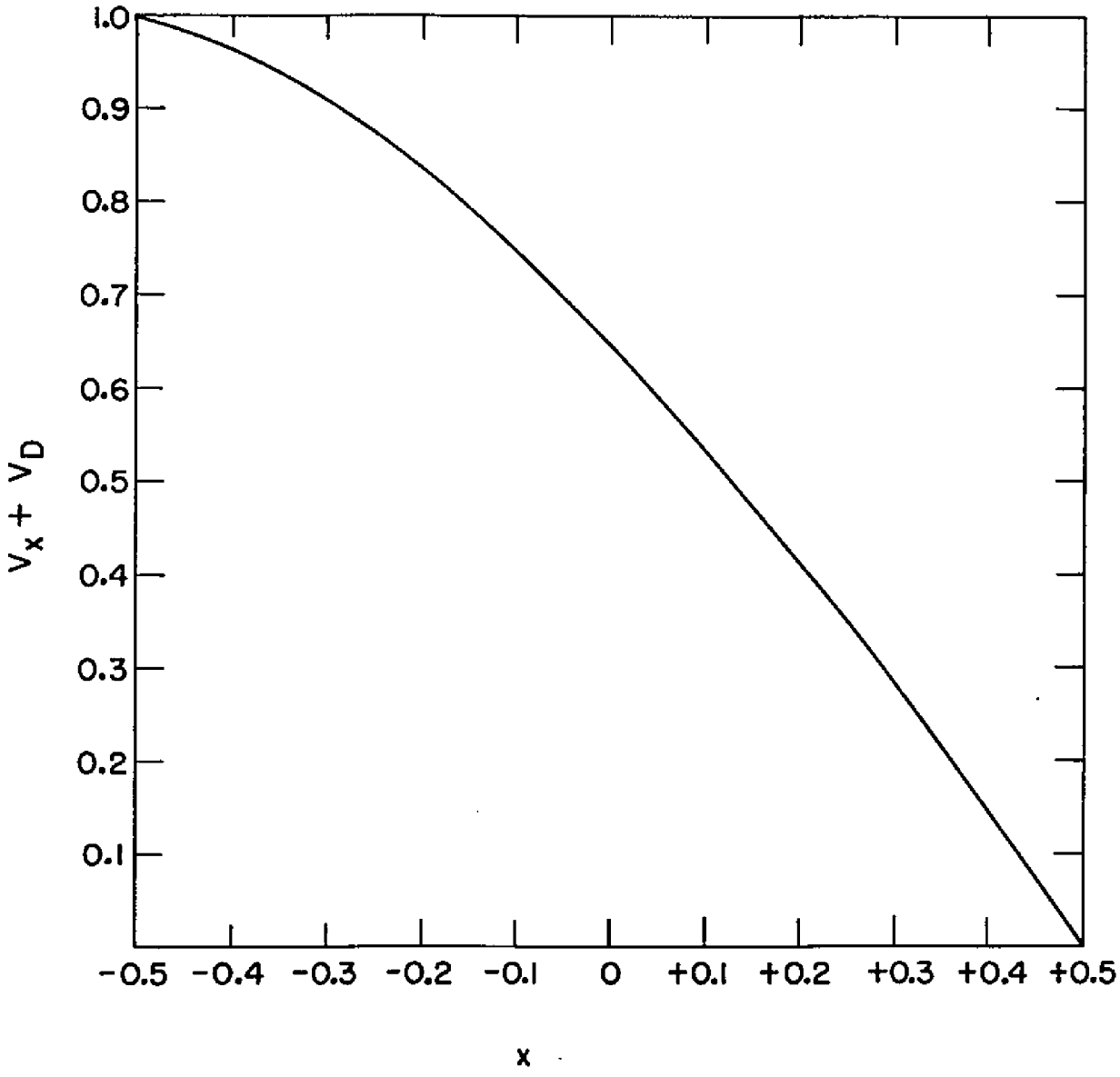

FIG. 2.6. THE CHARGE DENSITY DISTRIBUTION, $n(x) \cdot n(x)$, IN ARBITRARY UNITS PROPORTIONAL TO dE_x/dx, IS PLOTTED AGAINST x, MEASURED IN UNITS OF ℓ.

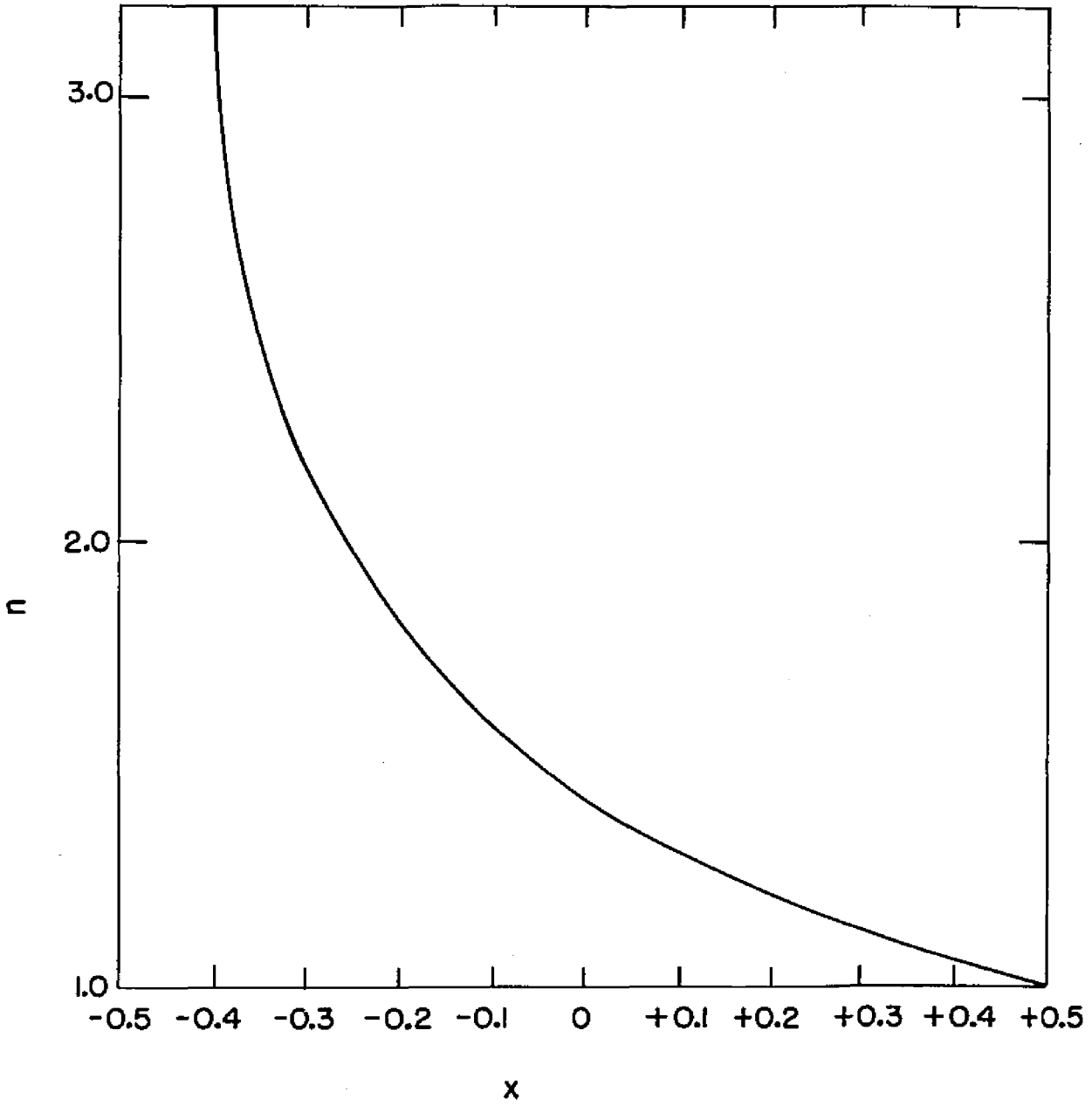

from equation 2.54. The result is:

$$x_o'/\ell^{3/2} = V_L/(V_L+V_D) = (x+\tfrac{1}{2}\ell)/\ell^{3/2} , \qquad 2.55$$

for $V_x(x_o') = 0$. Substituting equation 2.55 into equation 2.53, one obtains:

$$E_x(x_o) = (3/2)V_L^{1/3}(V_L+V_D)^{2/3}\ell^{-1} , \qquad 2.56$$

for $V_x(x_o) = 0$. The electric field and potential distributions are shown in Figs. 2.4 and 2.5 respectively. They are plotted as functions of x in arbitrary units. The charge density distribution, n(x), which is proportional to dE_x/dx, is shown in Fig. 2.6.

(2) Calculation of V_H from V_M.

It is convenient to write:

$$V_H = 2V_M/GS, \qquad 2.57$$

where G is a geometrical factor due to the finite dimensions of the sample, and S is a factor due to space charge effects.

(a) Evaluation of G.

The case where space charge effects are neglected is considered first. This is defined as S = 1. Here, $E_y \neq E_H$, where $E_H = V_H/w$, because of the finite dimensions of the sample. That is, when $\ell \lesssim w$, Fig. 2.3, the short circuiting effect of the current electrodes cannot be neglected. It is assumed that $\vec{E}_y = \vec{E}_y(x,y)$ for a sample with uniform thickness, t.

It is assumed that $\vec{E}_y$ has a **charge distribution** (neglecting the z direction) as its source, located at $y = \pm\frac{1}{2}w$ for $-\frac{1}{2}\ell \leq x \leq +\frac{1}{2}\ell$ (see Fig. 2.3). Therefore, $\vec{\nabla} \times \vec{E}_y = \vec{\nabla} \cdot \vec{E}_y = 0$ in the interior of the sample. Thus, one may write:

$$\vec{E}_y(x,y) = -\vec{\nabla} V_y(x,y), \qquad 2.58a$$

$$\nabla^2 V_y = 0. \qquad 2.58b$$

V_y must satisfy the following boundary conditions:

$$V_y(x, \pm\tfrac{1}{2}w) = \pm V_M, \quad (-\tfrac{1}{2}\ell \leq x \leq +\tfrac{1}{2}\ell), \qquad 2.59a$$

and $$V_y(\pm\ell, y) = 0. \qquad 2.59b$$

A solution to this problem has been obtained by Isenberg, Russell, and Green:[5]

$$V_y(x,y) = (4\ell V_H/\pi^2 w) \sum_{n=0}^{\infty} \frac{(-1)^n \sinh\left[(2n+1)\pi y/\ell\right] \cos\left[(2n+1)\pi x/l\right]}{(2n+1)^2 \cosh\left[(2n+1)\pi w/2\ell\right]} \qquad 2.60$$

Since $2V_M = V_y(x,\frac{1}{2}w) - V_y(x,-\frac{1}{2}w)$, and $\sinh(X) = -\sinh(X)$, one obtains:

$$G = (8/\pi^2)(\ell/w) \sum_{n=0}^{\infty} \frac{(-1)^n \tanh\left[(2n+1)\pi w/2\ell\right] \cos\left[(2n+1)\pi x/\ell\right]}{(2n+1)^2}. \qquad 2.61$$

$G\left[(x/\ell),(\ell/w)\right]$ is shown plotted against ℓ/w in Fig. 2.7 for $x/\ell = 0$.

FIG. 2.7. THE GEOMETRICAL FACTOR, $G[(x/\ell), (\ell/w)]$, AS GIVEN BY EQUATION 2.61, IS PLOTTED AGAINST ℓ/w FOR $x/\ell = 0$

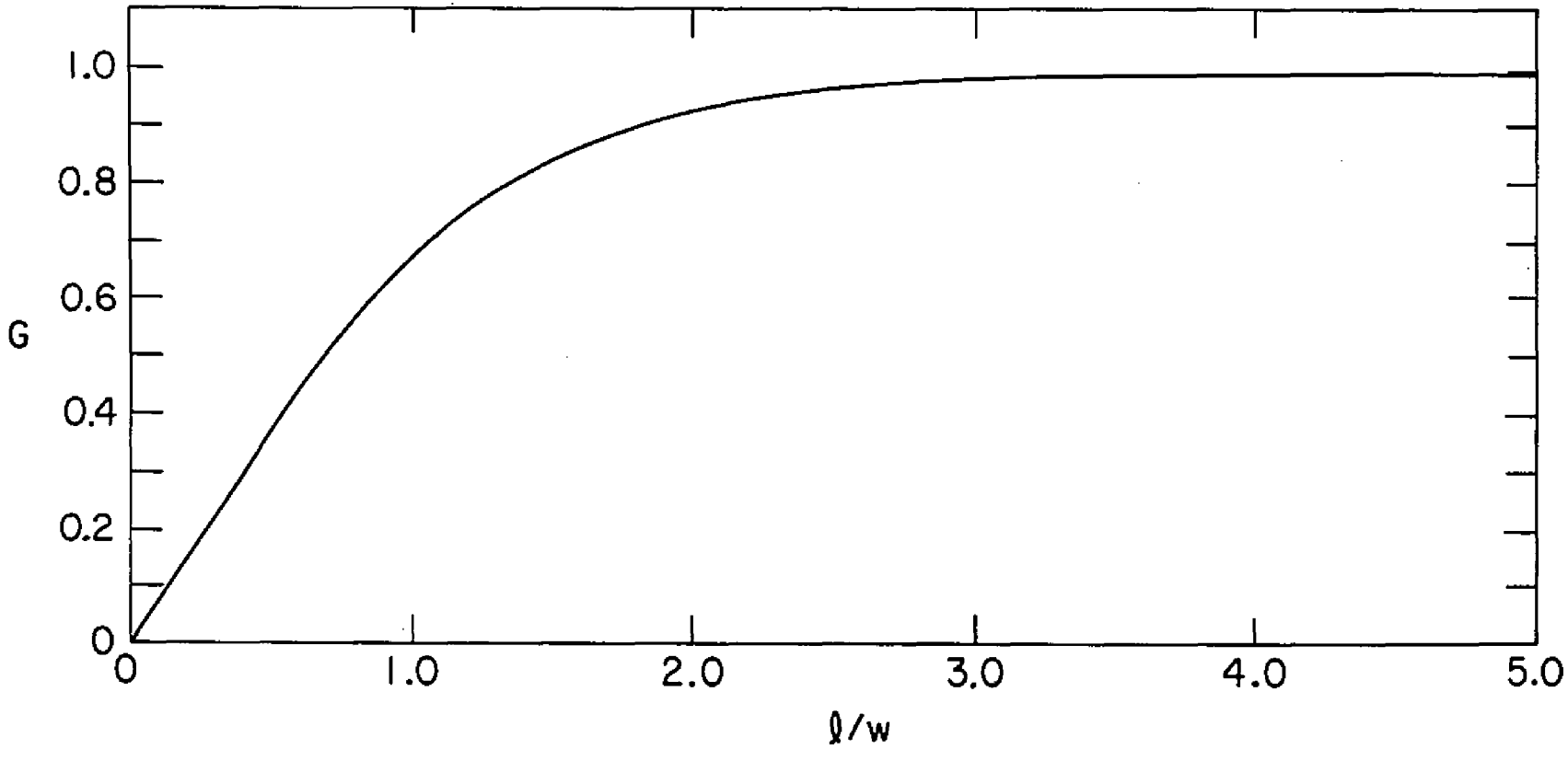

(b) Evaluation of S

One considers the particular yz plane defined by:

$$x/\ell = \left[V_L/(V_L+V_D)^{2/3}\right] - 0.5 \quad . \qquad 2.62$$

Equation 2.62 is obtained by combining equations 2.50 and 2.55. It is assumed that in this plane the density of positive charge carriers, n, is only a function of y. Then, for the steady state, one has:

$$j_y = e\mu_y E_y n + e\mu_y \mu_H E_x B_z n - eD(dn/dy) = 0, \qquad 2.63$$

where μ_y is the drift mobility along the y direction, μ_H is the Hall mobility as given by equation 2.8, and D is the diffusion constant for holes. Solving for dn/dy, one obtains:

$$dn/dy = (\mu_y n/D)(E_y + \mu_H E_x B_z). \qquad 2.64$$

With $E_y = -dV_y/dy$, equation 2.64 may be integrated to:

$$\ln(n/n_o) = -(\mu_y/D)V_y + (\mu_y \mu_H E_x B_z/D)y, \qquad 2.65$$

where $n_o = n(0)$ is the equilibrium value of the hole concentration, i.e. the value without an applied magnetic field. Since one has:

$$dE_y/dy = (e/\epsilon_y \epsilon_o)(n - n_o), \qquad 2.66$$

where ϵ_y is the dielectric constant in the y direction for an anisotropic material, and ϵ_o is the vacuum

permittivity. One now obtains the following equation for V_y from equations 2.65 and 2.66:

$$-d^2V_y/dy^2 = (e/\epsilon_y\epsilon_o)n_o\left[\exp\left[-(\mu_y/D)V_y + (\mu_y\mu_H E_x B_z/D)y\right] - 1\right]. \qquad 2.67$$

The boundary conditions for equation 2.67 are **assumed to be:**

$$V_y(0) = 0 \qquad 2.68a$$

and $$(dV_y/dy)_{y=\pm\frac{1}{2}W} = 0 \text{ (see Appendix C).} \qquad 2.68b$$

Equation 2.68a and $n_o = n(0)$, follow from symmetry considerations and from the assumption that the total space charge **has** a distribution, over the yz cross section being considered, that may be described by:

$$\int_{-\frac{1}{2}W}^{+\frac{1}{2}W}(n - n_o)\,dy = 0. \qquad 2.69$$

Equation 2.69 is justified by the principle of detailed balance applied to the generation and recombination of charge carriers for steady state conditions, i.e. for thermal equilibrium conditions. Equation 2.68b involves the neglect of edge effects due to the finite extension of the sample in the x and z directions. The solution to equation 2.67 was obtained by Banbury, Henisch, and Many[7] by defining the function, U(y), as:

$$U(y) = -(\mu_y/D)V_y + (\mu_y\mu_H E_x B_z/D)y = -AV_y + By. \qquad 2.70$$

Substitution of equation 2.70 into equation 2.67, leads to the following differential equation for U:

$$d^2U/dy^2 = (e/\epsilon_y\epsilon_o)n_oA \exp(U) - 1 \quad . \qquad 2.71$$

In general, it is seen that $U \ll 1$. ($U = 0$ in the conventional treatment of the Hall effect.) Thus, one may expand the term on the right side of equation 2.71 as:

$$\exp(U) - 1 \approx U + \tfrac{1}{2}U^2 + \ldots\ldots \quad . \qquad 2.72$$

With this expansion, equation 2.71 becomes:

$$d^2U/dy^2 \approx (e/\epsilon_y\epsilon_o)n_oA\ddot{U} \quad . \qquad 2.73$$

The solution to equation 2.73 is:

$$-AV_y + By = \alpha \sinh(y/L), \qquad 2.74$$

where L is similar to the Debye-Hückel length, referred to in Shockley's theory of p-n junctions.[8] L is given by:

$$L^2 = (\epsilon_y\epsilon_o D/en_o\mu_y) = (\epsilon_y\epsilon_o kT/e^2n_o), \qquad 2.75$$

where the Einstein relation[9] was used to obtain the last term. α may be obtained from differentiating equation 2.74 and substitution into equation 2.68b. One obtains:

$$\alpha = \frac{BL}{\cosh(\frac{1}{2}w/L)} \quad . \qquad 2.76$$

Substitution of equation 2.76 and A and B, as defined in

equation 2.70, into equation 2.74 leads to:

$$V_y = (B/A)\left[y - L\,\frac{\sinh(y/L)}{\cosh(\frac{1}{2}w/L)}\right] = V_H\left[(y/w) - (L/w)\,\frac{\sinh(y/L)}{\cosh(\frac{1}{2}w/L)}\right]. \qquad 2.77$$

Since $2V_M = V_y(+\frac{1}{2}w) - V_y(-\frac{1}{2}w)$, it is seen that:

$$S = 1 - (2L/w)\tanh(w/2L). \qquad 2.78$$

S is plotted as a function of 2L/w in Fig. 2.8. The expression for L (equation 2.75) may be modified by use of the following expression for the charge density n_o:

$$en_o = j_x/\mu_x E_x = (I_x/wt)(1/\mu_x E_x), \qquad 2.79$$

where I_x is the photocurrent of the photo-injected charge carriers. Thus, equation 2.75 becomes:

$$L = \left[\epsilon_y \epsilon_o (kT/e)(2t/\eta)(\mu_x/I_x)\right]^{\frac{1}{2}}, \qquad 2.80$$

where η is inversely proportional to E_x (E_x is given by 2.56) and is:

$$\eta = 2/wE_x = (4/3)(\ell/w)V_L^{-1/3}(V_L+V_D)^{-2/3}. \qquad 2.81$$

(3) μ_H from V_M

From equations 2.8, 2.57, and 2.81, one has:

$$\mu_H = (\eta/GS)(V_M/B_z). \qquad 2.82$$

FIG. 2.8. THE SPACE CHARGE FACTOR, S(2L/w), AS GIVEN BY EQUATION 2.78, IS PLOTTED AGAINST 2L/w.

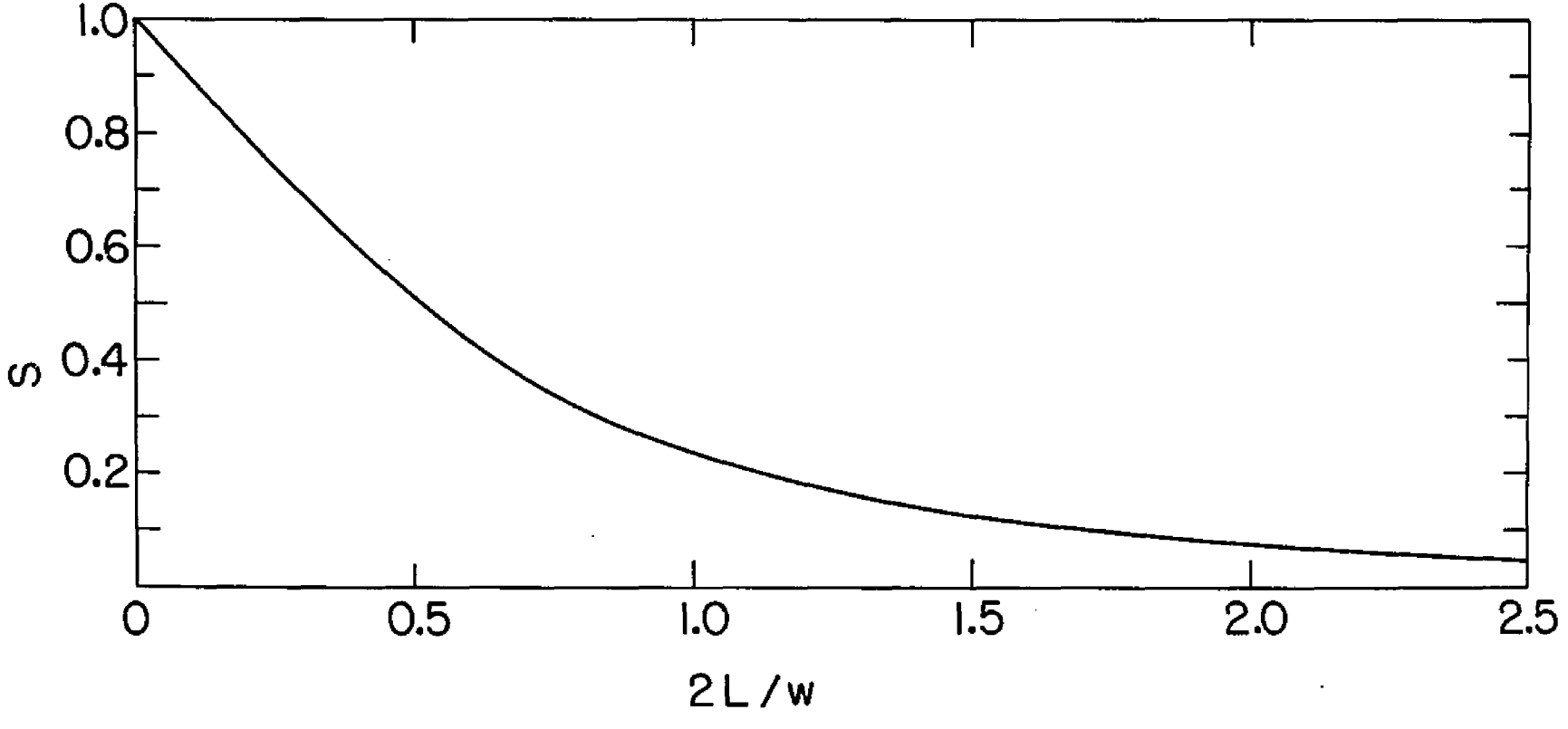

Since one Vsec/cm^2 is equivalent to 10^5 kilogauss, if μ_H is to be expressed in cm^2/Vsec, V_M in mV, B_Z in kilogauss, and η in V^{-1}, equation 2.82 must be written as:

$$\mu_H = (100\eta/GS)(V_M/B_Z). \qquad 2.83$$

From equations 2.78, 2.80, and 2.81 it can be seen that S is a function of the primary current, I_x. Therefore, one can conlude, from equation 2.83, that V_M is a function of I_x. The experimental results, presented in chapter 5, are consistent with this functional dependence of V_M on I_x.

References - Chapter 2

1. A.J. Dekker, Solid State Physics (Prentice Hall Inc., Englewood Cliffs, N.J., 1965), p.278.

2. H. Jones and C. Zener, Proc. Roy. Soc. 145A, 268 (1934).

3. E.L. Frankevich and I.A. Sokolik, Soviet Physics - Solid State 25, 790 (1967).

4. W. Helfrich, Space-charge-limited and volume controlled currents in organic solids in D. Fox, M.M. Labes, and A. Weisberger eds., Physics and Chemistry of the Organic Solid State (Interscience, New York, 1967), Vol. III, 1, p.1.

5. W. Helfrich, Phys. Stat. Sol. 7, 863 (1964).

6. I. Isenberg, B.R. Russell, and R.F. Green, Rev. Sci. Inst. 19, 685 (1948).

7. P.C. Banbury, H.K. Henisch and A. Many, Proc. Phys. Soc. 66A, 753 (1953).

8. W. Shockley, Bell System Tech. J. 28, 435 (1949).

9. Reference 1, p. 342.

3. Calculation of the Hall Mobility from the Energy Band Structure of Anthracene.

A. The Energy Band Structure of Anthracene

The energy band structure of crystalline anthracene was first calculated by LeBlanc[1], using linear combinations of single Slater carbon atomic orbitals (in the Hückel approximation) as basis functions in the tight binding approximation. LeBlanc's calculations led to bandwidths, W, such that $W < kT$, at room temperature. Thaxton et. al.[2] extended LeBlanc's calculations to other aromatic hydrocarbons. In addition, they corrected an error, made by LeBlanc, in the tight binding calculation for anthracene. Katz et. al.[3] employed self-consistent-field atomic orbitals in the linear combination of atomic orbitals scheme. These give a better description of the molecular wavefunctions in the region of configuration space which make the dominant contribution to the intermolecular overlap.[3] Katz et. al. obtained bandwidths such that $W \gtrsim kT$, at room temperature. Silbey et. al.[4] made calculations taking into account the additional degrees of freedom associated with intramolecular vibrations. Their results led to bandwidths of the same order as those obtained by LeBlanc and Thaxton et. al. Glaeser and Berry[5] used the results of Katz et. al. and Silbey et. al. to estimate the effects of electronic polarization.

Anthracene forms a base centered, monoclinic molecular crystal with two molecules per unit cell, located at (0,0,0) and ($\frac{1}{2}$a,$\frac{1}{2}$b,0) (see Fig.3.1). Since there are two molecules per unit cell in the crystal lattice, there are two bands for electrons and two bands for holes, arising from the symmetric and antisymmetric combinations of molecular wavefunctions in a unit cell. LeBlanc incorrectly assumed that the anthracene crystal lattice could be related to a hypothetical lattice with one molecule in a cell.

Katz et. al. used

$$\Psi_{\pm}(\vec{k},\vec{r}) = \sum_{\ell=0}^{2N-1} (\pm 1)^{h_\ell} \exp(i\vec{k}\cdot\vec{r}_\ell)\ \phi(\vec{r}-\vec{r}_\ell) \qquad 3.1$$

as one-electron, unnormalized, crystal wavefunctions, constructed from linear combinations of one-electron molecular wavefunctions, ϕ. LeBlanc and Thaxton et. al. used only the symmetric function, Ψ_+ in their calculations. The index h_ℓ labels the molecules of the unit cells so that the molecule at the corner of each cell has an even index while the one at the center of each cell has an odd index. $\vec{r}_\ell$ is the vector to the center of each molecule and N is the number of unit cells (one half the number of molecules). The Hamiltonian for an excess electron or hole has the form

$$H = -(\hbar^2/2m)\nabla^2 + V(\vec{r}) \qquad 3.2$$

where $V(\vec{r})$ determines the crystal field and was approximated

by

$$V(\vec{r}) = \sum_n V_n(\vec{r}-\vec{r}_n), \qquad 3.3$$

where V_n is the Hartree potential of an isolated neutral molecule for electrons, or the positive ion-molecule potential for holes. For an excess electron, the potential energy of a molecule was taken as a linear combination of neutral carbon atom potentials. V_n was obtained by averaging over the four 2s, $2p_x$, $2p_y$, and $2p_z$ electrons.

$$V_n = -\sum_i (Ze^2/R_i) + 2\sum_i J_{n,i} = \sum_i V_i , \qquad 3.4$$

where R_i is the distance from the i^{th} carbon nucleus to the electron, $J_{n,i}$ is the Coulomb potential of the i^{th} molecular orbital of the n^{th} molecule, and V_i is the Goeppert-Mayer and Sklar[6], screened Coulomb potential, of carbon atom i of molecule n. Exchange effects were neglected. The energy was obtained from:

$$E_\pm(k) = \frac{\langle \Psi_\pm | H | \Psi_\pm \rangle}{\langle \Psi_\pm | \Psi_\pm \rangle}, \qquad 3.5$$

where the brackets denote the usual quantum mechanical summations. Equation 3.5 was reduced to:

$$E_\pm(k) = \mathcal{E}_o + \sum_n{}' \mathcal{E}_n + \sum_\ell (\pm 1)^\ell \cos(\vec{k}\cdot\vec{r}_\ell)\,\mathcal{E}_\ell, \qquad 3.6$$

where $\mathcal{E}_o$ is the energy of an isolated negative or positive ion relative to infinite separation of the electron or hole

and the neutral molecule, and ε_n and ε_ℓ are given by:

and the neutral molecule, and ε_n and ε_ℓ are given by:

an

$$\varepsilon_n = \langle \phi(\vec{r}) \left| V_n(\vec{r}-\vec{r}_n) \right| \phi(\vec{r}) \rangle , \qquad 3.7$$

$$\varepsilon_\ell = \langle \phi(\vec{r}-\vec{r}_\ell) \left| V_\ell(\vec{r}-\vec{r}_\ell) \right| \phi(\vec{r}) \rangle . \qquad 3.8$$

The sums in equation 3.6 are taken over all molecules except the one with its center located at the origin (molecule 1 of Fig. 3.1). Three-center intermolecular integrals in which the centers were on three different molecules (see equation 3.13) were neglected since the large interatomic distances made these terms negligible. In addition, since the overlap between molecules is small, overlap integrals multiplied by ε_n or ε_ℓ were also neglected in obtaining equation 3.6 from equation 3.5. The k variation of the energy bands is obtained from the last term of equation 3.6:

$$\varepsilon(k)_\pm = \sum (\pm)^{\eta_\ell} \cos(\vec{k}\cdot\vec{r}_\ell)\, \varepsilon_\ell , \qquad 3.9$$

where ε_ℓ is the intermolecular resonance integral between molecule 1 and molecule ℓ of Fig. 3.1. η_ℓ is even for corner molecules and odd for center molecules of each cell. The molecular orbitals of a negative or positive ion were approximated by a linear combination of neutral carbon 2p wavefunctions, u_i:

$$\phi_s = \sum c_{s,i}\, u_i , \qquad 3.10$$

Fig. 3.1. Anthracene unit cell and molecular centers in the unit cell and at sites adjacent to the unit cell, showing the molecular numbering used by Katz et. al.[3]

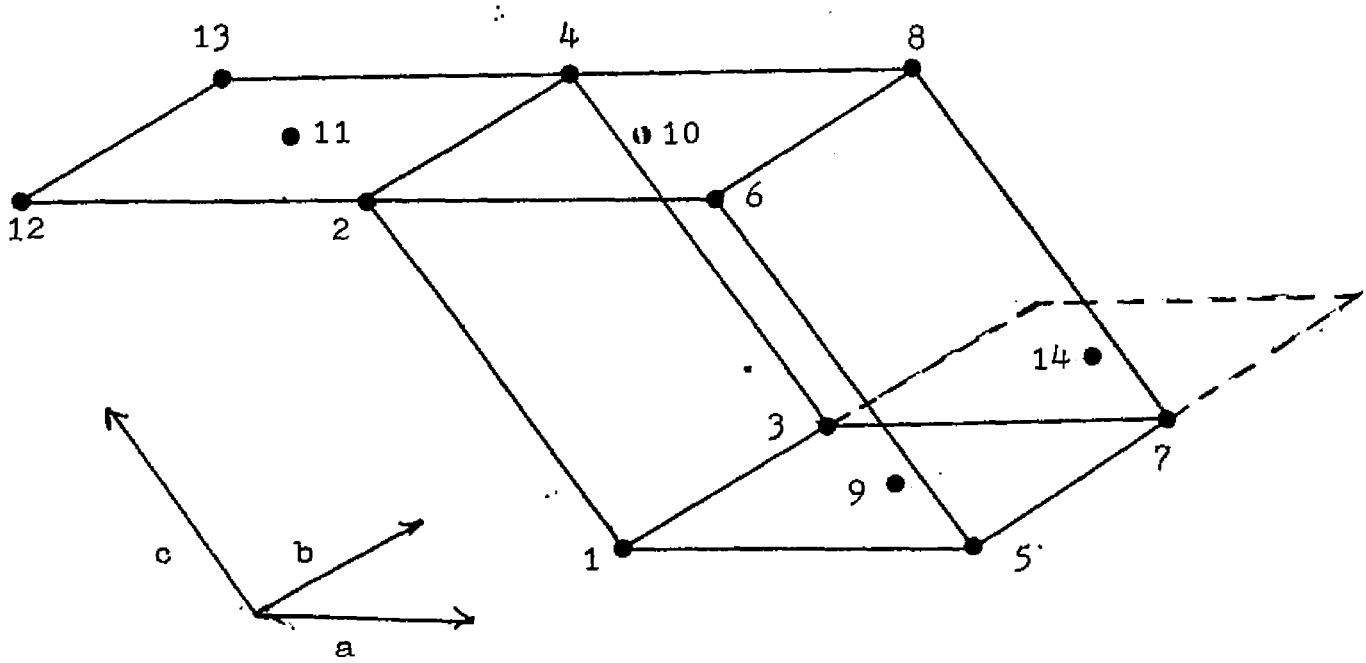

where the $C_{s,i}$ are Hückel coefficients for the lowest antibonding and highest bonding π orbitals for electrons and holes respectively.[7] s is the lowest unoccupied molecular orbital of a molecule for electrons and the highest occupied molecular orbital of a molecule for holes. Katz et. al. used:

$$u_i(r_i) = (\hat{n}_i \cdot \vec{r}_i) \sum_{i=1}^{4} a_j (\alpha_j^5/\pi)^{\frac{1}{2}} \exp(-\alpha_j r_i) \qquad 3.11$$

as the "best available carbon **atomic wavefunctions** represented in the form of a linear combination of four Slater wavefunctions". $\hat{n}_i$ is the unit vector defining the direction of the 2p orbital. The coefficients a_1 and the orbital exponent α_j were those given by Clementi and Roothaan.[8] LeBlanc and Thaxton et. al. used a single Slater wavefunction given by:

$$u_i = (\hat{n}_i \cdot \vec{r}_i)(\alpha_i^5/\pi)^{\frac{1}{2}} \exp(-\alpha_i r_i), \qquad 3.12$$

with the orbital exponent α_i given by Slater.[9] A knowledge of the detailed behavior of the molecular wavefunctions at large distances is required for the calculation of the excess electron and hole band energies. That is why Katz et. al. used a linear combination of Slater wavefunctions instead of a single Slater wavefunction to obtain a more accurate representation of the molecular wavefunction at large distances. Equation 3.8 may be expanded by substitution of equation 3.10 to:

$$\varepsilon_\ell = \sum_{i,j,m} C_{r,i} C_{s,j}\, u_i(\vec{r}-\vec{r}_i) V_m(\vec{r}-\vec{r}_m) u_j(\vec{r}-\vec{r}_\ell-\vec{r}_j) \; . \qquad 3.13$$

LeBlanc and Thaxton et. al. neglected those terms in the sum where $i \neq m$, i.e. they neglected all three-center integrals. Terms such as $i \neq m = j$ involve integrals where the potential and one wavefunction are on the same molecule. According to Katz et. al., these terms are not small and there are enough of them to change the energy by 25%.

Silbey et. al. extended the calculations of Katz et. al. by including the effects of molecular vibrations and adding an exchange potential to the Hartree potential. They represented their molecular wavefunctions as a product of an electronic part and a vibrational part. This corresponds to the weak-coupling limit of vibronic interaction where the nuclear part of the Hamiltonian is diagonalized before the crystal field part (the Born-Oppenheimer approximation). They used a wavefunction which represented the entire crystal instead of a one-electron wavefunction of the excess electron or hole. This was given by:

$$\Psi_{\pm}(k) = \sum_{\ell=0}^{2N-1} (\pm)^{n_\ell} \exp(i\vec{k}\cdot\vec{r}_\ell)\, \mathcal{A}\, \psi_{\ell,s}(1) \times \prod_{i=0}^{2N-1}{}' \left[\psi_{i,1}(1,1) \cdots\cdots \overline{\psi}_{i,a}(1,2a)\, \chi_1 \right] \quad 3.14$$

as the symmetrized wavefunctions of the crystal with an excess electron or hole. $\mathcal{A}$ is the unnormalized anti-symmetrization operator which permutes electrons between molecules. $\psi_{\ell,s}$ is the lowest unoccupied molecular orbital for electrons and the highest occupied molecular orbital

for holes of molecule ℓ. The ψ_i are the a occupied molecular orbitals of molecule i. The bar over $\overline{\psi}_{i,a}$ means that the electron in that molecular orbital has spin "$-\frac{1}{2}$". χ_i is the ground state vibrational wavefunction of molecule i. It was assumed that all vibrational wavefunctions were the same except that for the ions. This implies that every electron or hole band is split into many vibrational bands, each with its characteristic vibrational wavefunction. The K=0 (K is a vibrational quantum number) levels of these bands will be separated by the vibrational quantum which is of the order of 0.2 eV in aromatic molecules.[10] Since the calculated bandwidths are of the order of 0.01 eV, the bands are well separated. The potential used by Silbey et. al. was:

$$V_n'(\vec{r}-\vec{r}_n) = V_n(\vec{r}-\vec{r}_n) - \sum K_{n,i} \qquad 3.15$$

where

$$K_{n,i} = \langle \psi_{n,j} \left| (1/r_{ij}) \right| \psi_{n,j} \rangle \qquad 3.16$$

is the exchange potential of the i^{th} molecular orbital on molecule n. Thus, they obtained:

$$\epsilon_\ell = \left| \langle \chi^{\mp} | \chi^{o} \rangle \right|^2 \left[\langle \psi_{\ell,s}(\vec{r}-\vec{r}_\ell) \left| V_\ell (r-r_\ell) \right| \psi_{1,s}(\vec{r}) \rangle - \langle \psi_{\ell,s}(\vec{r}-\vec{r}_\ell) \left| K_{\ell,i} \right| \psi_{1,s}(\vec{r}) \rangle \right] \qquad 3.17$$

where $\chi^{\mp}$ represents the vibrational wavefunction of the negative or positive ion and χ^{o} that of the neutral molecule.

Glaeser and Berry, using the results of Katz et. al. and Silbey et. al., estimated the effects of electronic polarization. They represented the polarized orbitals of molecule j when an excess electron or hole is on molecule i by:

$$\psi_j^{(i)} = \left[\psi_j + \sum_x \delta_x^{(i)} \psi_j^{(x)}\right]\left[1 + \sum_x \left|\delta_x^{(i)}\right|^2\right]^{-\frac{1}{2}}, \quad 3.18$$

where the perturbation coefficients $\delta_x^{(i)}$ were expressed in terms of the known anisotropic polarizability and the oscillator strengths of the dipole-allowed transitions of the molecule. The sum over x was over the three principal directions of the molecule. Their calculations resulted in the following expression for the intermolecular resonance integrals:

$$\varepsilon_\ell = \varepsilon_\ell(\text{resonance}) + \Delta\varepsilon_\ell(\text{resonance}) + \varepsilon_\ell(\text{electrostatic})\, S. \quad 3.19$$

Here, ε_ℓ(resonance) is the intermolecular resonance integral given by Silbey et. al., assuming 100% vibrational overlap. $\Delta\varepsilon_\ell$(resonance) gives the corrections to ε_ℓ(resonance) which result from the use of polarized orbitals. ε_ℓ(electrostatic) represents a long-range interaction between the excess charge and the induced dipole moments on neighboring molecules. S represents the overlap of polarized wavefunctioons corresponding to two different locations of the electron or hole. Glaeser and Berry made calculations assuming that either only the highest π-orbital was polarized or that

all seven π-orbitals were polarized.

Chojnacki[11] has made calculation similar to those of Thaxton et. al. but including all integrals between molecules containing carbon atoms closer than 10 Å from each other in the two-center resonance integrals between molecule 1 and molecule ℓ.

Table 3.1 consists of the intermolecular resonance integrals for holes and electrons as calculated by Thaxton et. al., Katz et. al., Silbey et. al., and Glaeser and Berry. Table 3.2 consists of the intermolecular resonance integrals calculated by Chojnacki. The subscript ℓ labels the resonance integrals according to the scheme shown in Fig. 3.1. For example, ε_2 is the intermolecular resonance integral between the molecule at the origin (molecule 1) and molecule 2. Referring to the calculations presented in Tables 3.1 and 3.2, the energy band structure of anthracene, as given by equation 3.9, may be expanded to:

$$\begin{aligned} \varepsilon(k)_{\pm} = {} & 2\varepsilon_2 \cos \vec{k}\cdot\vec{c} + 2\varepsilon_3 \cos \vec{k}\cdot\vec{b} + 2\varepsilon_4 \cos \vec{k}\cdot(\vec{b}+\vec{c}) \\ & + 2\varepsilon_5 \cos \vec{k}\cdot\vec{a} + 2\varepsilon_6 \cos \vec{k}\cdot(\vec{a}+\vec{c}) \\ & \pm 4\varepsilon_9 \cos \tfrac{1}{2}\vec{k}\cdot\vec{a} \cos \tfrac{1}{2}\vec{k}\cdot\vec{b} \\ & \pm 4\varepsilon_{10} \cos \tfrac{1}{2}\vec{k}\cdot\vec{b} \cos \vec{k}\cdot(\tfrac{1}{2}\vec{a}+\vec{c}) \ , \end{aligned} \qquad 3.20$$

where ε_7, ε_8, ε_{11}, ε_{12}, ε_{13}, and ε_{14} have been neglected because, in general, their values are smaller than the other intermolecular resonance integrals.

Table 3.1. Intermolecular Resonance Integrals, ε_ℓ.

ℓ	(1)	(2)	(3)	(4)	
			HOLES		
2	.....	- 0.47	- 3.15	- 1.42	- 2.27
3	-16.2	-132.44	-438.14	-258.50	-405.95
4	.....	- 0.17	- 1.08	- 0.49	- 0.73
5	.....	0.20	1.30	0.68	1.26
6	.....	- 4.39	- 20.11	- 9.45	- 16.71
7	.....	0.03	0.26	.....	.....
8	.....	- 0.03	- 0.14	.....	.....
9	-14.9	- 93.05	-311.75	-196.40	-288.59
10	3.1	36.61	133.46	60.06	114.76
11	.....	0.01	0.08	.....	.....
12	.....	0.00	0.00	.....	.....
13	.....	0.00	0.00	.....	.....
14	.....	0.01	0.08	.....	.....
			ELECTRONS		
2	.....	0.15	- 4.23	- 1.90	- 3.02
3	11.9	71.61	224.51	132.46	208.53
4	.....	- 0.03	- 0.16	- 0.07	- 0.11
5	.....	0.25	1.59	0.83	1.56
6	.....	- 0.74	- 5.09	- 2.39	- 4.46
7	.....	0.04	0.24	.....	.....
8	.....	0.02	0.09	.....	.....
9	-19.7	-124.79	-403.69	-254.32	-372.68
10	0.65	2.48	9.46	4.26	8.72
11	.....	0.02	0.14	.....	.....
12	.....	0.00	0.00	.....	.....
13	.....	0.00	0.00	.....	.....
14	.....	0.00	- 0.01	.....	.....

Notes:

1. All energies are measured in units of 10^{-4}eV.

2. Calculations by: (1) Thaxton et. al.[2]; (2) Katz et. al.[3]; (3) Silbey et. al.[4]; and (4) Glaeser and Berry.[5]

3. The calculations in (3) by Silbey et. al. are for 100% vibrational overlap.

4. The calculations in (4) by Glaeser and Berry assume one orbital perturbed by the polarization effect and all seven π orbitals perturbed by the polarization effect, respectively.

Table 3.2. Intermolecular resonance integrals, ε_ℓ, calculated by Chojnacki.[11] ε_ℓ is measured in 10^{-4} eV.

ℓ	ε_ℓ
	HOLES
3	- 23.04
6	- 0.10
9	- 16.95
10	4.47
	ELECTRONS
3	- 17.57
6	- 0.03
9	- 25.16
10	0.77

Drift mobilities were calculated from equation 3.19 and equation 2.28 by assuming either a constant relaxation time or a constant mean free path. For a constant relaxation time one has:

$$\mu_x = (e\tau/kT)\langle v_x^2 \rangle \qquad 3.21$$

for charge carriers drifting along the x direction. For a constant mean free path, λ, one has:

$$\mu_x = (e\lambda/kT)\langle v_x^2 |\vec{v}(\vec{k})|^{-1} \rangle , \qquad 3.22$$

where $\hbar\vec{v} = \vec{\nabla}_k \mathcal{E}$.

LeBlanc and Thaxton et. al. neglected the variation of the Boltzmann factor in their calculations becauses their intermolecular resonance integrals gave bandwidths that were about 0.56 kT wide (kT is at room temperature). They evaluated μ_x as given by equation 3.21 in closed form and used a numerical integration (a 125 point Simpson's rule integration with a probable error of +50%)[1] for evaluating μ_x from equation 3.22.

Since Katz et. al. obtained bandwidths of the order of kT, they evaluated μ_x from equations 3.21 and 3.22 by numerical methods (a 1728 trapezoidal rule integration with a probable error in the fifth decimal place)[3].

Table 3.3 compares the theoretical and experimental values of the ratio of drift mobilities for various orientations of hole and electron drift currents in anthracene crystals. It can be seen that the band theory

Table 3.3. Band model and experimental values of ratios of drift mobilities in anthracene, at room temperature.

	I[1]	II[2]	III[3]	IV[4]	V[5]	VI[1f]	VII
	HOLES						
μ_b/μ_a	1.7	1.7	2.5	9.0	2.7	2.3	2.0
$\mu_c,/\mu_a$	0.2	0.2	0.3	1.1	0.4	0.04	0.8
	ELECTRONS						
μ_b/μ_a	0.8	0.9	0.7	2.2	0.4	0.99	0.6
$\mu_c,/\mu_a$	0.005	0.005	0.002	0.3	0.01	0.0025	0.2

Notes. 1. Columns I through VI are values obtained from band model calculations.

2. Column VII are experimental values obtained from Table 1.1.

3. **Reference numbers refer to references given at the end of the chapter.**

calculations agree with the experimental values given in column VII of Table 3.3 except for ratios involving the drift mobility along the c' direction.

B. Calculation of the Ratio of the Hall Mobility to the Drift Mobility.

In order to calculate μ_H/μ_D it is sufficient to consider integrals in k space over the first Brillouin zone. The reciprocal lattice may be constructed from the reciprocal lattice vectors $\vec{a}^{-1}$, $\vec{b}^{-1}$, and $\vec{c}^{-1}$, where[12]

$$2\pi\vec{a}^{-1} = \frac{2\pi(\vec{b} \times \vec{c})}{\vec{a}\cdot(\vec{b} \times \vec{c})} \qquad \text{etc.} \qquad 3.23$$

From Fig. 1.2, one has:

$$\begin{aligned} \vec{a} &= 8.56\ \text{Å}\ \hat{a}, \\ \vec{b} &= 6.04\ \text{Å}\ \hat{b}, \\ \vec{c} &= 11.16\ \text{Å}\ (\cos\beta\ \hat{a} + \sin\beta\ \hat{c}'), \\ \text{and} \quad \beta &= 124.7^{\circ}. \end{aligned} \qquad 3.24$$

The unit vectors $\hat{a}$, $\hat{b}$, and $\hat{c}'$ form a right handed coordinate system as shown in Fig. 1.2. Thus, one obtains:

$$\begin{aligned} 2\pi\vec{a}^{-1} &= 0.894\ \text{Å}^{-1}\ (-\cos\beta\ \hat{a} + \sin\beta\ \hat{c}'), \\ 2\pi\vec{b}^{-1} &= 1.04\ \text{Å}^{-1}\ \hat{b}, \\ 2\pi\vec{c}^{-1} &= 0.686\ \text{Å}^{-1}\ \hat{c}', \end{aligned} \qquad 3.25$$

and $\hat{c}^{-1}\cdot\hat{a} = \hat{a}^{-1}\cdot\hat{c} = 0$. The Brillouin zone is constructed

from a reciprocal lattice formed by the vectors, $2\pi\vec{a}^{-1}$, $2\pi\vec{b}^{-1}$, and $2\pi\vec{c}^{-1}$. Planes are drawn which are the perpendicular bisectors of these lattice vectors. The smallest volume enclosed by these planes is the first Brillouin zone[13], Fig. 3.2.

LeBlanc[14] and Friedman[15] expanded the Boltzmann factor and retained terms to first order in ξ_q/kT. They assumed a constant relaxation time and obtained an analytical solution to the k space integrals of μ_H/μ_D in the ab plane ($k_a k_b$ plane of k space). Their solution, verified in this investigation, resulted in $\mu_H/\mu_D = -8$ for both electrons and holes, using the intermolecular resonance integrals obtained by Thaxton et. al. LeBlanc and Friedman also used the intermolecular resonance integrals obtained by Katz et. al. and obtained $\mu_H/\mu_D = -1$ for electrons and holes. In this investigation, the Boltzmann factor was expanded to $(\xi_q/kT)^2$. In addition to the use of intermolecular resonance integrals calculated by Thaxton et. al. and Katz et. al., a calculation was made with the intermolecular resonance integrals obtained by Silbey et. al. A fifty per cent vibrational overlap was assumed so that ξ_q/kT would be less than one. The results gave $\mu_H/\mu_D = -1$ for both electrons and holes. This method cannot be applied to μ_H/μ_D in the ac' and bc' planes because of the shape of the Brillouin zone.

Fig. 3.2. A cross section of the first Brillouin zone of anthracene in the $\underline{a^{-1}c^{-1}}$ plane of reciprocal lattice space. k_a is the component of $\vec{k}$ along the $\underline{a}$ direction and $k_{c'}$ is the component of $\vec{k}$ along the $\underline{c'}$ direction.

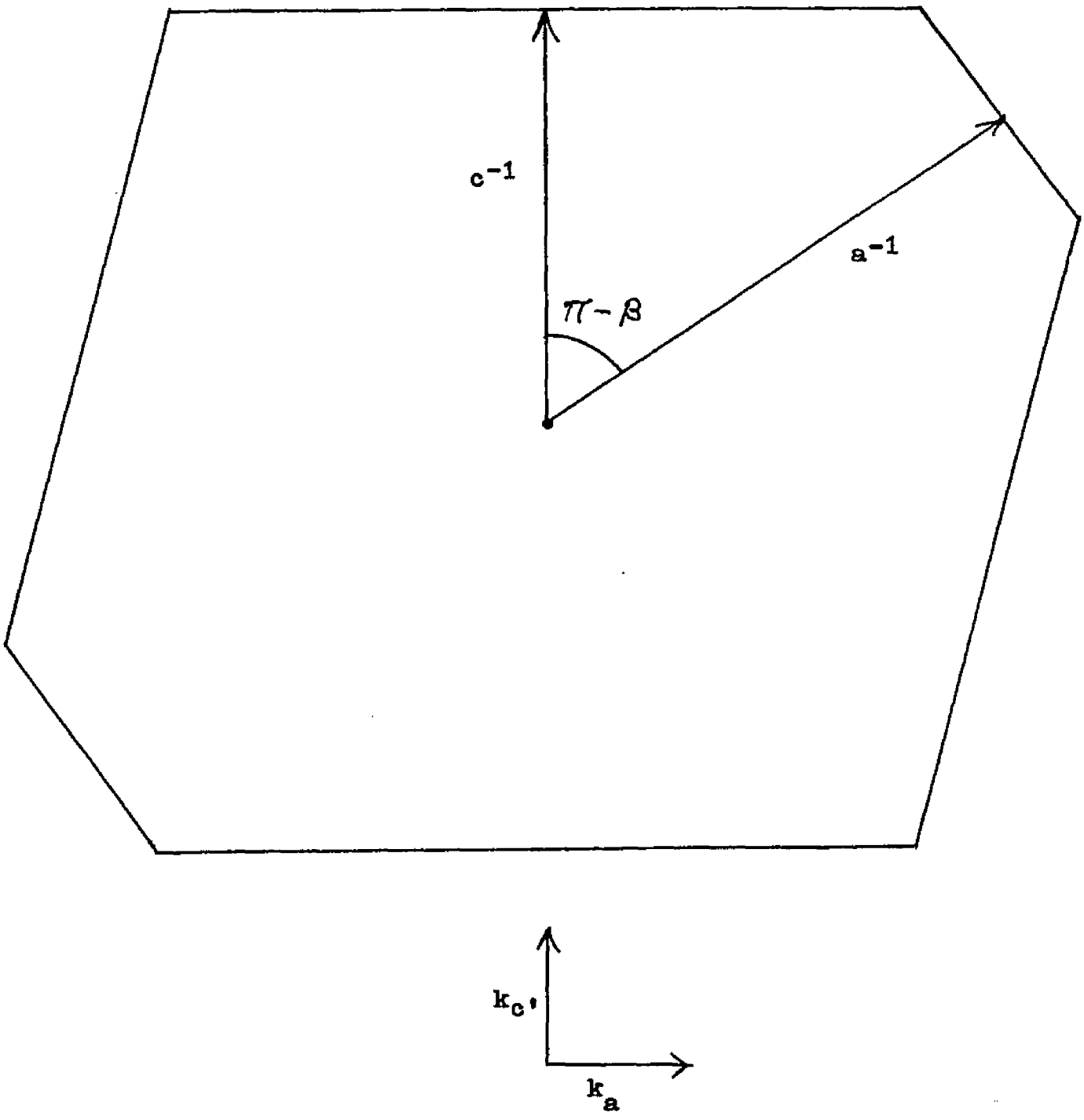

Toombs[16] has calculated μ_H/μ_D in the ab, ac', and bc' planes. He used the intermolecular resonance integrals calculated by Katz et. al. and Glaeser and Berry, and assumed a constant relaxation time. He used a computer and chose points in the first Brillouin zone and computed $\vec{v} = (1/\hbar)\vec{\nabla}_k \mathcal{E}$ and the effective mass tensor, M_{ij}^{-1} (see chapter 2, section B). The proper combinations were formed for μ_H/μ_D and weighted by the Boltzmann factor, $\exp\left[-\mathcal{E}(k)_{\pm}/kT\right]$. This was added to the results from previous points until the entire Brillouin zone was covered. The results, obtained by Toombs, are given in Table 3.4.

Table 3.4. μ_H/μ_D for nonzero Hall voltage at room temperature, calculated by Toombs[14].

		Katz			Glaeser and Berry OSC = 2			Glaeser and Berry OSC = 14		
I//	B//	a	b	c'	a	b	c'	a	b	c'
					HOLES					
a			1.7	-1.0		1.3	-0.3		1.4	0.01
b		-1.0		-1.0	0.3		-0.3	0.8		0.01
c'		-1.0	1.6		0.3	1.3		0.8	1.4	
					ELECTRONS					
a			0.03	-1.0		-0.8	-0.2		-0.6	0.06
b		-1.0		-1.0	-0.3		-0.2	-0.2		0.06
c'		-1.0	0.03		-0.3	-0.8		-0.2	-0.6	

Notes:

1. OSC = 2 corresponds to one orbital perturbed by the the polarization effect.
2. OSC = 14 corresponds to all seven π orbitals perturbed by the polarization effect.
3. The calculations using the intermolecular transfer integrals calculated by Glaeser and Berry are for 100% vibrational overlap.
4. B// and I// indicate the axes to which the magnetic field and the current are parallel.

References - Chapter 3

1. O.H. LeBlanc Jr., J. Chem. Phys. 35, 1275 (1961).

2. G.D. Thaxton, R.C. Jarnagin, and M. Silver, J. Phys. Chem. 66, 2461 (1962).

3. J.I. Katz, S.A. Rice, S. Choi, and J. Jortner, J. Chem. Phys. 39, 1683 (1963).

4. (a) R. Silbey, J. Jortner, S.A. Rice, and M.T. Vala Jr., J. Chem. Phys. 42, 733 (1965); (b) R. Silbey, J. Jortner, S.A. Rice, and M.T. Vala Jr., J. Chem. Phys. 43, 2925 (1965).

5. R.M. Glaeser and R.S. Berry, J. Chem. Phys. 44, 3797 (1966).

6. M. Goeppert-Mayer and A.L. Sklar, J. Chem. Phys. 6, 645 (1938).

7. E. Hückel, Z. Physik 76, 628 (1932).

8. E. Clementi and C.C.J. Roothaan, Phys. Rev. 127, 1618 (1962).

9. J.C. Slater, Phys. Rev. 36, 57 (1930).

10. B. Rosenberg, J. Chem. Phys. 29, 1108 (1958).

11. (a) H. Chojnacki, Molecular Crystals 3, 375 (1967); (b) H. Chojnacki, Molecular Crystals 5, 313 (1969).

12. A.J. Dekker, Solid State Physics (Prentice Hall Inc., Englewood Cliffs, N.J., 1965), p.278.

13. Reference 12, p.263.

14. O.H. LeBlanc Jr., J. Chem. Phys. 39, 2395 (1963).

15. L. Friedman, Phys. Rev. 133, A1668 (1964).

16. T. Toombs, Ph.D. Thesis, Princeton University (unpublished, 1968).

4. Experimental Procedures and Apparatus

A. Purification of Anthracene

Single crystals of high purity were required for the measurement of electrical transport properties in anthracene because impurities generate trapping states that alter these properties.[1,2,3] Purification of commercial grade synthetic anthracene (Eastman H480) was done by liquid adsorption chromatography, vacuum sublimation, and zone refining. All purification processes were performed under yellow "safe" lights to prevent photo-reactions from generating impurities.

The major impurities in synthetic anthracene have been isolated and identified. These are: anthraquinone, anthrone, bianthryl, and 9,10-dihydroanthracene.[4]

(1) Liquid, Adsorption Chromatography

Liquid, adsorption chromatography serves to remove polar impurities and to reduce the concentration of all impurities to levels at which the efficiency of the zone refining process is improved. Liquid, adsorption chromatography was performed using the apparatus shown in Fig. 4.1. A column packed with 28-200 mesh silica was continuously eluted with pentane that had been redistilled. The lower end of the column was closed with a wad of glass wool, that had been washed in redistilled pentane, to prevent the silica from passing into the lower three

Fig. 4.1. Apparatus for Adsorption Chromatography

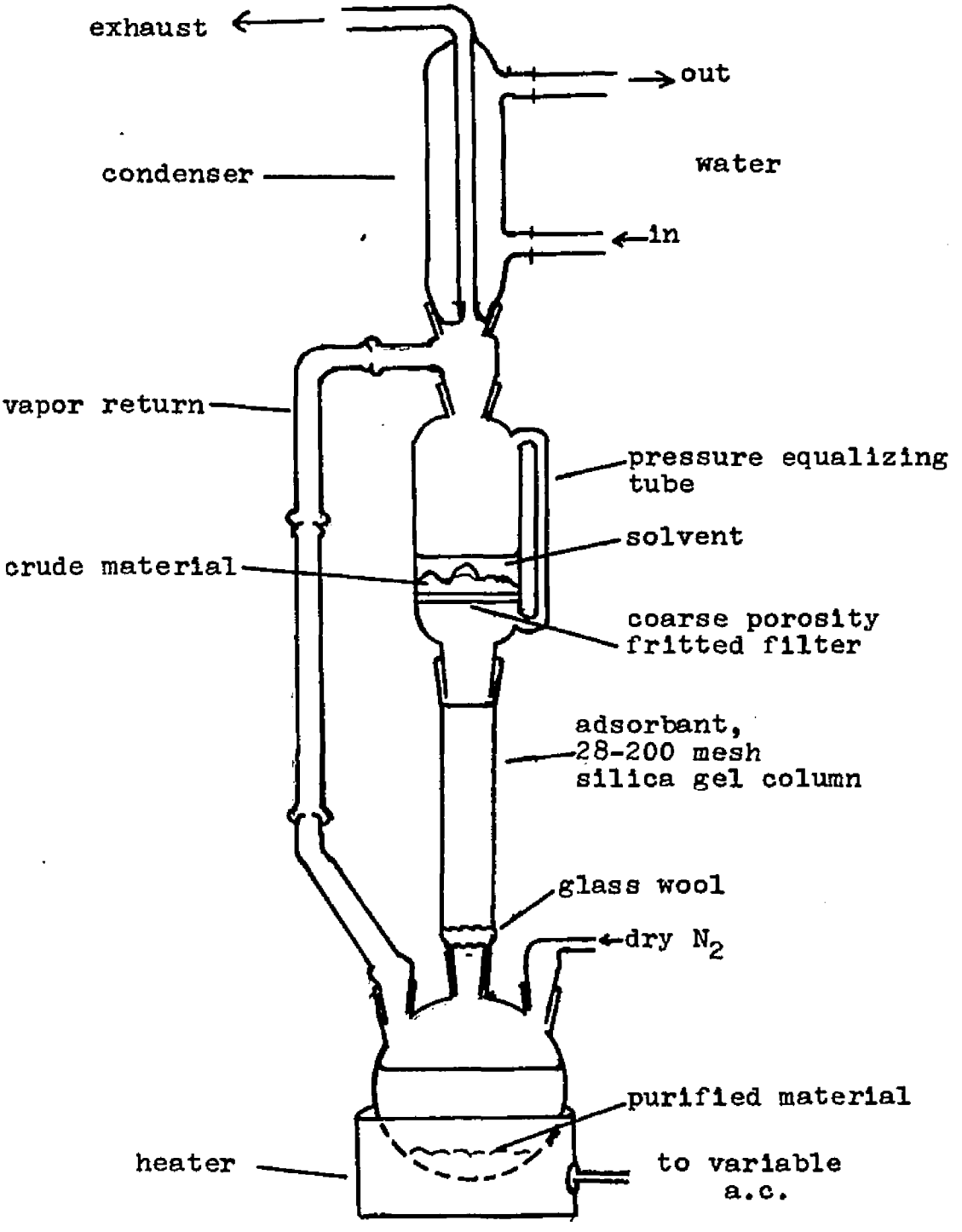

neck flask.

Impure synthetic anthracene was placed upon a coarse porosity fritted filter in the upper flask and a continuous slow stream of dry, oxygen-free nitrogen was then maintained through the apparatus (see Fig. 4.1) during the remainder of the process to minimize oxidation. Photo-oxidation was further reduced by the use of red glass for the column and the lower flask. The lower flask was heated and the pentane was distilled to the upper flask where it condensed and dripped upon the anthracene. The warm pentane dissolved the anthracene which, since it was not strongly adsorbed upon the column, passed in solution through the column into the lower flask. Typically, a column, 3/4 of an inch in diameter by 14 inches in length, passed 10 grams of anthracene per day and lasted two days before repacking was necessary to prevent impurities from passing through the column to the lower flask.

The more polar and less soluble impurities were adsorbed at the top of the column. When a used column was removed for repacking, red and green bands were noticeable at the top of the column. These were due to anthraquinone and tetracene respectively.[4] Also, a light brown coloration, due to tarry materials,[4] was seen spreading down the column.

As the pentane in the lower flask cooled, the anthracene crystalized from solution and was removed by filtration. The remaining anthracene was recovered by placing the cold concentrated solution into a lightproof

desicator and evaporating the pentane by pumping with a water siphon.

(2) Vacuum Sublimation

The chromatographed anthracene still contained those non-polar impurities which were soluble in pentane and also a high proportion of solvent. Further purification was done by vacuum sublimation. The apparatus used for this purpose was a combined sublimation and zone refining tube shown in Fig. 4.2.

70 to 80 grams of chromatographed synthetic anthracene were loaded into the left-hand bulb, the filling tube sealed, and the apparatus pumped down to a pressure that was less than 25 microns. The left-hand bulb was placed in a furnace, maintained at a temperature of 145 ^{o}C, and the anthracene sublimed under continuous evacuation into the second bulb. The most volatile impurities were pumped off and trapped. When approximately 95% of the anthracene had passed over to the second bulb, the furnace was turned off and the remaining 5% impure anthracene was sealed in the first bulb by melting the constriction between the first and second bulbs. The anthracene in the second bulb was then resublimed into the third bulb, which was then sealed at the constriction connecting the third bulb to the second bulb. The apparatus was flushed twice and filled to $\frac{1}{2}$ atm. with pure nitrogen (research grade). The remaining bulb and zone refining tube were then sealed off from the

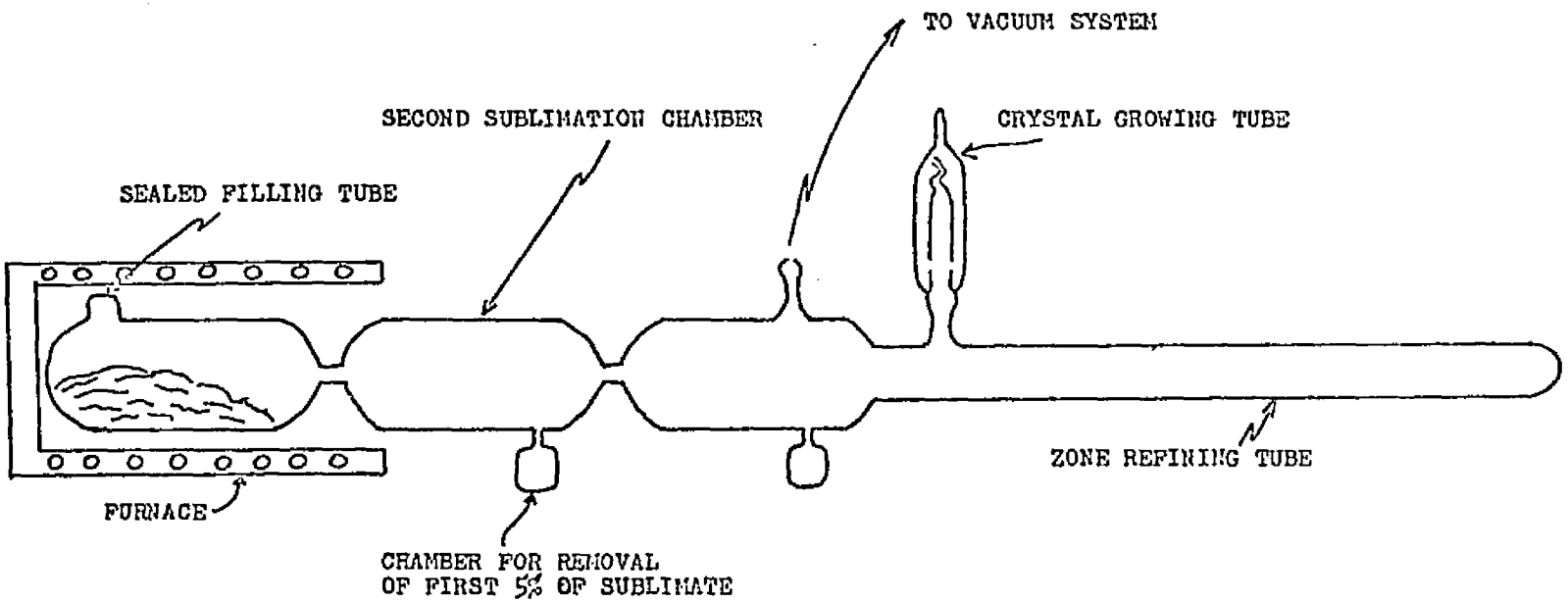

Fig. 4.2 COMBINATION TUBE CONSISTING OF VACUUM SUBLIMATION, ZONE REFINING AND CRYSTAL GROWING VESSELS

vacuum system and the anthracene was melted into the zone refining tube and allowed to solidify from the lower end of the zone refining tube.

(3) Zone Refining

Next, zone refining was carried out on a Fisher zone refiner, depicted in Fig. 4.3. The refining was carried out in thick walled, 20mm, pyrex tubing to reduce the possibility of breakage which could occur as a result of the considerable expansion on melting which is characteristic of organic compounds. Tube breakage was also avoided by the use of air coolers above the heaters to stabilize the width of the molten zone and by starting zone melting at the free surface. The presence of an inert gas in the tube prevented serious sublimation of anthracene up the tube.

About 30 zones of $\frac{1}{2}$ to 1 inch in length were passed down a 14 inch column at the rate of one inch per hour. The heaters were maintained at the lowest temperature that would permit the formation of a good zone so that thermal decomposition could be minimized.

The most obvious change of the anthracene column during zone refining was the concentration of yellow anthraquinone together with some dark brown material at the lower end of the tube.

Impurities which lower the freezing point of the host substance, anthracene, traveled with the molten zone, and tended to segregate at the bottom end of the

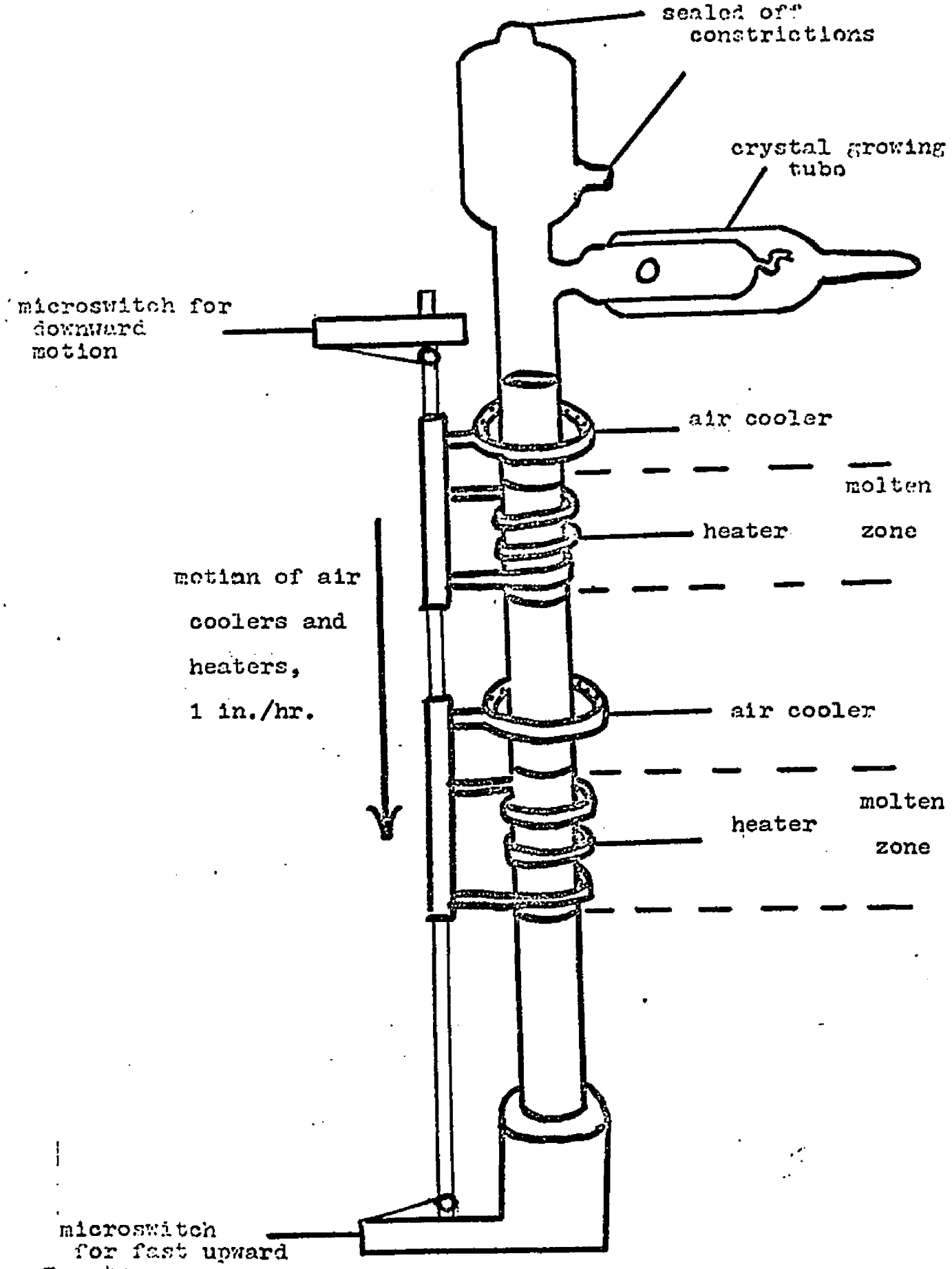

Fig. 3. A schematic representation of the zone refining apparatus.

anthracene column. These impurities have a segregation coefficient that is less than one. (The segregation coefficient is defined as the ratio of the impurity mole fraction in the solid to the impurity mole fraction in the liquid.)[5] Impurities which raise the freezing point traveled in a direction opposite to the molten zone and therefore tended to segregate at the top of the anthracene column. These impurities have a segregation coefficient that is greater than one. An impurity such as carbazole has a segregation coefficient that is approximately one and is therefore not efficiently removed by zone refining and must be removed by chromatography.

When zone refining was completed, the tube was cracked open and the upper and lower ends were rejected. The center portion of the anthracene column was then combined with other similar material and loaded into combined sublimation, zone refining, and crystal growing tubes. The material was then sublimed twice as before, and melted into the combined zone refining and crystal growing tubes. The material was then zone refined. After zone refining, the top end of the column was melted into the empty sublimation bulb. The center portion of the column was then melted into the crystal growing tube which was then sealed off from the zone refining tube. In this way the transfer was effected without exposing the anthracene to atmospheric oxidation and the crystal was grown in the same atmosphere as used for the final zone

refining.

B. Growth and Quality of Anthracene Crystals

Crystals were grown by the Bridgman method in which controlled cooling is carried out by slowly lowering the crystal growing tube at the rate of one inch per day through a vertical temperature gradient from the hot to the cold end.[6] A suitable temperature gradient was obtained by arranging two isothermal furnaces, as shown in Fig. 4.4, such that the upper furnace was at 240 °C and the lower furnace was at 205 °C. (The melting point of anthracene is 217 °C.)

A diagram of the crystal growing tube is shown in Fig. 4.5. The tube was suspended in the furnace, as shown in Fig. 4.4, so that the tip was just below the melting point isothermal, and the lowering mechanism was then turned on. Crystallization was begun by cooling the tip of the tube. This prevented supercooling and the subsequent formation of multicrystals.

As the tube is lowered, crystallites grow until, just below the bent capillary, several large crystallites occupy the tube. The bent capillary inevitably selects a particular seed which grows into the upper tube as a large crystal. If the angle between the capillary and the tube axis is less than 45°, the ab cleavage plane will grow parallel to the tube axis. If the angle is greater than 45°, it will grow perpendicular to the tube axis.[7]

Fig. 4.4. Crystal growing furnace.

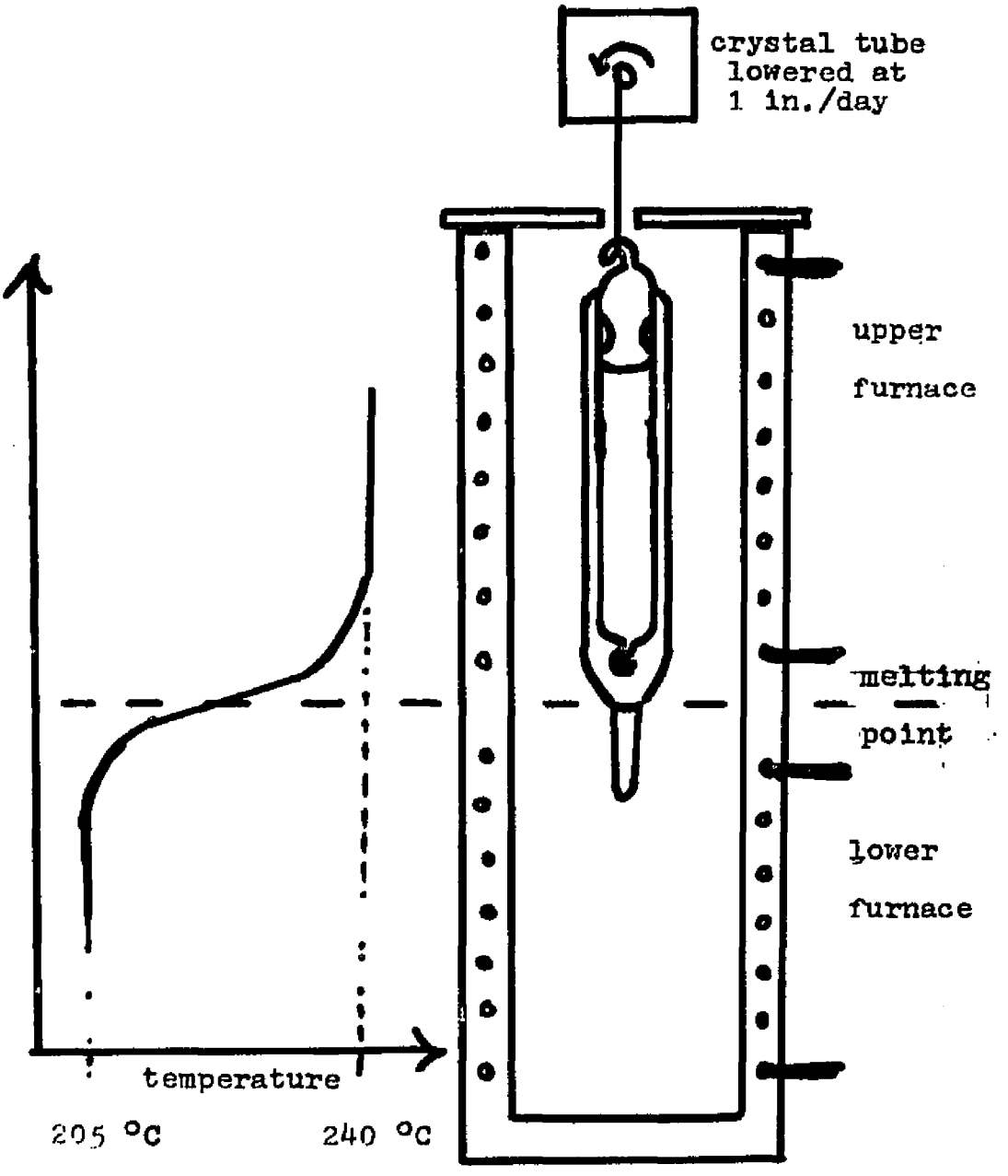

Scale: approximate

Fig. 4.5. Crystal growing tube.

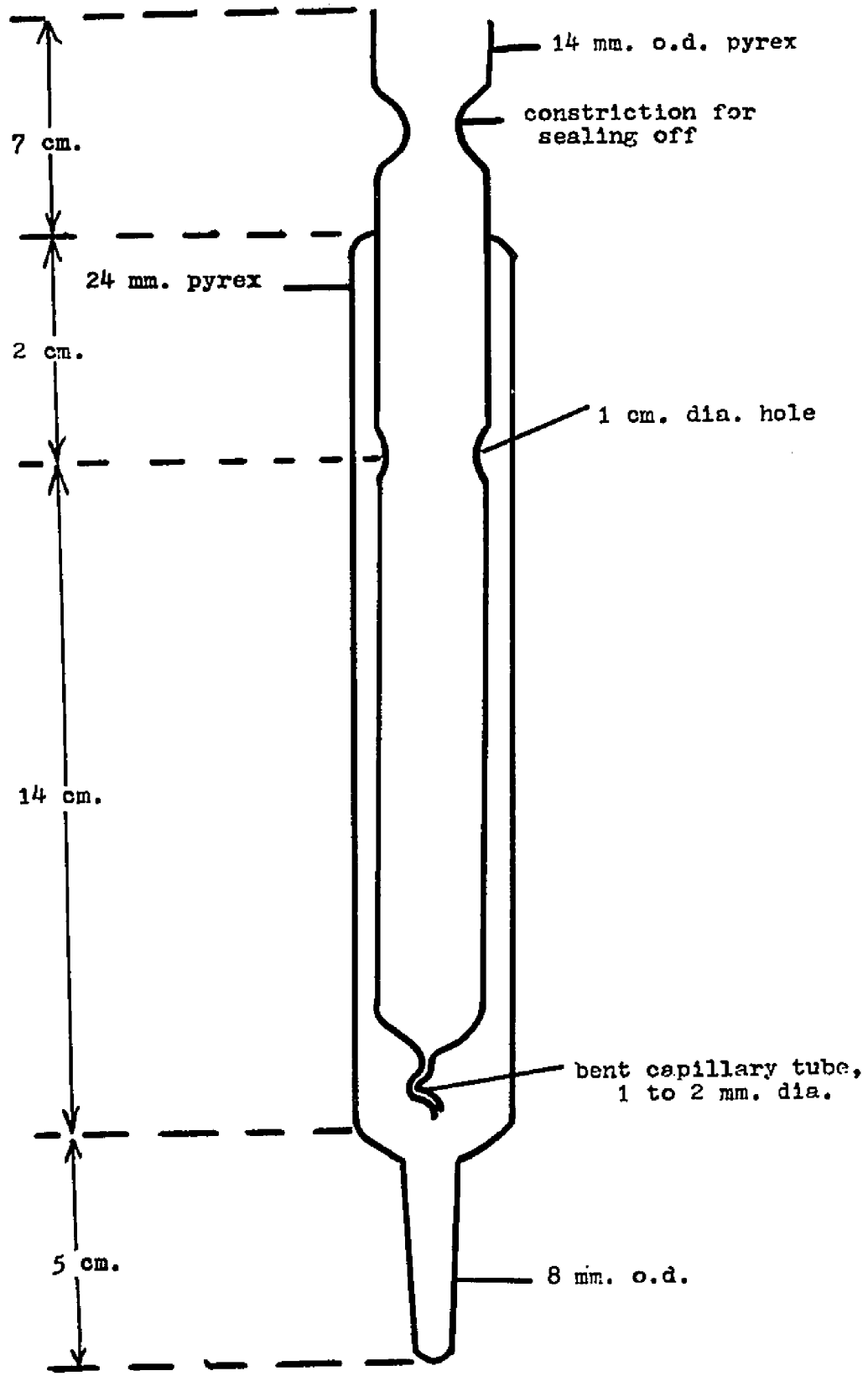

When growth was complete, the crystal in the tube was removed from the lower furnace and allowed to cool rapidly for a few minutes to let the crystal break away from the tube wall. There was usually a "cracking" sound as this occurred. The crystal and tube were then returned to the lower, annealing, furnace and cooled to room temperature over a period of three days. After this period, the crystal tube was opened and the crystal boule was easily slid from the tube because the inside surface of the crystal growing tube had been treated with "Dow Corning 200" silicone release agent, dissolved in methyl ethyl ketone. After treatment, and before filling, the tube had been baked for one hour at 275 ^{o}C. The release agent reacted chemically with the glass surface and when a crystal was grown, contamination of the crystal, due to the release agent, was unlikely.

No impurities were eluted in a gas chromatograph. Thus, it was concluded that the total impurity content was less than 1 p.p.m. The final purity and structural defect concnetration of the material was checked by the triplet lifetime which was found to be between 20 and 25 msec, equivalent to the longest which has been reported.[8]

C. Cutting, Orienting, and Shaping a Sample from a Crystal Boule.

A crystal boule usually had some cleavage cracks. Applying pressure with a razor blade in the direction of the crack readily cleaved the crystal apart. The cleavage face is the ab plane. The location of the a direction in this plane was obtained by the use of a polarizing microscope[9] or by observation of the double refraction of the crystal[10]. With this information and knowledge of the relative positions of the b and c' directions,[11] the crystal could be cut in any desired orientation of the a, b, and c' directions (see Fig. 4.6).

After orientation, the crystal was glued with "Duco" cement to a glass slide and cut with a xylene soaked razor blade, used as a microtome, and shaped by use of a xylene soaked strip of 600A grit emery paper, glued to a glass slide. An optical finish was obtained by polishing the crystal on a glass slide covered with a "Kleenex" tissue, soaked in xylene. Typical dimensions of a crystal used for a Hall effect measurement were 6 mm x 3 mm x 2 mm.

Fig. 4.6. Orientation of an anthracene crystal by double refraction. (a) A non-aligned crystal placed over intersecting vertical and horizontal lines. (b) A crystal aligned relative to intersecting vertical and horizontal lines with its a axis parallel to the horizontal line.

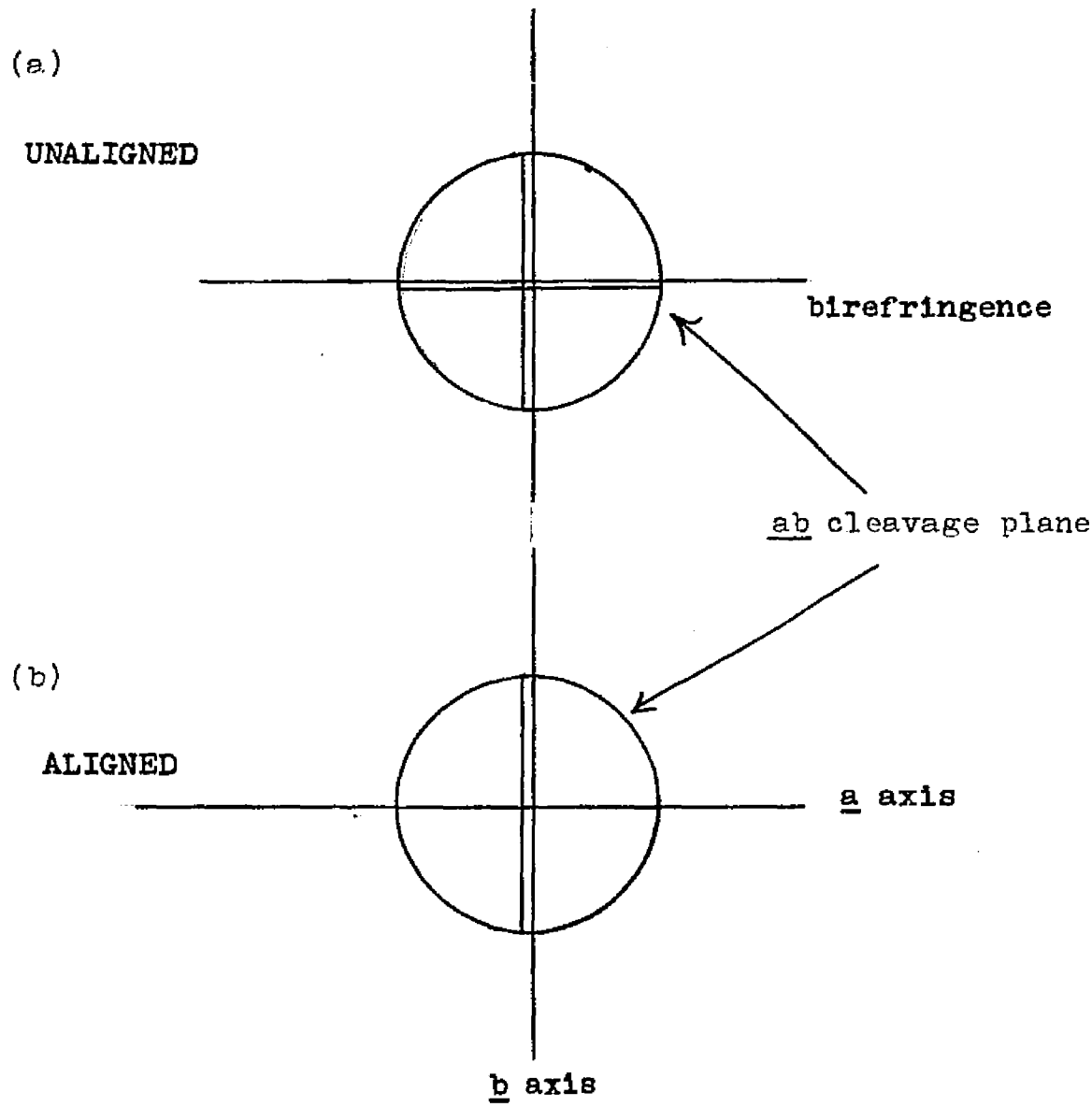

D. Hall Effect Apparatus.

The apparatus used to measure the Hall voltage and photoconductivity of anthracene consisted of the following: (1) a cryostat and superconducting solenoid; (2) an inner dewar insert; (3) an inner dewar cap and dry box; (4) a crystal holder; (5) a crystal chamber; (6) a vacuum and helium gas system; (7) temperature controllers; (8) an optical system; and (9) an electrical system (Fig. 4.7).

(1) Cryostat and Superconducting Solenoid.

The crysostat and superconducting solenoid were manufactured by Varian Associates. The cryostat was designed to cool the superconducting magnet with liquid helium. It consisted of an outer dewar which contained liquid nitrogen, a dewar which contained liquid helium and the superconducting solenoid, and an inner dewar which provided experimental access to the center of the superconducting solenoid (see Figs. 4.8 and 4.9).

In practice, the magnetic field was swept through a typical cycle of 10 minutes of increasing field, 10 minutes of steady field, and 10 minutes of field decreasing to zero.

(2) Inner Dewar Insert

The inner dewar insert is shown in Figs. 4.10, 4.11, and 4.12. It consisted of a solid brass cylinder, $1\frac{15}{16}$ inches in diameter by 3/4 of an inch in length, on which

Fig. 4.7. The Hall effect apparatus.

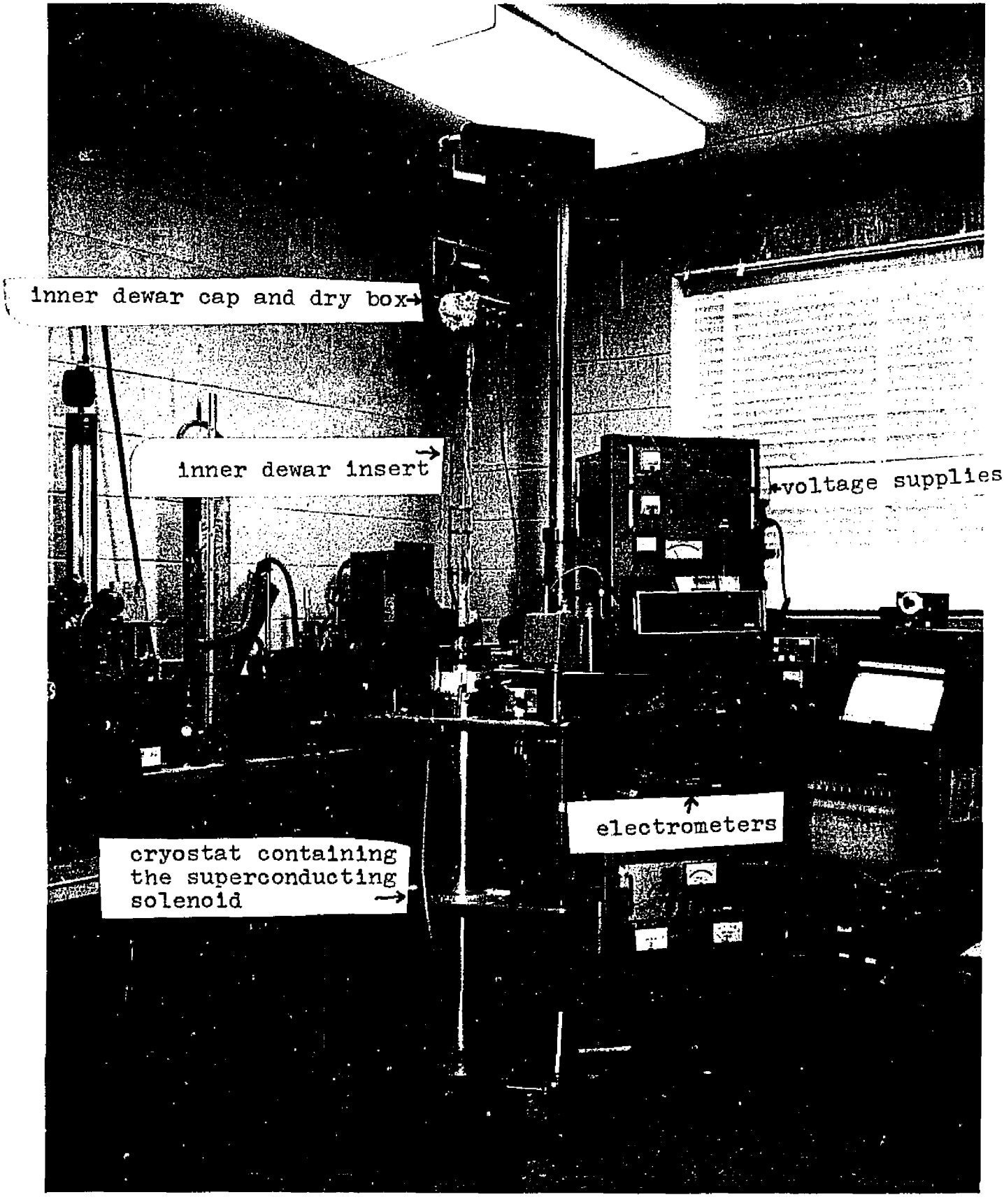

Fig. 4.8. Front surface mirror, inner dewar cap, dry box, and upper portion of cryostat.

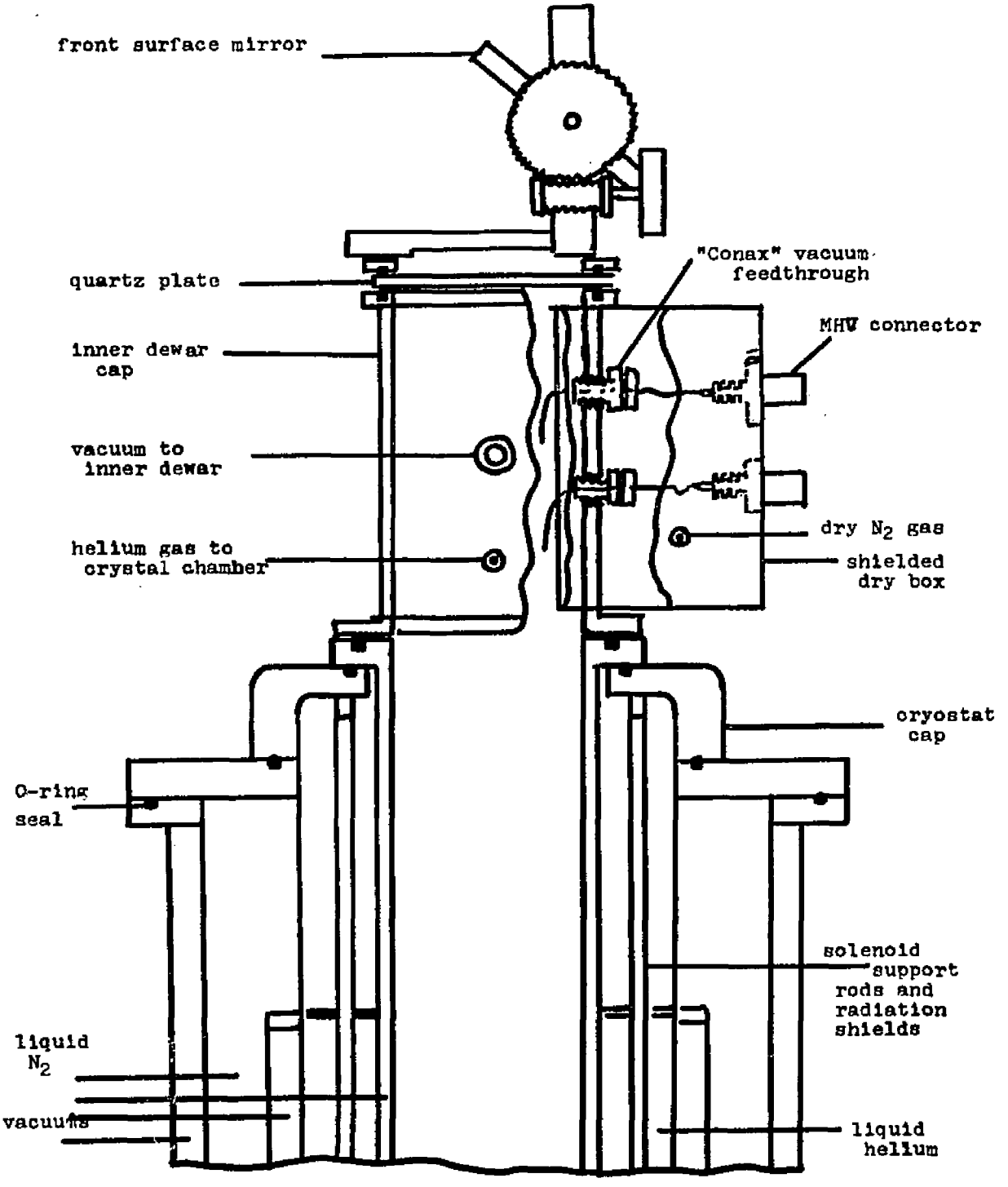

Fig. 4.9. The lower portion of the cryostat and superconducting solenoid.

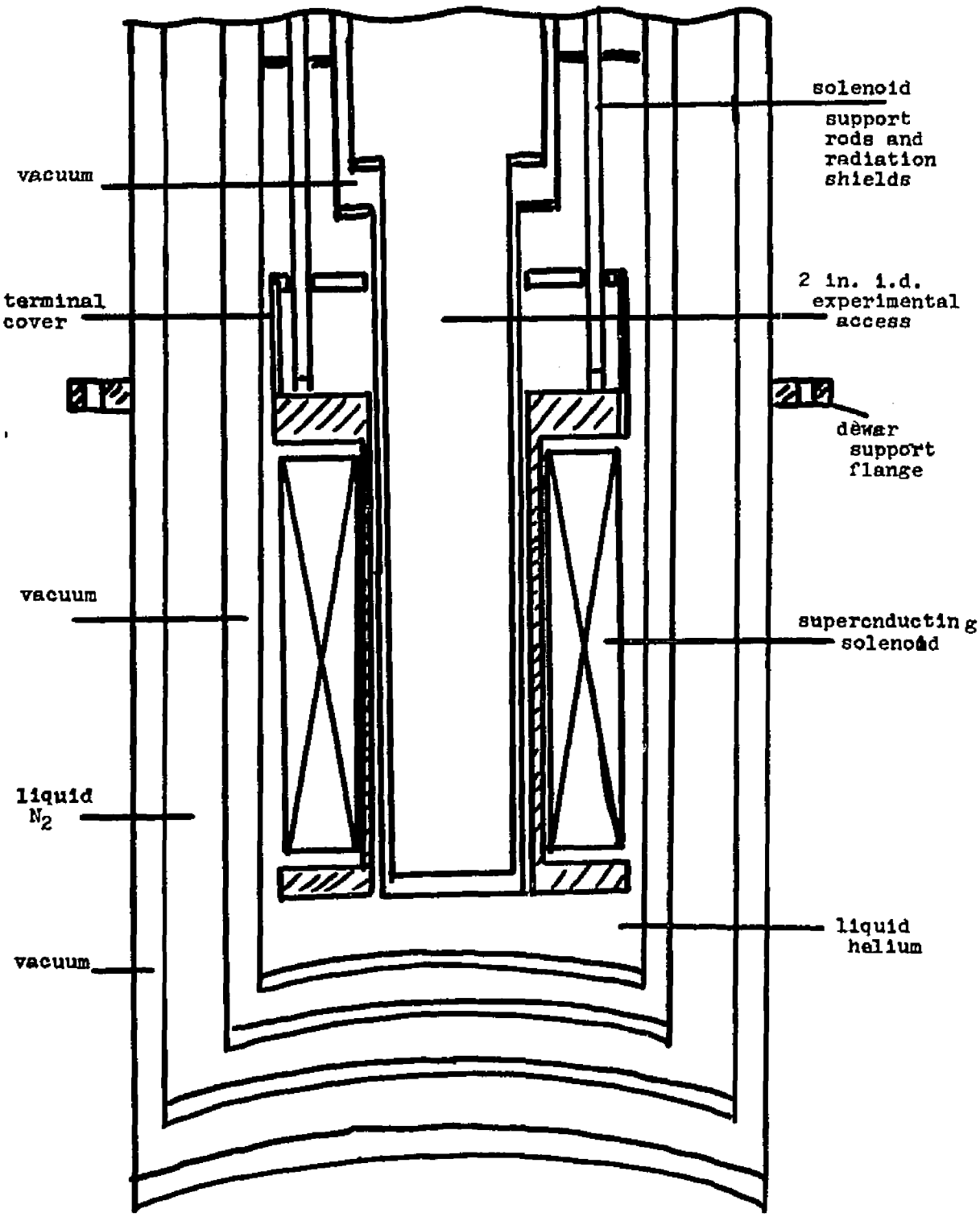

Fig. 4.10. Front surface mirror, inner dewar cap and dry box, and inner dewar insert.

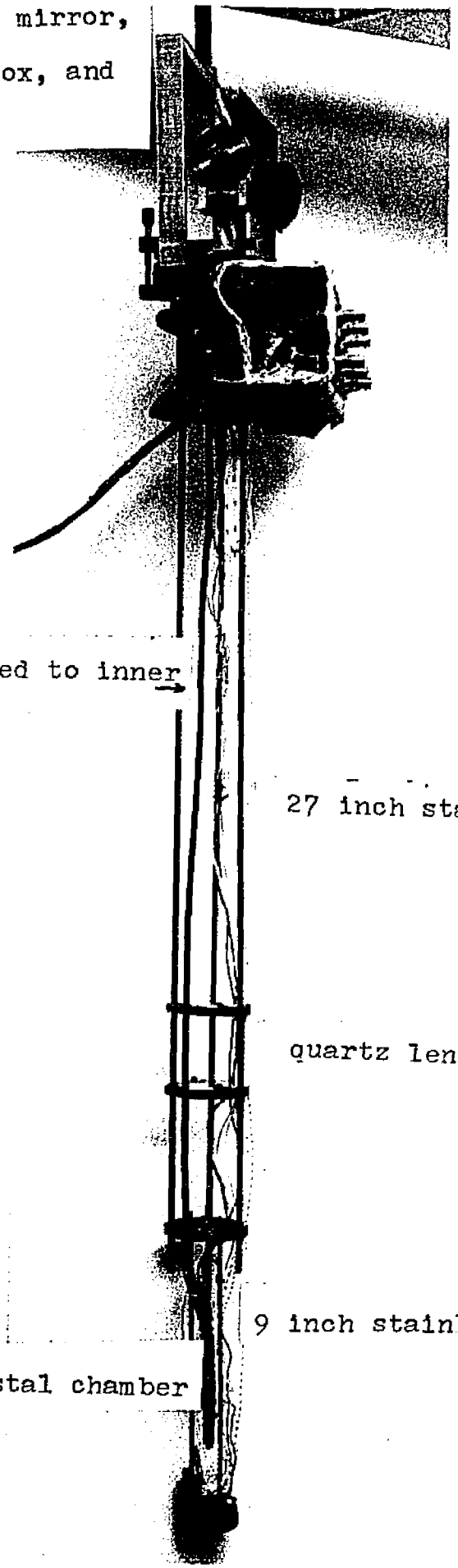

Fig. 4.11. Front view of the lower portion of the dewar insert.

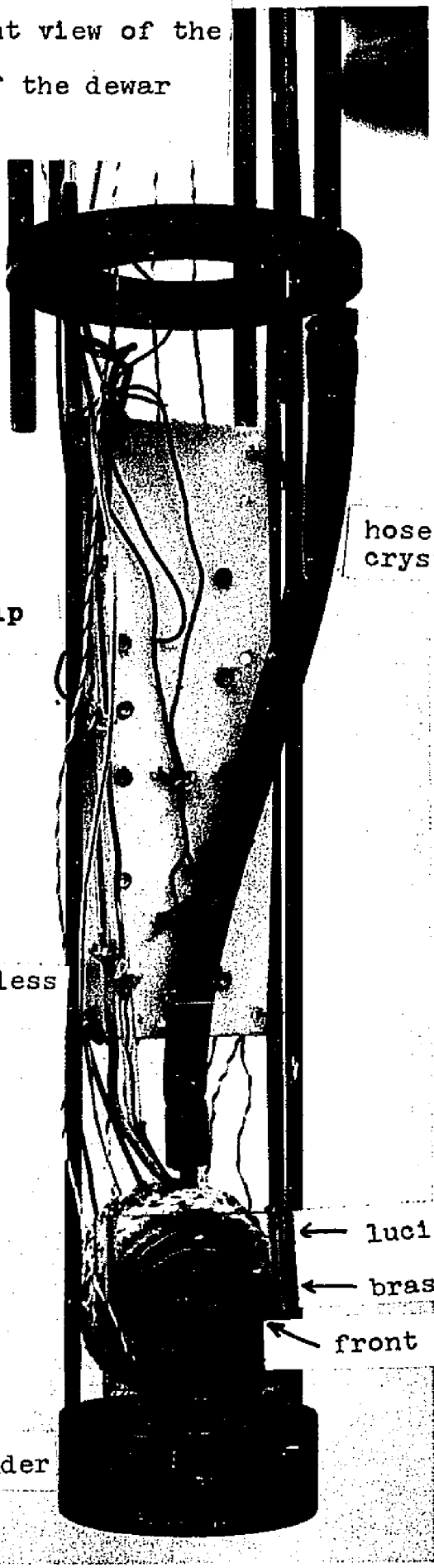

Fig. 4.12. Rear view of the lower portion of the dewar insert.

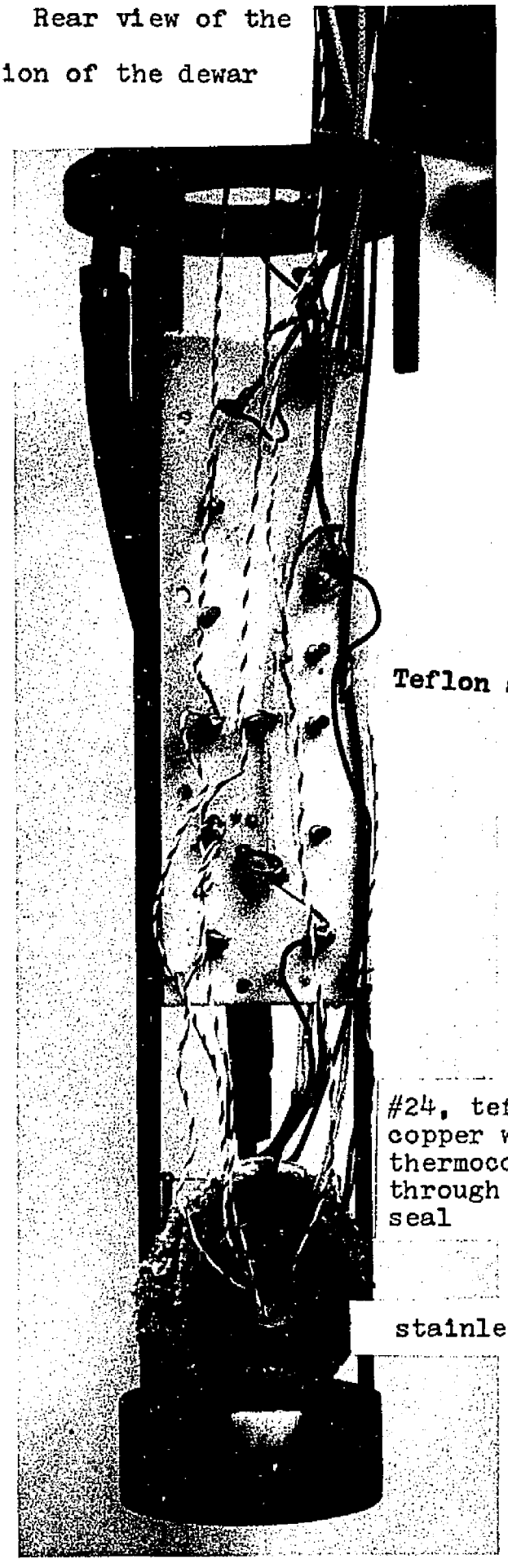

was mounted a front surface mirror, 1 cm. x. 1 cm., and the crystal chamber. Three 9 inch stainless steel rods, screwed into the brass cylinder, were bolted to a 1/4 inch thick brass ring ($2\frac{5}{8}$ in. o.d. by $1\frac{1}{2}$ in. i.d.). Three 27 inch stainless steel rods, bolted to the brass ring, were screwed into the bottom of the inner dewar cap. Two 5 cm. diameter, 65 cm. focal length quartz lenses focused ultraviolet light on the crystal. A copper tube, soldered to the inner dewar cap, was connected with a hose to the crystal chamber, and allowed helium gas to enter the chamber. The helium gas prevented the crystal from subliming and aided in the maintenance of a constant temperature inside the crystal chamber. Electrical leads from the crystal were soldered to lugs mounted on teflon strips. Thermocouple leads went directly through a "Conax" vacuum feedthrough, and heater leads were soldered to "Stupikoff" vacuum feedthroughs, mounted in the side of the inner dewar cap.

(3) Inner Dewar Cap and Dry Box

The inner dewar cap, Figs. 4.8 and 4.10, was fitted with "Conax" Teflon insulated, vacuum feedthroughs that were connected to Teflon insulated MHV connectors mounted in an electrically shielded dry box. The cap was covered with an O-ring sealed quartz plate, on top of which was mounted a front surface mirror, to direct ultraviolet light to the crystal. Two pipes on the side of the cap allowed the inner dewar to be connected to a vacuum pump and the

crystal chamber to be connected to a helium gas cylinder.

(4) Crystal Holder

The crystal holder and chamber are shown in Fig. 4.13. The crystal holder consisted of two Teflon discs held together by four 0-80 brass screws, a tin oxide coated quartz electrode, a spring-loaded copper electrode, a Teflon pressure seal, 5 Teflon insulated, copper wires, and a thermocouple consisting of #30 copper-constantan wires.

A guard ring was pasted with "Eccobond 57C" silver conducting paste (thinned with toluene) as close as possible around the surface of an anthracene crystal, which was in contact with the quartz electrode. The opposite surface of the crystal, which was in contact with the copper electrode, was covered with "Eccobond 57C" to insure uniform contact.

After the crystal had been placed in the holder between the quartz electrode and the spring-loaded copper electrode, the four brass screws of the holder were carefully tightened. The Hall probes were then connected by using spring-loaded brass wires that had been etched in hydrochloric acid and had been soldered to #24, Teflon insulated, copper wires. A #40 copper wire, soldered to a #24, Teflon insulated, copper wire, was pasted to the guard ring with quick drying "Dupont #4817" silver conducting paste (thinned with butyl acetate).

A mask was placed in front of the quartz electrode to

Fig. 4.13. Crystal holder and chamber, scale approximately 4X.

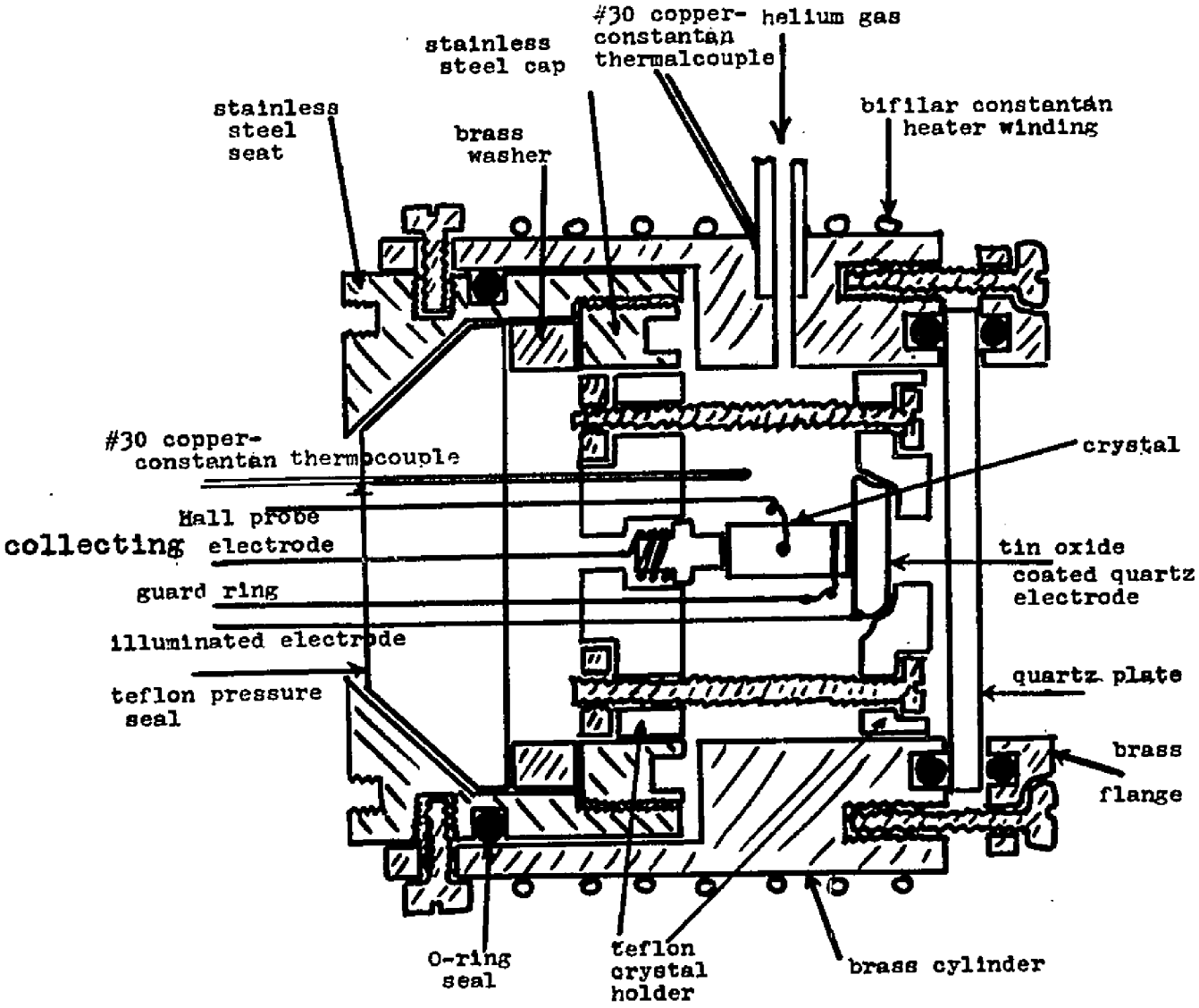

shield the guard ring from the light source so that it would not contribute photocurrent to the sample.

The brass spring for the copper electrode and the brass Hall probes were made from 0.020 inch diameter brass wire that had been drawn down to a diameter of 0.010 inches to increase its stiffness. Electrical contact to the tin oxide coated quartz electrode was made by fastening a #24, Teflon insulated, copper wire to the edge of the tin oxide surface with "Dupont #4817" paste. A layer of epoxy glue was then spread over the connection. The copper electrode was soldered to one end of the brass spring. The other end of the brass spring was soldered to a #24, Teflon insulated, copper wire. The five #24, Teflon insulated, copper wires and the two #30 thermocouple wires passed through separate, tight fitting, holes in the Teflon pressure seal.

(5) Crystal Chamber.

The crystal chamber consisted of a brass cylinder, quartz plate and brass flange, brass washer, stainless steel cap and seat, bifilar constantan heater winding, #30 copper-constantan thermocouple and a helium gas inlet pipe (see Fig. 4.13). The thermocouple and brass inlet pipe were soft soldered to the brass cylinder. The bifilar heater winding was tied around the outside of the brass cylinder. The quartz plate, sandwiched between two O-rings, was connected to one end of the brass cylinder with the brass flange. These pieces were then mounted on the base of the

dewar insert in a lucite frame as shown in Fig. 4.11.

The crystal, in its holder, was placed into the stainless steel seat. After the brass washer was in place, the stainless steel cap was carefully tightened with two spanner wrenches, compressing the Teflon pressure seal in the stainless steel seat. These pieces were then slid into the open end of the brass cylinder. The outer surface of the stainless steel seat was fitted with an O-ring which made a seal with the inner surface of the brass cylinder.

(6) Vacuum and Helium Gas System.

The vacuum and helium gas system is shown schematically in Fig. 4.14. The inner dewar was pumped down to a constant pressure of 20 to 40 microns by forepump (1). It was pressurized to one atm. with helium gas when one desired to remove a crystal. Helium gas was maintained in the crystal chamber at a constant pressure of 4 to 8 cm of Hg by adjusting valves leading to helium gas cylinder (1) and forepump (2). The helium gas served as a heat exchanger and also retarded sublimation of the crystal. The dewar containing the superconducting solenoid was precooled with liquid nitrogen. It was then connected to the vacuum and helium gas system via the helium side vent port of the cryostat (Fig. 4.16) and pumped to 66 cm of Hg below atmospheric pressure. This procedure cooled the dewar another 14 K below liquid nitrogen temperature.[12]

Fig. 4.14. Block diagram of the vacuum and helium gas system connected to the cryostat and crystal chamber.

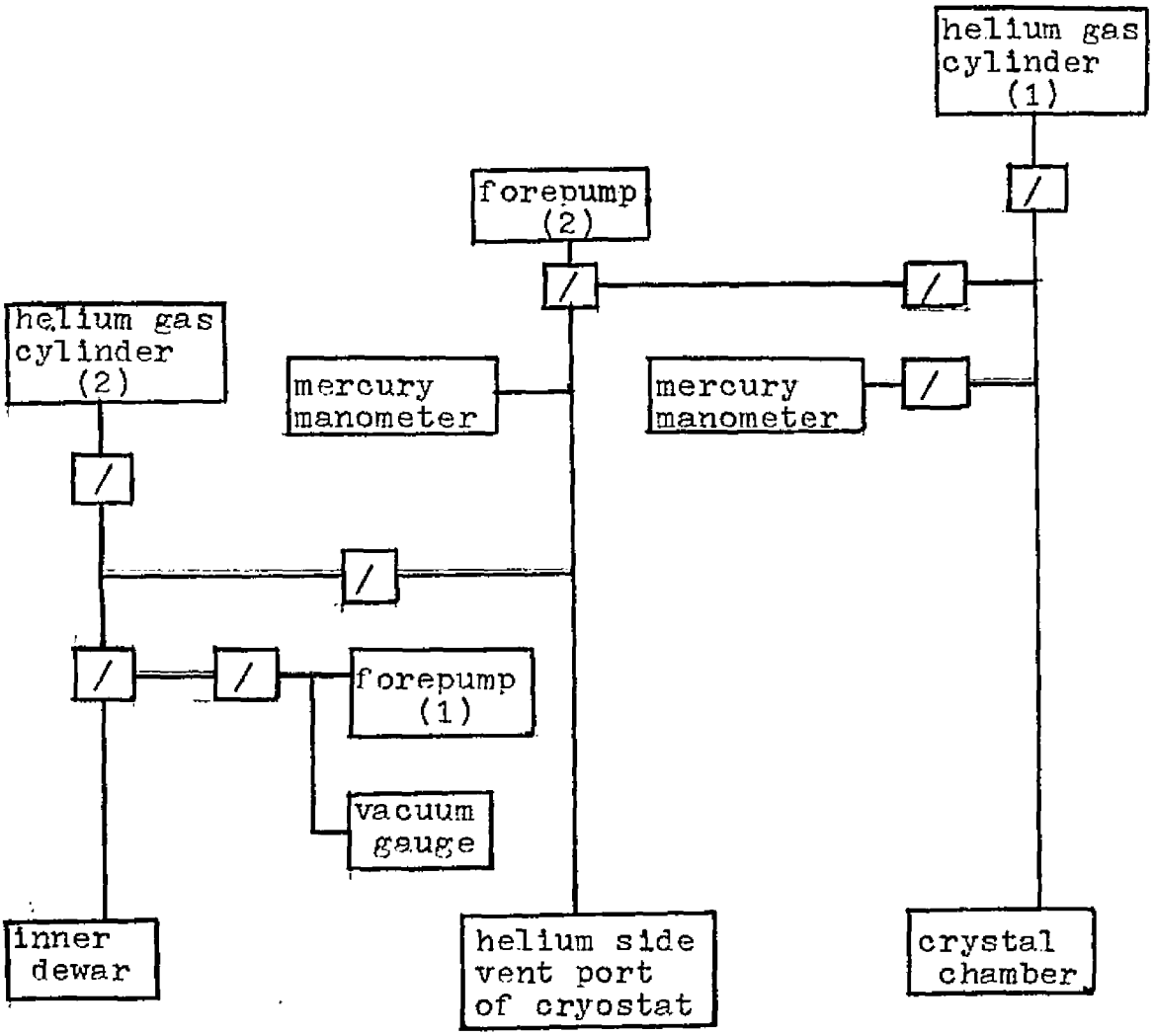

/ is used to represent a valve. The crystal chamber was placed inside the inner dewar.

(7) Temperature Controllers.

The temperature of the crystal chamber was controlled by connecting the thermocouple, soldered to the chamber wall, to an "A.P.I." on-off pyrometer, which turned the heater power supply on or off. During the Hall effect measurement, the temperature was controlled by connecting this thermocouple to a "Keithley" microvoltmeter. The output of the microvoltmeter was connected to a relay-potentiometer circuit, Fig. 4.15, which varied the heater current from a maximum to a 50% of maximum value. In this manner, the temperature in the crystal chamber, 25 °C, did not vary by more than six microvolts (approximately 1/7 of a °C) as measured by the copper-constantan thermocouple.

(8) Optical System.

A 100 watt, point source, mercury lamp ("P.E.K. 109") was used to illuminate the crystal. Because charge carriers are created by exciton-exciton interaction, the conduction is not intrinsic.[13] Therefore, in a crystal of high purity the carriers must be injected. The optical system is shown schematically in Fig. 4.16. In order to maintain a constant photocurrent through the crystal, the output of the vibrating reed electrometer, that was used to measure the photocurrent, was connected to a potentiometer and a d.c. amplifier. The output of the d.c. amplifier controlled a two phase motor which opened or closed a variable diaphragm.

Fig. 4.15. Circuit diagram of the crystal chamber temperature controller.

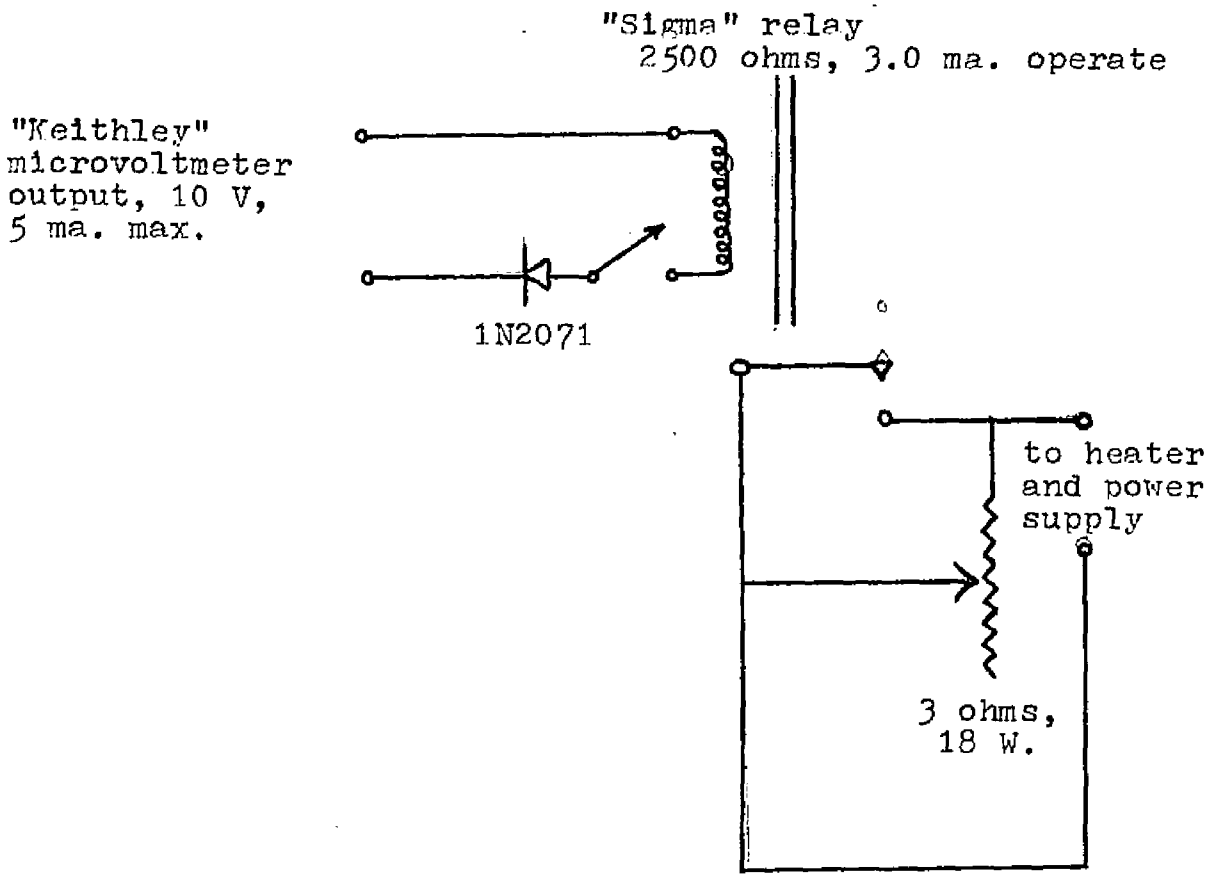

Fig. 4.16. Block and circuit diagram of the optical system used to illuminate the crystal.

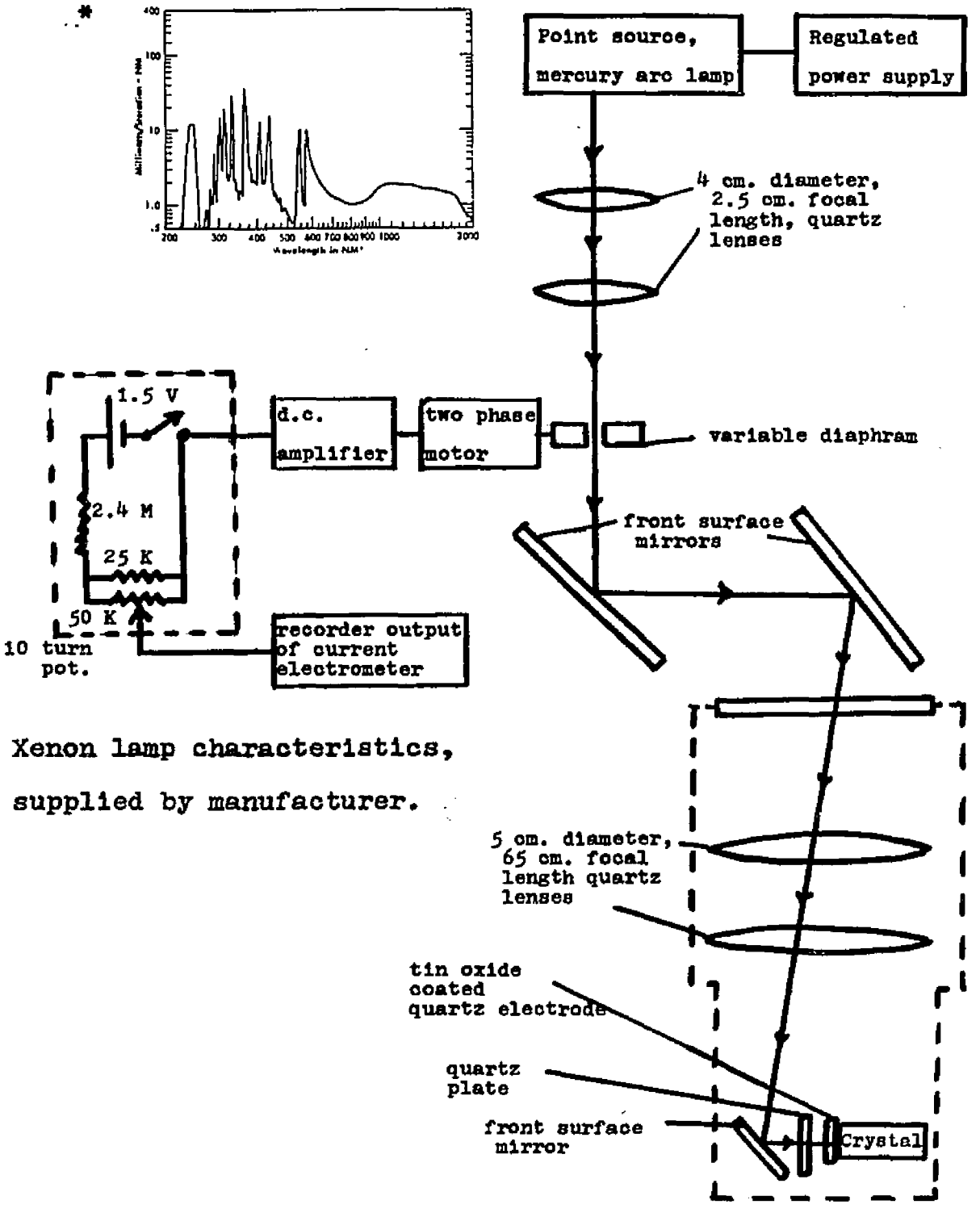

* Xenon lamp characteristics, supplied by manufacturer.

A constant photocurrent was necessary to reduce drift potentials at the Hall probes to a minimum. This can be seen from the following analysis. Referring to chapter 2, section C.1, if $V_x \neq 0$, equation 2.55 becomes

$$(x'/\ell)^{3/2} = (V_L - V_x)/(V_L + V_D). \qquad 4.1$$

Thus, the electric field distribution, given by equation 2.56, becomes

$$E_x = (3/2)(V_L - V_x)^{1/3}(V_L + V_D)^{2/3}\ell^{-1}. \qquad 4.2$$

To first order,

$$\Delta j \propto \Delta E_x = -\Delta V_x E_x / 3(V_L - V_x), \qquad 4.3$$

so that

$$\Delta V_x = -3V_L(\Delta j/j), \qquad 4.4$$

where j is the photocurrent density, Δj is the variation in the photocurrent density, and ΔV_x is the variation in the potential at a Hall probe with respect to ground potential.

A filter was inserted in the light path that absorbed any wavelengths lomger than 4000 Å to insure that carriers were not generated in the bulk of the crystal.

(9) Electrical System.

The circuit used for the measurement of the Hall voltage and the photoconductivity of anthracene is shown in

Fig. 4.17. In this investigation, anthracene had a dark resistivity of $\approx 10^{16}$ ohm cm. The photoresistivity was typically 10^{12} ohm cm. A vibrating reed electrometer, with a 10^{8} ohm resistor across its input, was used as an ammeter to measure the photoconductivity. The line, in Fig. 4.17, connecting the current electrometer to the light source represents the feedback system described above in section 8.

Besides the high input impedance of the vibrating reed electrometer, in excess of 10^{16} ohms, another useful property of this instrument was that compensating potentials for Hall probe misalignment voltage could be applied without destroying the high input impedance or adding to the circuit capacitance. Low circuit capacitance was necessary to reduce the time constnat of a Hall voltage measurement. Assuming an input capacitance of 100 picofarads to the Hall voltage measuring electrometer, the time constant for a measurement, without illumination, would be of the order of three hours. This value was obtained by using $\approx 10^{17}$ ohms for the dark resistance of a typical anthracene crystal. Since charge carriers were photogenerated, this time was reduced to the order of three minutes.

In practice, it was impossible to place a Hall probe on a crystal in such a manner that it would be on any desired, arbitrary, equipotential surface. Therefore, with an applied electric field that was typically 200 V/cm,

Fig. 4.17. Block diagram for the measurement of the Hall voltage and the photoconductivity of anthracene.

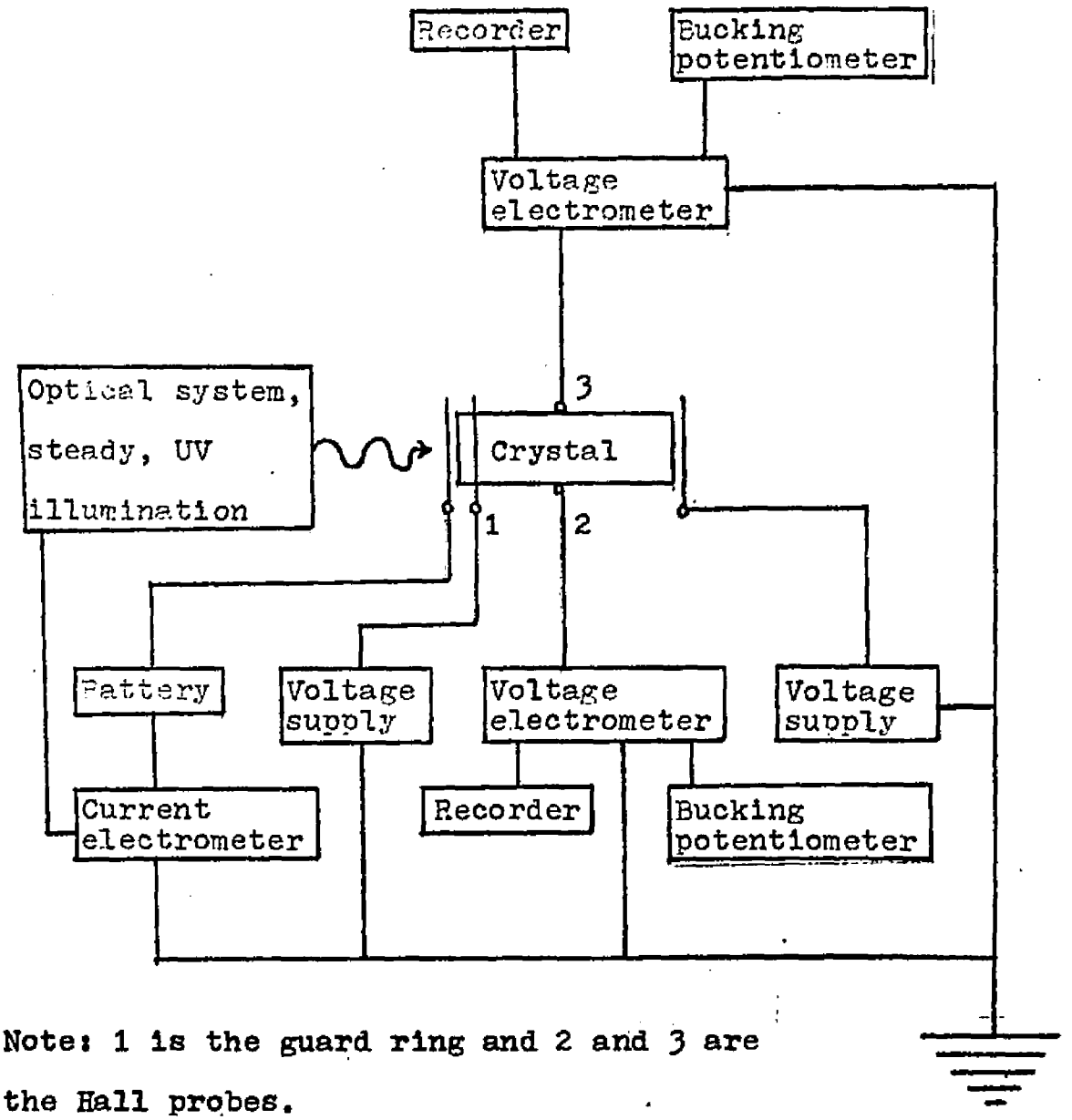

Note: 1 is the guard ring and 2 and 3 are the Hall probes.

one could not do better than align the Hall probes so that the misalignment voltage was a few volts. This voltage had to be balanced out by a suitable bucking potential in order to observe a Hall voltage. A circuit diagram of a bucking potentiometer is shown in Fig. 4.18.

The Hall voltage expected with a magnetic field of 25 kilogauss, an electric field of 200 V/cm, and crystal dimensions of 6 mm x 3 mm x 2 mm, was of the order of 10 mV. This value was obtained by assuming $|\mu_H/\mu_D| \approx 1$ (see chapter 3, section B), and using the elementary theory of of chapter 2, section A. The value of the electric field was chosen as a compromise to enhance the Hall voltage and diminish the drift voltage. Space charge effects, described in chapter 2, section C.2.b, reduced this value by a factor of two. Even with continuous recording of a probe potential (half the Hall voltage), the maximum drift tolerable during a measurement was about one order of magnitude larger than the signal to be measured. A larger drift did not permit one to detect a change in a probe potential upon application of the magnetic field.

Separate electrometers were used to measure the potential at each Hall probe because it was necessary to ground one input terminal of an electrometer when using it to measure voltages (Fig. 4.17). Also, by measuring the potentials of the individual Hall probes, one could discriminate between a Hall voltage and drift voltages due to instabilities in interelectrode leakage resistances and thermal and photo-

Fig. 4.18. Circuit diagram of a bucking potentiometer.

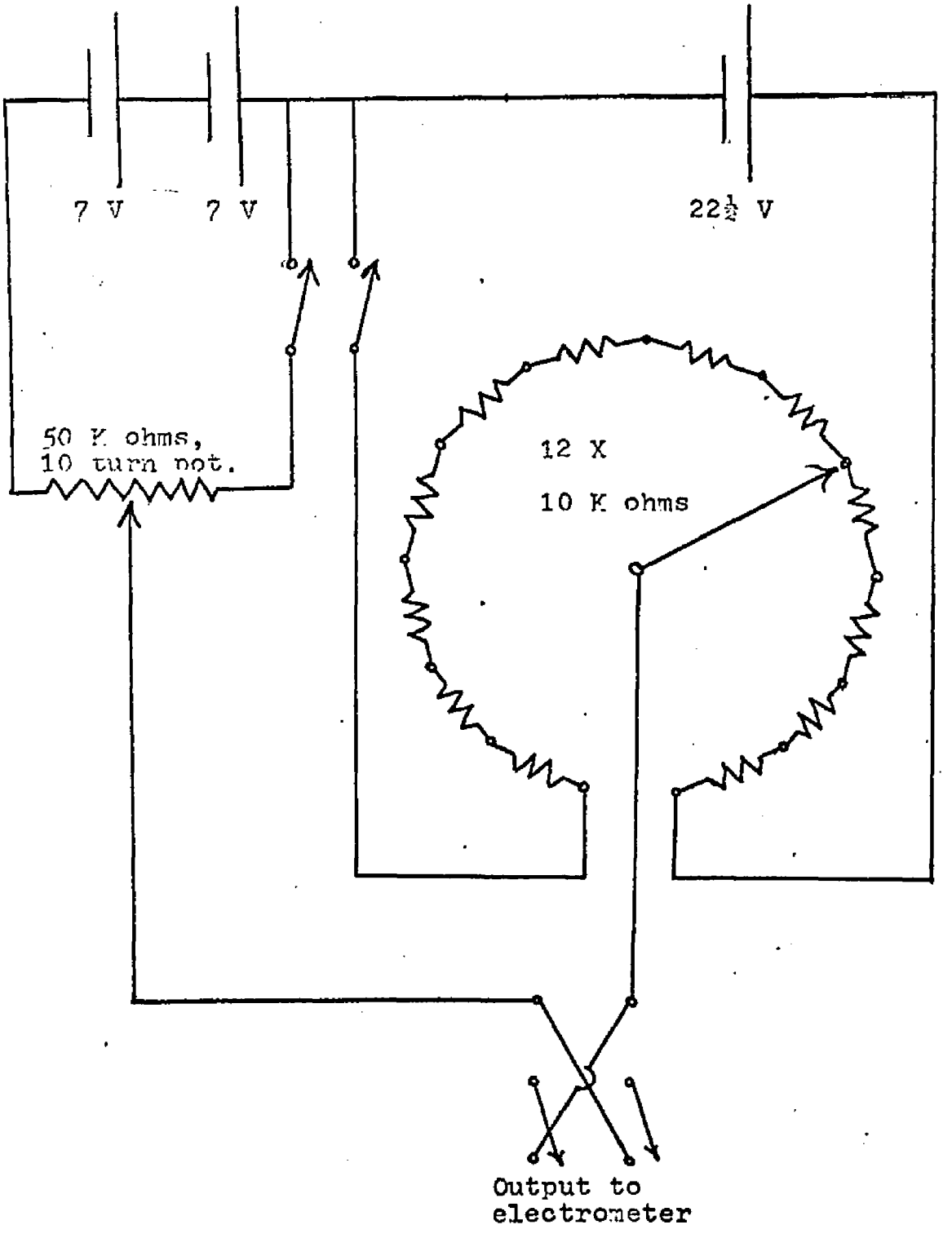

current variations. In response to a Hall voltage, the Hall probes registered in different directions, i.e. one probe became more positive and the other became more negative. In response to drift voltages caused by unstable interelectrode leakage resistances and thermal and photocurrent variations, both probes registered in the same direction.

E. Drift Molbility Apparatus.

The drift mobility of anthracene crystals was measured by a pulsed photoconductivity method, developed by Kepler.[2] A block diagram of the drift mobility apparatus is shown in Fig. 4.19. A xenon flash tube was triggered to emit a 2 microsec pulse of light. A monochromator selected light that was strongly absorbed by an anthracene crystal (3900 A).[14] A photo-generated pulse of charge then drifted across the crystal, and a voltage pulse was developed across a resistor, R, in series with the crystal. A typical value of R was 20 megohms. The amplifier (gain ≈ 1) was used to match the impedance of R to the input impedance of the oscilloscope (≈ 1 megohm) and to reduce the input capacitance so that the time constant was less than 5 microsec. The trace of the voltage pulse, developed across R, was then displayed on the oscilloscope and photographed. One then had a record of the voltage developed across R as a function of time. This enabled one to measure the transit time of the pulse of charge across the crystal,

Fig. 4.19. Block diagram for pulsed photoconductivity measurement of the drift mobility in anthracene.

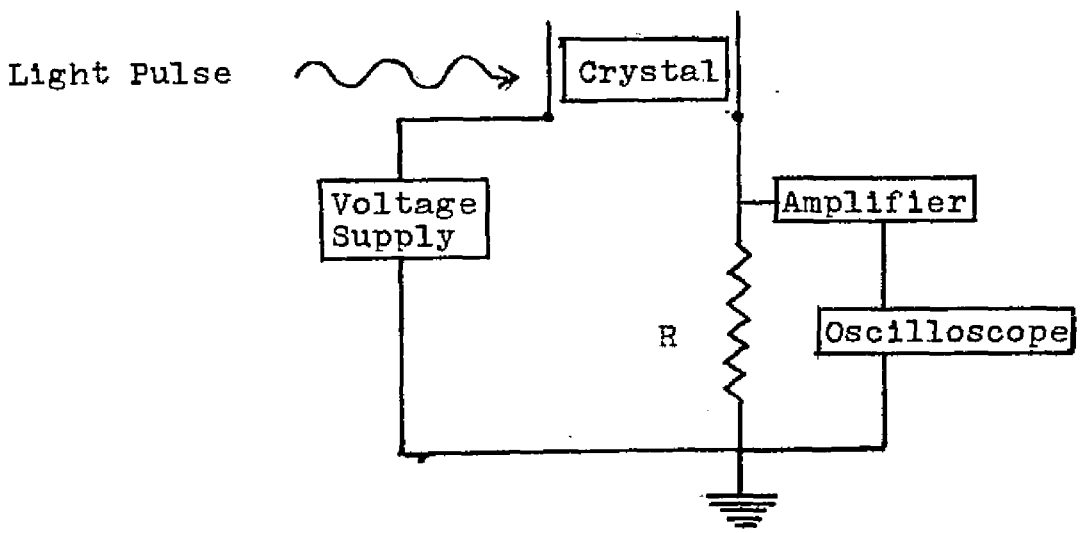

and hence the drift mobility. Although the drift mobility of one type of charge carrier was measured, holes, with the proper bias applied to the crystal, the drift mobility of electrons could also be measured within the sensitivity of the apparatus.

References - Chapter 4

1. D.C. Northrop and D. Simpson, Proc. Roy. Soc., 244a, 377 (1958).

2. R.G. Kepler, Phys. Rev. 119, 1226 (1960).

3. D.C. Hoesterey and G.M. Letson, J. Phys. Chem. Solids, 24, 1609 (1963).

4. J.N. Sherwood, Purification and Growth of Large Anthracene Crystals in M. Zeif editors. Methods and Techniques of Fractional Solification (M. Dekker, New York, 1969).

5. F. Gutmann and L.E. Lyons, Organic Semiconductors (J. Wiley & Sons, Inc., New York, 1967), p. 130.

6. F.R. Lipsett, Can. J. Phys. 35, 284 (1957).

7. J.N. Sherwood and S.J. Thomson, J. Sci. Instr. 37, 242 (1960).

8. S. Singh et. al., J. Chem. Phys. 42, 330 (1965).

9. R.C. Jarnagin et al., J. Chem. Phys. 39, 573 (1962).

10. I. Nakada, J. Phys. Soc. of Japan 17, 113 (1962).

11. J.M. Robertson, Revs. Mod. Phys. 30, 155 (1958).

12. J.E. Jensen et. al. eds., Bubble Chamber Group Selected Cryogenic Data Notebook, (Brookhaven National Laboratory, B.N.L. 10200, 1966), p. V1-A-1.1.

13. M. Silver et. al., Phys. Rev. Letters 10, 12 (1963).

14. E. Clar, Aromatic Hydrocarbons (Academic Press, New York, 1964) p.291.

5. Experimental Techniques, Results and Discussion

A. Hall Effect Measurement

The Hall effect measurement was made as follows. The negative bias, V_D, applied to the **collecting electrode (see** chapter 2, section C), was adjusted so that one of the Hall probe potentials was zero with respect to ground potential. One could then determine the primary electric field intensity at this probe by equation 2.56. The applicability of equation 2.56 to the present measurements was verified by placing probes along the length of a crystal and measuring the potential distribution. Hall probe potentials were recorded, as a function of time, while the magnetic field was varied periodically as a function of time.

A Hall probe recording and a plot of magnetic field, as functions of time, are shown in Fig. 5.1. The oscillations, which have a period of approximately 1½ minutes, in the recording of the Hall probe potential, Fig. 5.1, are due to the temperature controller (see chapter 4, section D.7) turning on and off. The RC time constant of the circuit caused the time lag in Fig. 5.1 between the application of the magnetic field and the onset of the increase in the Hall probe voltage V_M. This Hall voltage was determined from the change in average slope of V_M compared to that of the magnetic field. This could be done at the several regions of change indicated in Fig. 5.1. Thus, a check was available for internal consistency of any measurement cycle. Errors

FIG. 5.1. (a) HALL PROBE POTENTIAL RECORDING, V_M AS A FUNCTION OF TIME. (b) CORRESPONDING PLOT OF MAGNETIC FIELD, B_Z, AS A FUNCTION OF TIME.

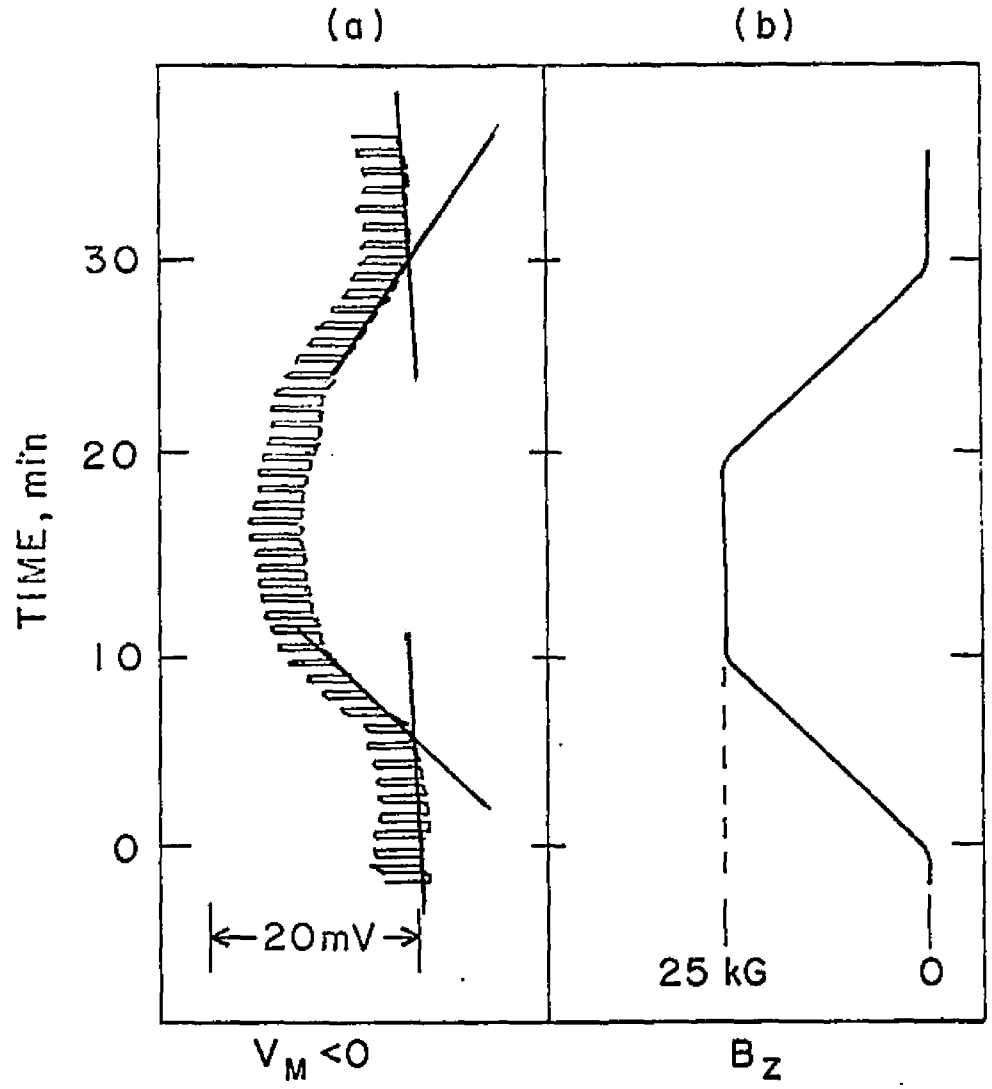

in the values arise from errors in choosing the average slopes and were not believed to exceed 30%. The slope could be affected by instabilities in the photocurrent and thermal effects around the Hall probes. Only those traces showing reasonable stability were accepted for analysis. About five runs were made for each of the orientations and the reported data are the averages of these runs.

Experimental data and computed Hall mobilities are shown in Tables 5.1, 5.2, and 5.3. The data are for holes at room temperature. The Hall mobility for electrons was not measured because electrons could not be photogenerated as efficiently as holes. The notation used for the crystal dimensions, is the same as that used in chapter 2. η was computed from equation 2.81. The space charge factor, S, was computed from equation 2.78 which is:

$$S = 1 - (2L/w) \tanh(w/2L), \qquad 2.78$$

where L was computed from equation 2.80. L is a function of the anisotropic dielectric constant of the sample. The anisotropic dielectric constant of anthracene is given in Table 5.4. The geometrical factor, G, was computed from equation 2.61. The infinite series, given in equation 2.61, converges rapidly. This was verified by a computer calculation to the first 16 terms. The Hall mobility, μ_H, was then computed from equation 2.83, which is given in Tables 5.1, 5.2, and 5.3.

Table 5.1. Experimental data and computed Hall mobility, at room temperature, for magnetic field parallel to the c' direction.

$$\mu_H = (100\eta/GS)(V_M/B_Z)$$

Crystal Orientation and Dimensions (ℓ x w x t) (mm^3)	V_L (V)	V_D (V)	Photo-current (10^{-11}A)	$\lvert V_M/B_Z \rvert$ (mV/kG)	100η (V^{-1})	S	G	μ_H (cm^2/Vsec)
I_{photo}//b (5.5x3x2.5)	46	86	0.8	0.21	2.63	0.191	0.906	-3.2
	46	106	1.0	0.29	2.40	0.211	0.908	-3.4
	46	106	1.0	0.19	2.40	0.211	0.908	-2.4
	46	106	0.9	0.26	2.40	0.194	0.908	-3.5
I_{photo}//a (6x3x2)	46	100	0.6	0.15	2.68	0.274	0.929	-1.6
	46	100	0.75	0.15	2.68	0.303	0.929	-1.4
	46	80	1.0	0.13	2.96	0.366	0.928	-1.1
	46	100	0.5	0.17	2.68	0.240	0.929	-2.0

V_L is the positive bias applied to the illuminated electrode.

V_D is the negative bias applied to the collecting electrode.

V_M is the voltage measured at a Hall probe.

B_Z is the magnetic field intensity.

$\eta = 2/wE_X$, where E_X is the electric field intensity.

S is a factor due to space charge effects.

G is a factor due to the finite dimensions of the sample.

Table 5.2. Experimental data and computed Hall mobility, at room temperature, for magnetic field parallel to the b direction.

$$\mu_H = (100\eta/GS)(V_M/B_z)$$

Crystal Orientation and Dimensions (ℓ x w x t) (mm^3)	V_L (V)	V_D	Photo-current (10^{-11}A)	$\lvert V_M/B_z \rvert$ (mV/kG)	100η (V^{-1})	S	G	μ_H (cm^2/Vsec)
I_{photo}//a (7x2.5x2.5)	70	70	0.8_5	0.49	3.36	0.245	0.961	+6.9
	70	70	0.8_5	0.60	3.36	0.245	0.961	+8.5
	70	70	0.8_5	0.45	3.36	0.243	0.961	+6.4
	70	120	1.0	0.65	2.74	0.229	0.977	+7.9
I_{photo}//c' (5.5x3x3)	70	70	0.2	0.28	2.20	0.097	0.882	+7.1
	70	70	0.2	0.27	2.20	0.097	0.882	+6.9

V_L is the positive bias applied to the illuminated electrode.

V_D is the negative bias applied to the collecting electrode.

V_M is the voltage measured at a Hall probe.

B_z is the magnetic field intensity.

$\eta = 2/wE_x$, where E_x is the electric field intensity.

S is a factor due to space charge effects.

G is a factor due to the finite dimensions of the sample.

Table 5.3. Experimental data and computed Hall mobility, at room temperature, for magnetic field parallel to the a direction.

$$\mu_H = (100\eta/GS)(V_M/B_Z)$$

Crystal Orientation and Dimensions (ℓ x w x t) (mm^3)	V_L (V)	V_D (V)	Photo-current (10^{-11})	$\lvert V_M/B_Z \rvert$ (mV/kG)	100η (V^{-1})	S	G	μ_H (cm^2/Vsec)
I_{photo}//c' (5.5x3x3)	70	110	0.3	0.25	1.86	0.104	0.908	-4.8
	70	130	0.3	0.19	1.73	0.098	0.909	-3.7
	70	120	0.4_5	0.19	1.80	0.141	0.909	-2.6
	70	120	0.6	0.32	1.80	0.179	0.909	-3.6
	70	105	0.6	0.41	1.90	0.187	0.907	-4.5
I_{photo}//b (6.5x3.5 x3.5)	70	80	0.6	0.28	2.13	0.096	0.897	-7.0
	70	80	1.3	0.73	2.13	0.183	0.897	-9.5
	70	80	0.6	0.36	2.13	0.096	0.897	-9.0
	70	60	2.6	1.0_5	2.34	0.319	0.871	-8.8

V_L is the positive bias applied to the illuminated electrode.

V_D is the negative bias applied to the collecting electrode.

V_M is the voltage measured at a Hall probe.

B_Z is the magnetic field intensity.

$\eta = 2/wE_x$, where E_x is the electric field intensity.

S is a factor due to space charge effects.

G is a factor due to the finite dimensions of the sample.

Table 5.4. The anisotropic dielectric constant of anthracene.

ϵ_a	2.79 [1]
ϵ_b	3.24 [1]
$\epsilon_{c'}$	3.8 ± 0.3 [2]

B. Drift Mobility Measurement.

The drift mobility of holes, at room temperature, was measured in anthracene crystals that were cut either from crystals used in the Hall effect measurement or from the same boule that furnished crystals for the Hall effect measurement.

The pulsed photoconductivity method that was used is described in chapter 4, section E. The measurements were made in an Ohmic region since the applied voltage was proportional to the voltage developed across resistor R, Fig. 4.16. The voltage developed across R is proportional to the photocurrent. Thus,

$$V \propto I, \qquad 5.1$$

where V is the voltage applied to the crystal and I is the photocurrent. For Ohmic conditions, the drift mobility is given by:

$$\mu_D = d^2/Vt , \qquad 5.2$$

where μ_D is the drift mobility, d is the crystal thickness, and t is the transit time of charge carriers across the crystal.

A photograph of a typical voltage pulse developed across R and displayed on an oscilloscope is shoen in Fig. 5.2. Measurements were made along the a, b, and c' crystallographic directions. The values of the drift mobility, that were obtained, are given in Table 5.5. t was obtained by

Fig. 5.2. Drift mobility measurement for holes drifting along the b crystallographic direction in anthracene at room temperature. d = 2.2 mm. V = 1500 V. t = 16 microsec. Time is measured from right to left.

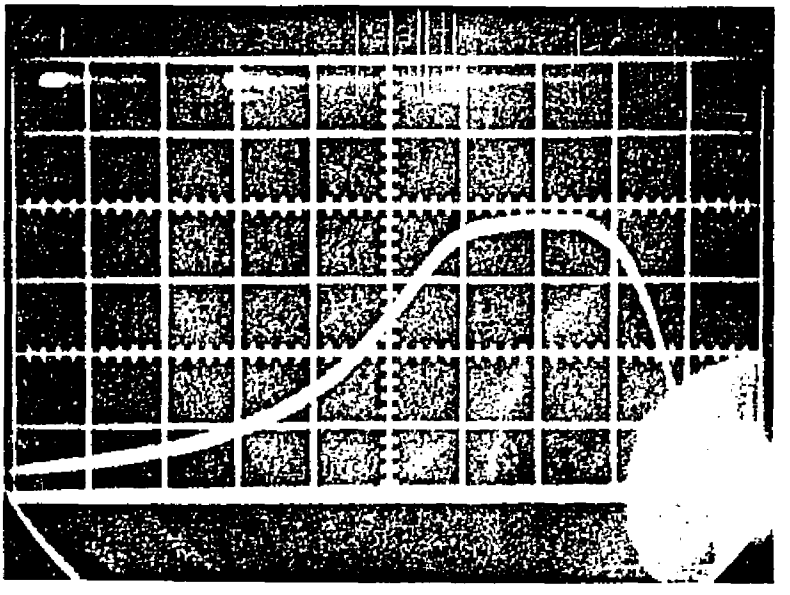

Vertical scale: 0.2 V/cm.

Horizontal scale: 5 microsec/cm.

Table 5.5. The drift mobilities, measured in anthracene at room temperature, for holes drifting along the a, b, and c' directions. The drift mobilities are given in $cm^2/Vsec$.

μ_a	1.0
μ_b	2.0
$\mu_{c'}$	0.8

measuring the time from the start of the pulse (right side of photograph) to the beginning of the decaying tail of the pulse (center portion of the photograph). The tail is due to charge carriers being released from traps.[3] The measured values of the drift mobility, given in Table 5.5, are exactly the same as the values obtained by Kepler.[4]

C. Discussion.

The results, given in Tables 5.1 and 5.3, show the Hall mobility of holes to have an anomalous sign when the magnetic field is parallel to the a and a' crystallographic directions in anthracene crystals. This means that the holes were deflected in the direction opposite to the direction in which positive charge carriers would normally be deflected by a Lorentz force. This agrees precisely with the predictions of band theory, given in chapter 3, where the hole bands are so narrow one can conclude that the negative effective mass states have been populated at room temperature. Since the effective mass states are weighted more heavily than the positive effective mass states in the numerator of equation 2.43, a reversal in sign for the Hall mobility is obtained.[5] The results, given in Table 5.2, show the Hall mobility of holes to have a normal sign and a value that is larger than the drift mobility when the magnetic field is parallel to the b crystallographic direction in anthracene crystals. The normal sign for this orientation has also been predicted by the band theory, given in chapter 3. The earlier experimentalists who found Hall mobilities much larger than drfit mobilities concluded that the conduction bands in anthracene are very narrow compared to kT at room temperature. The results presented here indicate that the hole bands are narrow but not so narrow as others have reported.

Table 5.6. (a) The Hall mobility in anthracene, computed from the measured photo-Hall voltage for photo-injected holes at room temperature. The Hall mobilities are given in $cm^2/Vsec$. (b) The ratios of the Hall to the drift mobility in anthracene for photo-injected holes at room temperature. B// and I// indicate the axes to which the magnetic field and the photocurrent are parallel.

(a)

I// \ B//	a	b	c'
a		+7.4	-1.5
b	-8.6		-3.1
c'	-3.8	+7.0	

(b)

I// \ B//	a	b	c'
a		+7.4	-1.5
b	-4.3		-1.5
c'	-4.8	+8.8	

Note: Minus signs indicate anomalous deflections.

Table 5.6 summarizes the results obtained in this investigation by giving the ratios of the Hall to the drift mobilities for holes in anthracene. It should be noted in Table 5.6 that when the current is in the c' direction μ_H/μ_D is negative for the magnetic field in the a direction and positive for the magnetic field in the b direction. Since anthracene cleaves readily only in the ab plane, it is presumed that the measurements discussed in chapter 1, in which the directions were not specified, were made on cleavage plates and therefore, the current was probably in the c' direction. In view of this and the findings reported here, disparity in sign of the ratio among the investigators discussed in chapter 1 is understandable in cases in which care was not taken in knowing the orientation of the magnetic field. It should be further noted that if a thin cleavage plate was used, then a significant fraction of the current could be due to electrons generated in the bulk of the material. It is not yet determined if anomalous behavior of electrons follows that of holes. The band theory calculations, given in chapter 3, are ambiguous for the case of electrons. If there is no anomalous behavior for electrons, then it is possible to observe a larger Hall voltage than would be observed with a single type of charge carrier.

Unfortunately, a unique band width cannot be determined from the experimental data presented in this work. In order to obtain a unique bandwidth, the exact depen-

dence of μ_H/μ_D on the energy band structure of anthracene would be required. This dependence, will, most likely, be a long time in development because of the difficulty in the required calculations (chapter 3).

An important result of this work is the anomalous sign for the Hall mobility of holes in anthracene. Since strongly absorbed light was used to generated the charge carriers and a positive bias was applied to the directly illuminated electrode no doubt exists about the sign of the charge carriers. Although the exact magnitude of the Hall mobility is not known (because of the small signal to noise ratio and the corrections applied for space charge conditions), the direction of the Hall field is known. This result, as presented earlier, is consistent only with conduction by a band mechanism since band theory is the only theory which predicts an anomalous Hall effect.

From these results and those of other investigators, presented in chapter 1, one can conclude that the bulk Hall effect is quite different from the surface Hall effect.

References - Chapter 5

1. F. Gutmann and L.E. Lyons, Organic Semiconductors (J. Wiley & Sons, Inc., New York, 1967), p.348.

2. D. Spielberg, private communication.

3. M. Silver, M. Swicord, and R.C. Jarnagin, J. Phys. Chem. Solids 23, 419 (1962).

4. R.G. Kepler, Charge carrier mobility and production in anthracene in J.J. Brophy and J.W. Buttrey, eds., Organic Semiconductors, (Macmillan, New York, 1962),p.1.

5. L. Friedman, Phys. Rev. 131, 2445 (1963).

Appendix

A. The validity of the first order expansion of the distribution function in terms of the electric field.

Consider the Boltzmann transport equation, equation 2.9, with no magnetic field and with the electric field along the x direction. Then,

$$-(f-f_o)/\tau = -(eE_x/\hbar)(\partial f/\partial k_x) , \qquad A.1$$

or

$$f - f_o = (e\tau E_x/\hbar)(\partial \varepsilon/\partial k_x)(\partial f/\partial \varepsilon) = e\tau v_x E_x(\partial f/\partial \varepsilon). \qquad A.2$$

In the expansion of f, used in chapter 2, it is assumed that:

$$\left|(f-f_o)/f_o\right| \ll 1 . \qquad A.3$$

This is equivalent to assuming,

$$\left|e\tau v_x E_x(\partial f/\partial \varepsilon)/f_o\right| \approx \left|e\tau v_x E_x(\partial f_o/\partial \varepsilon)/f_o\right| \ll 1. \qquad A.4$$

For anthracene, since the band gap is greater than 3 eV (see chapter 1), one may use the classical Bolzmann distribution given by:

$$f_o = A \exp(-\varepsilon/kT). \qquad A.5$$

Therefore,

$$(\partial f_o/\partial \varepsilon)/f_o = - 1/kT , \qquad A.6$$

and A.4 becomes:

$$\left| e\tau v_x E_x/kT \right| \ll 1 \; . \qquad \text{A.7}$$

$$e\tau = m\,\mu_D \; .^{1} \qquad \text{A.8}$$

m is the effective mass of a charge carrier and μ_D is the charge carrier drift mobility. v_x may be obtained from band theory calculations. Typically, $v_x \approx 15 \times 10^5$ cm/sec,[2] and $\mu_D E_x \approx 200$ cm/sec in this investigation. Therefore,

$$\left| e\tau v_x E_x/kT \right| = \left| m v_x \mu_D E_x/kt \right| \approx 7 \times 10^{-6} \qquad \text{A.9}$$

when the electron mass is used for m. It is seen that A.9 would be less than one if an effective mass of even 1000 m would be used instead of m. Thus, it is seen that $(f-f_o)/f_o$ must indeed be less than one.

B. The validity of the Jones and Zener expansion used in equation 2.18.

The expansion employed in equation 2.18 is in terms of $eB\tau/m$, and is thus valid if:

$$eB\tau/m \ll 1 \; . \qquad \text{B.1}$$

From equation A.8, it is seen that:

$$eB\tau/m = \mu_D B. \qquad \text{B.2}$$

Typically, $\mu_D \approx 1$ cm^2/V sec for anthracene (see chapter 1). Since B was not greater than 40 kilogauss = 4×10^{-4} V sec/cm, it is seen that $\mu_D B \approx 4 \times 10^{-4}$ and is less than one.

C. Examination of the Boundary Condition Imposed on the Electric Field in Calculating the Space Charge Factor.

In calculating the space charge factor, S, it was assumed that one had the following boundary condition:

$$(dV_y/dy)_{y=\pm\frac{1}{2}w} = 0. \qquad C.1$$

Here, one examines the effect of the following upper bound on the electric field at $y = \pm\frac{1}{2}w$:

$$-(dV_y/dy)_{y=\pm\frac{1}{2}w} < 2V_M/w \ , \qquad C.2$$

where

$$2V_M = SV_H \ . \qquad C.3$$

From equation 2.74, one has:

$$-V_y = -By/A + (\alpha/A)\ \sinh(y/L) \ . \qquad C.4$$

Differentiating equation C.4 with respect to y and using C.2 and C.3, one obtains:

$$\alpha/A < \frac{LV_H(1+S)}{w\ \cosh(w/2L)} \ . \qquad C.5$$

Thus,

$$V_y > V_H\left[(y/w) - (L/w)(1+S)\frac{\sinh(y/L)}{\cosh(w/2L)}\right] \ , \qquad C.6$$

or

$$2V_M > V_H\left[1 - (2L/w)(1+S)\tanh(w/2L)\right] \ . \qquad C.7$$

Therefore,

$$S > (1-\beta)/(1+\beta) \ , \qquad C.8$$

where

$$\beta = (2L/w) \tanh(w/2L). \qquad C.9$$

Since β was found experimentally to be of the order of one, it can be seen from C.8, that a lower bound for S is approximately $\frac{1}{2}(1-\beta)$.

References - Appendix

1. W. Shockley, Electrons and Holes in Semiconductors (D. Van Nostrand Co. Inc., New York, 1950), p.198.

2. J.I. Katz, S.A. Rice, S. Choi, and J. Jortner, J. Chem. Phys. 39, 1683 (1963).